MODELLING THE RECRYSTALLISATION-STOP TEMPERATURE OF VANADIUM AUSTENITE BY SINGLE PASS ROLLING

PRAFUL PATEL

A thesis submitted to the University of Manchester for the degree of Doctor of Philosophy in the faculty of Technology.

Department of Metallurgy
and Material Science,
University of Manchester
Institute of Science and Technology.

APRIL 1997

In memory of my late father, Prabhubhai, who constantly encouraged the philosophy of Caius Julius Victor:

'Rem tene; verba sequentur'

Grasp the subject; the words will follow.

ACKNOWLEDGEMENTS

The author is indebted to Dr.Ron Priestner, for initiating this research, his guidance and stimulating discussions throughout the course of this study. I am indeed grateful to Dr Zhou Chuanjie, for practical assistance with much of the experimental work and technical discussions.

My thanks are also extended to my colleagues both at Royal SunAlliance Engineering and UMIST for their constant support and constructive discussions throughout the course of this study. I am most indebted to my wife Lila, daughter Maya and son Kapil for their encouragement, support and above all, their patience throughout the course of this study.

THE AUTHOR

The author was awarded the degree of 'Associateship in Metallurgy' in 1979. He is a Professional member of the Institute of Materials, of Chartered Engineer status, and was with Royal SunAlliance Engineering Insurance Co, Manchester, from 1985 to 1996. He was awarded the degree of M.Sc (UMIST) following submission of a research thesis in 1992.

As with the degree of M.Sc, the research for the award of Doctor of Philosophy was also undertaken entirely on a part-time, self-financing and without support from his employer.

DECLARATION

The work described in this thesis was carried out at the University of Manchester, Institute of Science And Technology over the period 1992-1997. The work reported here is original, except where due reference is made. None of the material in this thesis has been submitted in support of an application for another degree or qualification of this, or any other University or other Institute of learning.

Praful Patel

April 1997.

ABSTRACT

The recrystallisation-stop temperature (RST) of vanadium microalloyed steels containing 0.20 and 0.43 wt% V was determined experimentally by single pass rolling in the austenitic phase field. Conventional Controlled Rolling (CCR) of each composition was simulated by rolling of reheated slabs, whereas Hot Direct Rolling (HDR) was simulated by rolling as-cast 0.2 wt% V austenite directly after it solidified. The experimental recrystallisation-stop temperature of the HDR and CCR austenites containing 0.2 wt% V were similar, despite a large difference in grain size (92 μm compared with 1150 μm) and process routes. The RST model, proposed by Dutta and Sellars for niobium steels, was modified to suit the current materials, process routes and experimental methodology. The original model overestimated the experimental RST of all the three steels studied. However, good agreement was found between the modified model and the experimental RST of both the as-cast and reheated austenites. The initiation of recrystallisation was more rapid in V austenite than in Nb austenite, and not so strongly dependent upon grain size as proposed by the Dutta and Sellars model.

LIST OF SYMBOLS

α	measure of the strength of a solute's effect on the RST
a	lattice parameter
a_α	lattice parameter of matrix phase
A	constant in the solubility product equation (1.6)
A_M	constant in equation (2.3)
A_{RX}	constant in equation (2.1)
A_{PPT}	constant in equation (2.5)
B	constant in the solubility product equation (1.6)
B_{RX}	constant in equation (2.1)
B_P	constant in equation (2.5)
C_s	concentration of solute in equilibrium with particle
d	matrix grain diameter
d_o	initial austenite grain size (μm)
D_o	Diffusion coefficient ($m^2\ s^{-1}$)
D_{eff}	effective diffusion coefficient
$\dot{\varepsilon}$	strain rate
$\bar{\dot{\varepsilon}}$	equivalent mean strain rate
ε	strain
f	volume fraction of particles
F	solute drag effect factor
F_{gb}	the total drag force per unit area of grain boundary
F_{max}	the drag exerted by a single particle on a grain boundary
F_G	energy provided by grain growth
f_o	modifying factor
ΔG^*	critical free energy for nucleation
ΔG_V	free energy change arising from the chemical driving force
G	ASTM grain size number
H	original slab thickness (mm)
h	slab thickness after reduction r (mm)

J_s	steady state nucleation rate
k	Avrami exponent
k_β	Boltzmann's constant
γ	particle/matrix interfacial energy
γ_{gb}	grain boundary energy
k_S	supersaturation ratio
K	solubility product
K_C	constant in equation (1.7)
l	mean intercept distance (μm)
L_{LT}	the total length of traverse in the longitudinal
L_{TT}	the total length of traverse in the transverse direction
$\bar{L}_{\gamma L}$	average austenite grain intercepts in the longitudinal direction (μm)
$\bar{L}_{\gamma T}$	average austenite grain intercepts in the transverse direction (μm)
$\bar{L}_L$	mean linear intercept in the longitudinal direction
$\bar{L}_T$	mean linear intercept in the transverse direction
n	number of particles per unit volume
N	rotating speed of rolls during deformation (ms^{-1})
N_o	Avagadro's number
N^*	density of nucleation sites per unit volume
Nb_{RX}	time to 20% softening of a Nb steel at 1000 °C
N_{GB}	the number of grain boundaries intersecting the line of traverse
Q_d	activation energy for diffusion
Q_{deff}	apparent activation energy for deformation (J/Mol)
Q_{diff}	apparent activation energy for diffusion (J/Mol)
Q_{RX}	apparent activation energy for recrystallisation (J/Mol)
r	rolling reduction (H-h/H)
r_o	mean particle radius at zero time
r_t	mean particle radius at time t
r_p	particle radius
R	gas constant

R_D	roll radius (mm)
t	time (s)
t_x	time required for the start of static recrystallisation in the steel containing the element
t_{ref}	is the equivalent time for reference plain C steel
$t_{0.5RX}$	time to 50% recrystallisation
$t_{0.05RX}$	time to 5% recrystallisation
$t_{0.5P}$	time to 50% strain induced precipitation
$t_{0.05P}$	time to 5% strain induced precipitation
T	temperature, Kelvin
T_{GC}	grain coarsening temperature
T_{deff}	temperature of deformation
V_{RX}	time to 20% softening of a V steel at 1000 °C
V_m	molar volume
X	fraction recrystallised
X_α	solute concentration
Z	Zener-Holloman parameter

CONTENTS

CHAPTER 1

INTRODUCTION AND OBJECTIVE

1.1 Introduction

Microalloyed (MA) steels were first introduced as a term by Noren[1] in 1962. He defined them as:

" a steel, the basic composition of which is simply an un-alloyed structural or in many cases a manganese alloy one or even a low alloy one to which a small amount of an alloying element has been added - this element having a very strong or remarkable effect on one or several of the steel properties. The amount of microalloying element to be added is one or two powers of ten less than would have been added for an alloying element in the conventional meaning."

The history of MA steels is documented extensively by, for example, Woodhead and Keown[2]. Tanaka[3] reviewed controlled rolling of plate and strip, and developments in the alloy design of microalloyed and other High Strength Low Alloy Steels (HSLA) were reviewed by DeArdo *et al*[4].

The most important feature of MA steels is their higher strength, relative to the common low-carbon steels used in many formed-and-welded applications. These steels are an extension of the carbon-manganese structural grades and fill the strength gap between the 250 MPa yield-strength carbon-manganese steels and the 700 MPa yield-strength quenched-and-tempered alloy steels. The properties of such steels are strongly dependant on the thermo-mechanical interactions during deformation.

MA steels containing niobium (Nb), titanium (Ti), vanadium (V), singly or in combination, now form a most important family of commercial steels, which during the last decade or so have been subject to more detailed scientific investigation than any other group of steels. Their unique combination of properties arise from the precipitation of carbides, nitrides or

carbonitrides and the interaction of these precipitates with the processes of recrystallisation and grain growth of austenite and of transformation from austenite to ferrite plus pearlite or bainite on cooling. Controlled thermomechanical processing (TMP) is essential if optimum benefit is to be obtained from these interactions. The excellent properties currently achieved are a direct result of the relatively mature understanding of two relationships:

(a) The relationship between microstructure and properties.
(b) The relationship among composition, processing and microstructure.

Much of the enhanced mechanical properties of control rolled microalloyed steels is attributed to precipitation hardening and the refinement of transformed microstructures. Grain refinement is unique, in that it is the only mechanism which simultaneously increases the strength and toughness[5], Fig. 1.

Grain refinement can occur by:

(a) Static recrystallisation during holding after deformation or during multi-pass rolling. However, grain growth between passes is very rapid for austenite grain sizes below about 30 μm. It is not possible to obtain a stable austenite grain size below this limit by static recrystallisation alone.

(b) Effectively refining the austenite by preventing its recrystallisation. The accumulation of rolling strain following the inhibition of recrystallisation below a Recrystallisation-Stop Temperature (RST), results in flattened and elongated austenite grains, and also introduces transgranular deformation bands within the grains, effectively increasing the grain boundary area for ferrite nucleation.

Microalloying elements are crucial to the inhibition of the austenite recrystallisation and to the accumulation of strain below the RST.

There are essentially two basic variants of TMP. Conventional Controlled Rolling (CCR) is where the steel is reheated from ambient temperature to a specific soaking temperature after

which it is deformed in the single austenitic phase field. The second variant is Hot Direct Rolling (HDR), in which the ingot is cooled to the rolling temperature after casting and rolled. The economics of the processing are enhanced by HDR due to the saving of energy by avoiding reheating and soaking at temperature prior to rolling, and due to reduced capital costs.

The as-cast austenite at the start of HDR differs in several forms. As-cast austenite has a very coarse grain size, is dendritic, and its alloy content is segregated interdendritically both on a micro and macro scale. Reheated austenite on the other hand, will be strongly conditioned by the gamma-alpha and alpha-gamma transformations during cooling and reheating. The austenite grain size is refined, and soaking results in a degree of chemical homogenisation. Microalloy carbonitrides precipitate in austenite and ferrite during cooling, and redissolve according to their equilibrium solubilities at the reheating temperature. In as-cast austenite, the concentration of the microalloy elements in solution may well depend on the kinetics of precipitation during and after solidification and to the effects of segregation, rather than on equilibrium solubilities.

Among HSLA steels, vanadium microalloyed steels may not be ideal candidates for conventional controlled rolling due to their low recrystallisation stop-temperature[6]. Owing to its greater solubility V(C,N) does not precipitate as extensively as Nb(C,N) in austenite, hence, vanadium is more effective as a precipitation-strengthening addition.

The importance of the RST is that, deformation below it results in 'pancaked' austenite grains containing transgranular deformation bands, thus increasing the density of potential ferrite nucleation sites. On transformation, a much finer grain size is obtained, with associated enhanced mechanical properties.

A number of metallurgical and processing variables influence the RST. The effects of these variables, composition, strain, strain rate, temperature, grain size, were incorporated by Dutta and Sellars[7] in a mathematical model to predict the RST. In the model, the kinetics of strain induced precipitation and of recrystallisation are used to predict the influence of composition

and process variables on the temperature at which recrystallisation is effectively stopped by strain induced precipitation.

1.2 Objective of Present Research

There is a large volume of literature on thermomechanical processing of Nb or combination of Nb-Ti-V microalloyed steels, but relatively, little on steels microalloyed with vanadium only. Such steels are commonly used for truck frames, storage tanks, low temperature storage tanks, pressure vessels[8].

The objective of the present research, therefore, is to evaluate the recrystallisation and precipitation kinetics of a CCR steel microalloyed with vanadium only, and to investigate the RST for comparison with the prediction of the Dutta and Sellars model. A second objective is to compare the results with a steel of similar composition but which is hot direct rolled. Should such modelling be possible, then it would permit the quantitative evaluation of the RST of vanadium microalloyed steels for most combinations of pre-conditioning and processing variables.

1.3 Structure of the thesis

Tables and figures relating to the text in each chapter are provided at the end of the appropriate chapters. The scope of the following chapters is:

Chapter 2: Review of the literature

The history of MA steels and the pertinent features of TMP is introduced. Structural changes during hot deformation processes are described and mathematical expressions are introduced where appropriate. The role of microalloys and the interacting aspects of hot deformation such as recrystallisation and strain induced precipitation are reviewed and comparisons made between microalloys. The concept of the RST and the models for its determination are discussed.

Chapter 3: Experimental procedures

The methodology of CCR and HDR experiments, choice of materials and an initial modification to the Dutta and Sellars model required to initiate the experimental campaign are

described. The model predictions of RSTs' that was used as a basis for planning the experiments are described.

Chapter 4: Results

Experimental results are presented and comparisons made between the different materials and process routes used. The differences in the experimental and model RSTs' are discussed.

Chapter 5: Discussion

The results from chapter 4 form the basis of a more detailed discussion and the proposal of modifications to the established equations to suit the current materials and experimental methodology. Predictions of the model RST's are compared with the experimental RST's.

Chapter 6: Conclusions and suggestions for further work

Conclusions are drawn based on the work carried out and suggestions are made for further research.

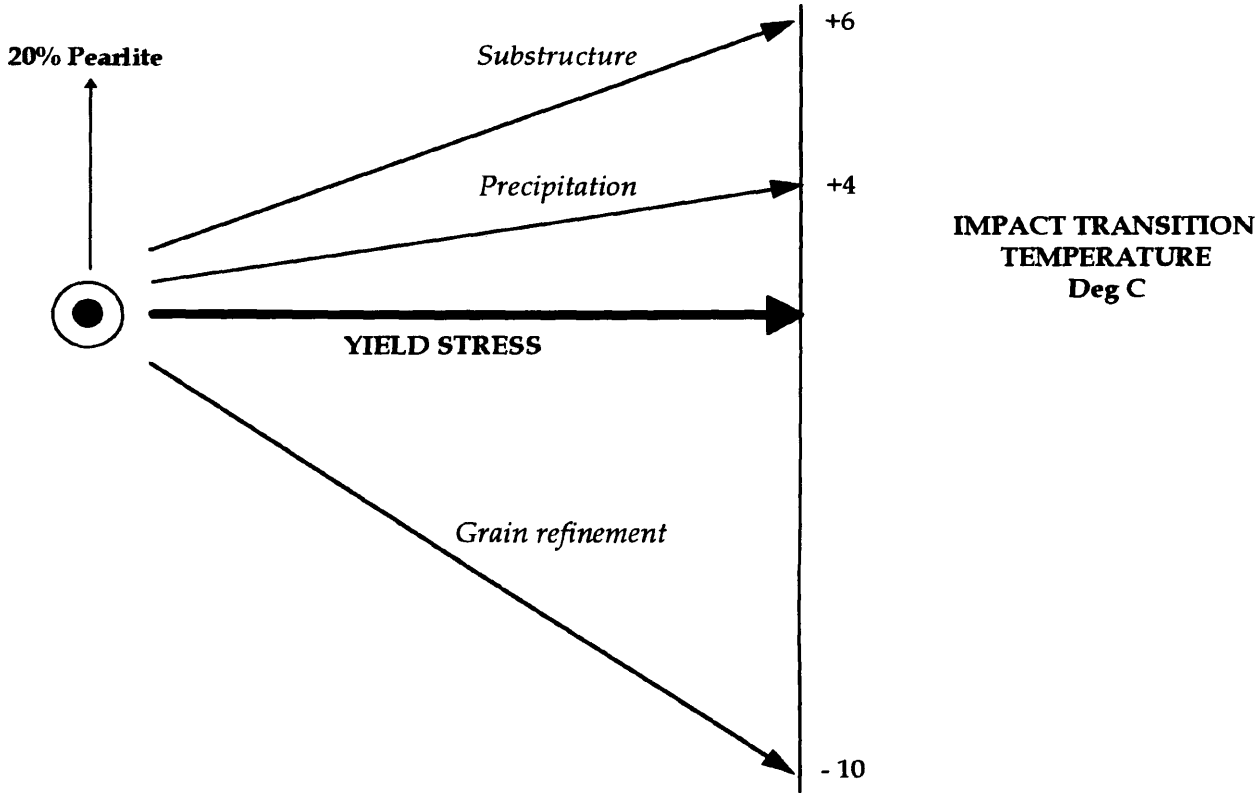

Fig. 1 **Schematic illustration of factors affecting yield strength and impact transition temperature. Numbers indicate the change in transition temperature (°C) per 15 MPa increase in yield strength, after Pickering [5].**

CHAPTER 2

REVIEW OF LITERATURE

2.1 Outline Of Thermomechanical Processing (TMP)

As early as 1954, it was recognised that the properties of steel could be significantly improved by the application of non-traditional cycles of thermal and deformation processing[9]. The traditional hot-rolling process has gradually become a more closely-controlled operation, and is being increasingly applied to MA steels with compositions carefully chosen to provide optimum mechanical properties when the hot deformation is complete. This practice is relatively inexpensive because the micro-alloying elements are required only in small concentrations[10,11].

One of the first attempts to study the microstructural alterations in iron and steel austenite during hot working was made by Grange[12,13]. He demonstrated that a refined austenite grain size developed during hot rolling transformed to a finer-grained transformation product. The control of the final microstructure begins during solidification and proceeds during reheating, hot rolling and final transformation. Because the final transformed microstructure reflects the microstructure and composition of the austenite, final microstructure of the austenite is critical to obtaining the optimum final microstructure and properties of the ferrite. It is the ability to control microstructure during processing that has allowed significant, cost-effective improvements in the final properties of the steel[14]. TMP conditions the parent phase for the subsequent formation of a product phase with an optimised microstructure. The relative difference between TMP and other deformation processes [15] is schematically illustrated in Fig. 2.0. The process, in which the various stages of rolling are temperature-controlled, the amount of reduction in each pass is predetermined and the finishing temperature is precisely defined, so allowing microstructural control, is called controlled rolling[16] (CR).

Basic conclusions of early work, reviewed by Sage[17,18], by Walsh and DeArdo[19] were:

(a) It is difficult by thermomechanical processing steels that do not contain microalloying to achieve the benefits in mechanical properties.

(b) Steels containing microalloying elements displayed lower toughness than their plain-carbon counterparts without thermomechanical processing.

The results from early research revealed a synergy between thermomechanical processing and microalloying.

TMP involves three essential steps:

(a) reheating;

(b) austenite conditioning by controlled rolling, and

(c) controlled cooling following rolling.

Accurate, quantitative knowledge of microstructural and constitutional changes that occur in austenite during thermomechanical processing thus enables control of the final properties in the rolled product without subsequent heat treatment.

2.2 Reheating

Conventional controlled thermomechanical processing starts with the reheating of the slab from ambient to a specific soaking temperature for an appropriate period of time, before subsequent deformation. The major events which may occur during the reheating stage include:

(a) the nucleation, growth and coarsening of austenite grains;

(b) dissolution, precipitation and coarsening of microalloy precipitates inherited from the original slab microstructure;

(c) reduction of inhomogeneties in solute distribution.

The differences in austenitic grain-growth behaviour[20] are illustrated in Fig. 2.1, for various steels during reheating. Carbon (Si-Mn) steels progressively coarsen as the solution temperature is increased. The Nb steel exhibits similar characteristics to the carbon steel at

temperatures above 1050 °C. However, small Ti additions (e.g 0.01 to 0.02%) to a carbon steel provide resistance to austenitic grain growth. As dissolution and coarsening of particles takes place the critical condition for abnormal grain growth may be reached, leading to rapid grain coarsening above a "grain coarsening temperature", which depends on steel composition and particle distribution[21]. Weiss *et al* [22] studied the grain coarsening characteristics of three steels microalloyed with Nb, V and V+Nb, under isothermal conditions at temperatures between 950 and 1300 °C. The grain coarsening temperatures were observed to increase with microalloying elements in the order V, Nb and V+Nb. This temperature was further increased by an increase in the nitrogen level in increments from 0.006 to 0.025% in the V+Nb steel.

Amin and Pickering[23] concluded that, of Nb and V steels, the grain coarsening temperature was higher for the Nb steel. Further, the maximum grain coarsening temperature occurred at the stoichiometric ratio of Nb:C in Nb steels, but the effect of stoichiometric proportion was less marked in the V steel. A further characteristic is the grain growth with increasing time at temperature, shown in Fig. 2.2 for a 0.14% V steel investigated by Mazzare *et al* [24]. This work was on three different steels; a base plain carbon steel, 0.14%V and V+0.043 wt%Nb. At austenitising temperatures of 900 and 1000°C, little grain growth occurred for heating times up to one hour. At higher temperatures, significant grain growth occurred, the curves displaying the classic parabolic shape associated with grain growth in metals. It was noted that the amount of grain coarsening was dependant on the microalloying elements. The V+Nb steel coarsened less rapidly than the V steel which in turn coarsened less rapidly than the base steel. Saito *et al* [25] modelled the variation of austenite grain size during reheating by a simple equation for a 0.07%C-0.03%Nb. It was found that the reheating temperature was a more important factor in the control of grain size than holding time.

The results quoted have shown that the type of microalloying element, reheating temperature and the duration at the reheating temperature all have an effect on the coarsening of austenite grains. Apart from the coarsening characteristics and control of grain size during reheating, the amount of the element in solution at the end of the reheating will influence the recrystallisation kinetics, recrystallised grain size, grain growth and further precipitation or strain induced precipitation in austenite and ferrite.

2.2.1 Role of microalloying elements during reheating.

Austenite grain growth can be inhibited by the interaction of second-phase particles with austenite-grain boundaries. This interaction results from the elimination of grain-boundary area when the boundary intersects a second-phase particle[26]. Movement of the grain boundary away from the particle results in a local energy increase and has a drag effect on the migrating boundary. It has been suggested that the binding force between particle and boundary is greater than could be supplied by thermal activation[27], and consequently the energy for unpinning has to be supplied from some other source, for example from the energy release resulting from grain growth.

Gladman[28] has shown that the energy provided by grain growth, F_G, is given by:

$$F_G = \frac{2\gamma_{gb}}{d} \qquad \textbf{(1.0)}$$

where F_G is the energy released per unit area of the advancing grain boundary; γ_{gb} is the grain boundary energy and, d is the matrix grain diameter.

The drag, F_{max}, exerted by a single particle on a grain boundary when the angle of contact, θ is 45° is expressed as:

$$F_{max} = \pi\, r_p\, \gamma_{gb} \qquad \textbf{(1.1)}$$

where r_p is the particle radius.

For a single particle of volume $4/3\ \pi r_p^3$, in volume fraction of particles f, the number of particles per unit volume n is given by:

$$n = \frac{3f}{4\pi r_p^{\,3}} \qquad \textbf{(1.2)}$$

and the total number of particles in volume n is $2r_p n$. As each particle exerts a drag F_{max} on the boundary, the total drag force per unit area of boundary, F_{gb}, is expressed as:

$$F_{gb} = \frac{3 f \gamma_{gb}}{2 r_p} \qquad (1.3)$$

For the prevention of grain coarsening, $F_{gb} \geq F_G$, that is:

$\frac{3 f \gamma_{gb}}{2 r_p} \geq \frac{2 \gamma_{gb}}{d}$, and the critical particle radius, r_p (critical), is expressed as:

$$r_p \text{ (critical)} = \frac{3}{4} \cdot f \cdot d \qquad (1.4)$$

This relationship shows that the critical particle radius increases with an increase in the volume fraction of particles, or an increase in matrix grain diameter. It is also noted that the critical particle radius is the maximum value that permits effective pinning.

The significance of this result is that stability of austenite grain size at high temperatures requires:

(a) A high solvus temperature, to ensure a sufficient volume fraction of particles;
(b) A low rate of coarsening, so that the particles remain fine enough to prevent grain growth.

These factors are governed by the solubility of the microalloying elements and their diffusivity in solid solution. The reheating conditions therefore determine:

(a) the reheated austenite grain size for TMP, and
(b) the amount of microalloy taken into solution.

The ultimate response of a steel to subsequent processing will, to a large extent, be strongly influenced by these two factors.

2.2.2 Solubility of Precipitate Dispersions

The usual form of the solubility product equation for a binary compound MX is expressed as:

$$K = [M]\,[X] \qquad (1.5)$$

and the general solubility relationship can be expressed as:

$$\log [M]\,[X] = A - B/T \qquad (1.6)$$

Where M is the concentration (wt %) of Nb, V or Ti and X is the concentration (wt %) of carbon or nitrogen in solution at equilibrium, K is the solubility product, A and B are experimentally derived constants, and T is the absolute temperature. A and B differ for different carbides and nitrides, and typical values[29,30,31] are given in Table 1.0 for VC and VN.

Vanadium carbide is much more soluble in austenite than niobium carbide or titanium carbide which possess similar solubilities. The nitrides are substantially less soluble than the corresponding carbides, vanadium nitride being the most soluble and titanium nitride having particularly low solubility. In practical terms, as applied to TM processing of microalloyed steels, the least soluble compounds will be precipitated at the highest temperatures in the austenite. To assure that the precipitation necessary to produce grain refinement will be present in the hot rolling range, steels are designed with a knowledge of the solution and precipitation behaviour of the alloy carbides and nitrides. Solubility data indicate that alloy precipitates can be thermodynamically stable over most of the rolling range, but do not consider the kinetics of precipitation or the stability of the precipitates against coarsening.

The Lifshitz-Wagner[106,107] theory of diffusion-controlled particle coarsening leads to a relationship:

$$\left(r_t^{\,3} - r_0^{\,3}\right) = \left(\frac{K_c}{RT}\right) V_m^2 C_S . D_0 . t . \gamma \qquad (1.7)$$

where r_o and r_t are mean particle radii at zero time and time t respectively, C_s is the concentration of solute in equilibrium with a particle of infinite radius, γ is the particle/matrix interfacial energy, V_m is the molar volume of precipitate, D_o is the solute diffusion coefficient and K_c is a constant. It follows that, other things being equal, a less soluble precipitate will coarsen more slowly than a more soluble one. Substitutional alloying elements diffuse more slowly than interstitial ones, and it is the diffusivity of Nb, V or Ti that controls the coarsening rate of microalloy carbides or nitrides. The diffusion coefficient of Ti is considerably smaller than those of V or Nb. The combination of low solubility and low diffusivity make T:N the most effective austenite grain refiner.

2.2.3 Precipitation and Matrix Austenite Compositions

Microalloyed steels often contain single or multiple additions of Nb, Ti and V. Their various roles can be best described by comparing their solubilities in austenite. A good comparison can be made of the various precipitation systems through the use of the appropriate solubility relations. For instance, the driving force for precipitation at a given temperature is the solute supersaturation at that temperature. A comparison of the variation of supersaturation with temperature is shown in Fig. 2.3 for several important systems[32]. This figure reveals that the Ti system shows a comparatively large supersaturation at temperatures well above those associated with hot rolling. The VC and VN system, on the other hand, show large supersaturation at temperatures at the very lowest range of hot rolling. The Nb system on the other hand, shows a large supersaturation at temperatures which are well situated within the hot rolling range. Hence, Ti precipitates are very effective for high temperature control (e.g. during reheating), Nb precipitates are effective for intermediate temperature exploitation (e.g. recrystallisation temperature control) and the V can easily be kept in solution in the austenite for the eventual precipitation hardening of the ferrite.

A detailed study of carbonitride precipitation in Nb-V microalloyed steels was presented by Speer *et al* [33]. The thermodynamic model can be used to estimate equilibrium austenite and carbonitride compositions, and the amounts of each phase, as a function of steel composition and temperature. The agreement between the measured and predicted precipitate compositions was found to be quite good for two experimental (0.03%Nb plus 0.05 and 0.20%V) steels. The main conclusion was that the precipitate composition was a function of

the steel composition and the temperature. In addition, the carbonitride solution temperature increased with increasing levels of either Nb, V, C, or N in the steel.

For vanadium steels, the two compounds, vanadium carbide and vanadium nitride, are mutually soluble, and thus a continuous series of vanadium carbonitride is possible[34]. Most authors have argued carbonitrides that precipitate in austenite are nitrogen rich[35,36]. Roberts *et al* [37,38] applied a regular solution model using a finite-difference technique to model changes in particle composition during precipitate growth. Their results suggest that vanadium carbonitride particles which precipitate in the austenite consist of a nitrogen-rich core with increasing carbon levels toward the periphery of the particles. The compositional gradients within the particle persists during the precipitation reaction.

Another model proposed by Speer *et al* [39] , assumes that the free energy of mixing of VC and VN can be described using the regular solution model developed by Roberts *et al.* At a given temperature, T , the steel, matrix, and the precipitate compositions must lie on a common tie line which satisfies the mass balance relationships. Assuming that the carbonitrides are perfectly stoichiometric, that is VC_xN_{1-x} , five non-linear simultaneous equations need to be solved to predict equilibrium conditions. The observations from their model were:

(i) The carbonitride need not be expected to be virtually VN, as commonly assumed. For instance the results in Table 1.1 show that in a steel containing 0.1%C, 0.005%N, and 0.1%V, the equilibrium precipitate at 800^oC would have the composition $VC_{0.66}\ N_{0.34}$. The nitrogen content of the precipitate increases with increasing nitrogen or decreasing carbon.

(ii) The equilibrium precipitate composition also depends on the vanadium concentration in the steel.

(iii) The temperature influences the precipitate chemistry, the nitrogen content of the precipitate increasing with increasing temperature.

Rios[40] also proposed a computer model for evaluating the composition and mole fraction of carbonitrides of the form (Nb,V,Ti....)(C,N) and the matrix composition from the solubility products of the individual carbides and nitrides. When applied to (Nb,V)(C,N), his model was in good agreement with that of Speer *et al*[39]. The model was similar to a thermodynamic model presented by Adrian[41], for HSLA steel austenite containing up to four microalloying elements. For three microalloying elements, the carbonitride is described by the chemical formula, $M'_xM''_vM'''_{1-x-v}C_vN_{1-v}$, neglecting vacancy formation, where $0 \leq x \leq 1$, $0 \leq v \leq 1$, $x+v \leq 1$, and $0 \leq v \leq 1$.

These models assume equilibrium conditions and might be considered to be relevant to the constitution of austenite after soaking and prior to TMP. However, it has been shown that deformation significantly enhances precipitation kinetics.

The 'conditioning' of the austenite by soaking and the amount of microalloying elements dissolved, will influence its response to deformation and, ultimately, the final properties of the steel.

2.3 Hot Deformation of austenite

During deformation at the strain rates and temperatures of interest in hot-working operations, all metals undergo work-hardening and dynamic recovery and some may also undergo dynamic recrystallisation. The microstructures produced by these processes are unstable and, on holding at temperature after the end of deformation, further structural changes occur by static recovery, recrystallisation and grain growth. In hot-rolling operations, the dynamic and static structural changes that occur during and between passes interact to determine the overall evolution of the final microstructure. During hot-working, the original coarse austenite grains are replaced by a new refined microstructure due to the recrystallisation processes. Depending on the hot deformation conditions, static, dynamic or metadynamic recrystallisation can occur. Static recrystallisation takes place when both the nucleation and growth of new grains occur after deformation. When these two processes occur simultaneously during deformation, dynamic recrystallisation results. Metadynamic recrystallisation is related to the formation of new grains during deformation but with growth occurring after deformation [42].

During this deformation, the flow stress initially rises with strain as a result of work hardening and recovery; dislocation density rises and a subgrain structure tends to develop. Because dynamic recovery is relatively slow, in steel austenite the subgrain boundaries are ill formed, and sufficient strain energy is stored to nucleate dynamic recrystallisation when a critical strain ε_c is reached. This provides an additional softening mechanism and results in a fall in flow stress from a maximum value at $\varepsilon_p > \varepsilon_c$ until a steady-state level is reached after a strain interval ε_x, when a large fraction of recrystallisation has taken place [43], Fig. 2.4 (a).

On holding these deformed structures isothermally, softening takes place as a function of time, as illustrated in Fig. 2.4 (a). Fig 2.4 (b) shows schematically as a function of prestrain how this softening is related to the occurrence of static recovery and recrystallisation[44]. In industrial thermomechanical processing operations, the temperature and strain rate may change continually, and in rolling and forging the deformation takes place in a series of passes separated by intervals of time. The dynamic structural changes are sensitive to strain rate and temperature. These determine the flow stress and hence the working forces, but also control the stored energy present at the end of deformation. This drives the static structural changes of recovery and recrystallisation, thereby influencing the kinetics of these thermally activated processes. Grain growth may follow recrystallisation and is again temperature sensitive. The static structural changes between passes determine the initial microstructure for the next pass. Modelling must consider these dynamic and static structural changes in sequence, as illustrated[45] in Fig. 2.5.

The main emphasis of the work in this thesis is concerned with single pass rolling and static recrystallisation. However, the introduction to this section has highlighted the complexities of mathematical modelling and the need to encompass each of the interacting aspects if realistic predictions are to be obtained.

2.4 The need for Mathematical Models in Hot Rolling

The past decade has seen a number of workers in many countries developing mathematical models to predict the final mechanical properties of controlled rolled steels. Many of these models are based on the work of Sellars and co-workers[46,47]. Mathematical

models for the individual metallurgical events that occur during rolling and transformation, combined in the correct metallurgical sequence with process models for a given rolling mill, allow the evolving microstructure to be followed as a function of macroscopic process changes. This permits alterations to composition, processing route or mill hardware to be quickly evaluated for their effects on final mechanical properties and, if incorporated with a microstructure-based, hot strength model, on rolling loads.

There are basically four types of model. The phenomenological models attempt to predict the progress of the actual physical processes that occur, for example, by solving the appropriate equations for heat flow and mechanical behaviour. The Empirical models are characterised by statistical analysis of data to provide relationships between the process variables and the parameters of interest, that is inputs and outputs. Here, simple regression has been the most commonly applied modelling tool.

The semi-empirical models combine a mixture of the two, and contain a representation of the physical processes occurring based upon the likely physical dependencies which could necessitate regression of certain model constants. A typical example is the high temperature recrystallisation behaviour of steel. The mathematical model for the time to a certain degree of recrystallisation uses an Arrhenius temperature term, combined with expressions relating the Avrami-Mehl kinetics to changes in the driving force for recrystallisation with deformation (strain or dislocation density) and austenite grain boundary surface area per unit volume (grain size). Such semi-empirical models have the potential for extrapolation beyond the current processing conditions.

The fourth type are the rule-based models which are now gaining widespread application within the steel industry such as the Expert-systems and Diagnostic models. These do not contain mathematical representation of a physical process, but can still predict an outcome of a series of events based on previous experience.

Models have been developed to handle plate, bar, rod, structural and strip rolling. The data required for these models have been primarily obtained through hot torsion testing which allows large strains and close control of the heating and deformation parameters.

Controlled thermomechanical processing of quality grades of C-Mn and microalloyed HSLA steels is itself sophisticated. The ability to achieve the final desired mechanical properties without subsequent heat treatment depends on accurate, quantitative knowledge of microstructural and constitutional changes that occur in austenite during processing. These include:

austenite grain growth during reheating;
precipitate coarsening and dissolution during reheating;
amount of microalloying element in solid solution;
dynamic recrystallisation during deformation;
metadynamic and static recrystallisation during interpass time intervals;
growth of austenite grains;
equilibrium and strain induced precipitation of microalloy carbonitrides;
the inhibition of recrystallisation due to strain induced precipitation below the RST;
retained strain during rolling below the RST with consequent pancaking of austenite grains and the creation of deformation bands;
transformation to ferrite, and control of the final ferrite grain size.

Generally, expressions for the progress of static recrystallisation, the time to 5% recrystallisation and the onset of strain induced precipitation in deformed austenite, have been found to be necessary parts of models intended to predict the final microstructure of microalloyed steels. The differences in models are the absolute values of various constants, which have essentially been established by fitting the expressions to data in the various authors' data bases.

The following sections describe the various metallurgical phenomena which occur both during and after hot rolling. Mathematical expressions are introduced where appropriate.

2.5 Static recrystallisation

The kinetics of static recrystallisation are a central part of models of controlled rolling[48]. The progress of recrystallisation can be represented according to the JMAK

(Johnson-Mehl-Avrami-Kolmogrov) equation[49], referred to in the following as the Avrami equation.

$$X = 1 - \exp\left[(-\ln 2)\left(\frac{t}{t_{0.5RX}}\right)^{k}\right] \qquad \textbf{(1.8)}$$

where X is the fraction recrystallised after time, t, $t_{0.5RX}$ is the time to X = 0.5, and k is the Avrami exponent which adopts typical values of 1 to 2. The value of k is of importance because it determines the time interval between the start ($t_{0.05RX}$) and end ($t_{0.95RX}$) of recrystallisation. When k = 2, $t_{0.95RX}/t_{0.05RX}$ is 7.7, whereas when k = 1, the ratio is 58.4. The Avrami exponent is obtained from plots of log(1/1-X) versus log t for a given set of deformation conditions and isothermal recrystallisation temperature. The effect of working variables on the recrystallisation rate is determined by their effect on the time to 50% recrystallisation, $t_{0.5RX}$. It is generally agreed that

$t_{0.5RX}$ = a function of (d_o, ε, Z) exp Q_{RX}/RT

where d_o is the initial austenite grain size, ε is the prior strain, Q_{RX} is the activation energy for recrystallisation and Z is the Zener-Holloman parameter of the prior deformation. Z is defined as

$$Z = \dot{\varepsilon} \exp\frac{Q_{def}}{RT_{def}} \qquad \textbf{(1.9)}$$

where T_{def} is the deformation temperature, R is the gas constant, $\dot{\varepsilon}$ the strain rate and Q_{def} is the apparent activation energy for deformation.

Various empirical relationships have been proposed to relate $t_{0.5RX}$ to the strain (ε), initial grain size d_o, absolute temperature (T) and the Zener-Hollomon parameter (Z). These are mostly of the form:

$$t_{0.5RX} = B \cdot \varepsilon^{p} \cdot d_o^{q} \cdot Z^{r} \cdot \exp\left(\frac{Q_{RX}}{RT}\right) \qquad (2.0)$$

where Q_{RX} is the apparent activation energy for recrystallisation (J/Mol), and B,p,q and r are material constants.

A critical assessment of recrystallisation kinetics led Dutta and Sellars[7] to propose the following equation for Nb microalloyed steel taking into account the influence of solute drag due to Nb in solid solution (the last exponential term):

$$t_{0.05RX} = A_{RX} \cdot d_o^{2} \cdot \varepsilon^{-4} \cdot \exp\frac{Q_{RX}}{RT} \cdot \exp\left\{\left(\frac{B_{RX}}{T} - 185\right) \cdot [Nb]\right\} \qquad (2.1)$$

where $t_{0.05RX}$ is the time (s) for 5% recrystallisation, [Nb] is the concentration in solid solution and A_{RX} and B_{RX} are constants whose values are 6.75×10^{-20} and 2.75×10^{5} respectively.
The effect of the individual variables on $t_{0.5RX}$ will now be considered.

2.5.1 Effect of strain and temperature

Medinas and Mancillas'[50] data for a 0.095 wt% V steel tested at different temperature and after different strains are shown in Fig. 2.6. Increasing strain and temperature decreases the time to 50% recrystallisation, $t_{0.5RX}$, as both the driving force and number of nucleation sites for recrystallisation are also increased. The dependence on strain of the characteristic time $t_{0.5RX}$, measured by either metallographic or restoration methods, is shown in Fig. 2.7 from Sellars[51] data. The plotted data all show a steep dependence on strains for strains less than ~0.8 ε_p and fit the relationship

$$t_{0.5RX} \propto \varepsilon^{m} \qquad (2.2)$$

where the mean value of m = -4.

The observations of Djaic and Jonas[44] in Fig. 2.7 indicates that an abrupt change takes place from strain dependence to independence at a strain of approximately ~0.8 ε_p. This

corresponds reasonably with the strain expected for ε_c and arises because pre-existing recrystallisation nuclei are always present in deformed austenite at strains greater than ε_c. Static recrystallisation under these conditions has been referred to as 'metadynamic' to distinguish it from classical recrystallisation after lower strains. Restoration measurements[52] indicate that the recrystallisation kinetics may have a complex form after strains between ε_c and the start of steady state, and direct metallographic observations of static recrystallisation after strains well into the steady state show that the Avrami exponent k drops to a value ~1. This means that $t_{0.05} = 0.074 \cdot t_{0.5}$ and $t_{0.95} = 4.33 \cdot t_{0.5}$, that is, static recrystallisation proceeds over about two orders of magnitude in time after strains which give partially dynamically recrystallised microstructures during deformation.

Increasing strain increases the number of grain boundary sites, as well as leading to intragranular sites, such as deformation bands at large strains, and subgrains at large initial grain sizes. The increase in driving force with increasing strain arises in spite of the increasing level of dynamic recovery, because the dislocation density in the subgrain boundaries increases and the size of the subgrains decreases, leading to an increase in the stored energy. The subgrain boundaries provide the largest contribution to the stored energy[53] and as their misorientation increases with strain, the driving force for recrystallisation also increases.

The times to $t_{0.5RX}$ for a C-Mn, V and Nb steels are plotted against the reciprocal of absolute temperature in Fig. 2.8 taken from the data of Medina and Fabregue[54]. The C-Mn plot in this figure and the plots of the data of Sellars for C-Mn and low alloy steels (Fig 2.7), all fall on reasonably straight lines where the time to $t_{0.5RX}$ increases with decreasing temperature. It is interesting to note that the plots for the V and Nb steels (Fig. 2.8) deviate from linearity at lower temperatures. Hodgson[55] for Nb steel and Medina et al[56] for V steel showed that the temperature at which this change occurs decreases with increasing strain and decreasing solute content. In the high temperature regime the recrystallisation kinetics are affected by a solute drag effect, while the deviation to much longer recrystallisation times below the critical temperature is considered to be due to strain-induced precipitation. Both these effects are discussed in a later section.

2.5.2 Effect of initial grain size

The effect of initial grain size on $t_{0.5RX}$ does not appear to have been studied systematically, especially for V microalloyed steels. Equation 2.0 shows that $t_{0.5RX} \propto d_o^q$. A value of q = 2 has been observed for stainless steels[57]. The data of Kozasu *et al* [58] on a 0.04 wt% Nb steel is also consistent with this value.

Nucleation sites for new grains are predominantly triple junctions and grain boundaries[59] in non-pancaked austenite. On the basis that the total grain boundary area in fine grained austenite will be larger than in coarse grained austenite, then $t_{0.5RX}$ will be expected to be smaller in the fine grained austenite for identical conditions. An example is the data of Medina *et al* [60]. For a 0.09 wt% V steel at $\varepsilon = 0.2$, $t_{0.5RX}$ was 6.2 seconds for a grain size of 125μm and 7seconds for 165μm. His data for the three V steels (0.043, 0.06 and 0.093 wt%) found that the quantitative influence of d_o on $t_{0.5RX}$ was linear. The resulting equation for $t_{O.5RX}$ is:

$$t_{0.5RX}\,(s) = A_M \cdot \varepsilon^{-2} \cdot \dot{\varepsilon}^{\,-0.44} \cdot d_0 \cdot \exp\left(\frac{Q_{RX}}{RT}\right) \qquad \textbf{(2.3)}$$

The constant A_M varied with the concentration of V solute having values of 6.767×10^{-10}, 5.355×10^{-10} and 5.081×10^{-10} for V contents of 0.043, 0.060, and 0.093 wt% respectively. The three individual equations for each composition studied, only differed in the constant A_M, which infers that the static recrystallisation kinetics was very similar in the three steels with a minimal influence of the solute content.

The effect of initial austenite grain size, strain and deformation temperature for the same time interval of (isothermal hold for 3 seconds) on the kinetics of recrystallisation is illustrated in Fig 2.9 from the data of Tanaka *et al* [61] for a Nb steel. At any deformation temperature, the critical amount of deformation decreased as the initial austenite grain size decreased. The critical strain increased with decreasing deformation temperature.

2.5.3 Effect of solute drag

Part of the results of an extensive study on a series of V and Nb microalloyed steels by Amin and Pickering[62] are shown in Fig. 2.10 For the 0.14%V steel, the grain coarsening temperature was 1000 °C, and the calculated VN solvus, 1050 °C.

Reheating at 1300 °C, followed by 50% reduction at 1100 °C, isothermal holding at the rolling temperature for 1 second and then quenching, results in 97.5% recrystallisation of the C steel but only 42.5% for the 0.14 wt% V steel. At these temperatures, the V would be expected to be in solution as solute. The slower recrystallisation kinetics in the V steel are probably, it has been argued, seem most likely to be attributable to solute drag effect, being slightly less at higher rolling temperatures.

There are few observations on V microalloyed steels compared with Nb steels. Irvine *et al* [63] found very little effect of 0.15 wt% V additions on recrystallisation kinetics. Cordea and Hook[64] observed some retardation of recrystallisation in a 0.059 wt% V steel below 925°C, but the effect was less than with 0.011 wt% Nb. Korchynsky[65] reported that the retardation of recrystallisation was less in a V steel than in a Nb steel. It is thus clear, that V is less effective than Nb in retarding recrystallisation.

The effect of single additions of Mo (0.30 wt%), Nb (0.035 wt%) and V (0.115 wt%) to a base steel of 0.05 wt% C and 1.40 wt% Mn on the occurrence of static recrystallisation and recovery after high temperature deformation (interrupted hot compression tests) was reported by Andrade *et al* [66]. The solute effects of Mo, Nb and V were distinguished from their effects as precipitates by the determination of the influence of these elements on the static softening rates after intervals of deformation as short as 0.05 seconds and, therefore, prior to strain induced precipitation. Even though the Nb content was almost a third of V, the greatest solute retardation of static recrystallisation and recovery was produced by Nb addition, followed by Mo and lastly by V.

They further attempted to quantify the retardation effect by calculating the 'Solute Retardation Parameter' (SRP) proposed by Akben *et al* [67] :

$$SRP = \log\left(\frac{t_x}{t_{ref}}\right) \cdot \left(\frac{0.1}{\text{atomic\% x}}\right) \cdot 100\% \qquad (2.4)$$

where t_x is the time required for the start of static recrystallisation in the steel containing the element x, and t_{ref} is the equivalent time for the reference plain C steel. Since solute effects are frequently non-linear with concentration and saturate at different levels, the SRP calculated provide an approximate value, but allow solutes to be ranked in order of effectiveness. Typical calculated values[68] are given in Table 1.2.

Experiments by Luton *et al* [69] on a decarburised and denitrided Nb steel also showed that Nb retarded recrystallisation by about one order of magnitude in time compared to an equivalent plain C steel. In a similar way, the work of White and Owen[70] on a V steel conducted above the solubility temperatures of VN and VC demonstrated the retarding effect of V in solution with respect to a plain C steel.

The exact mechanism which leads to inhibition of static recrystallisation by a solute has been the subject of considerable debate over the last decade. Jonas and Akben[71] noted that between 900-1000°C, the start of recrystallisation in microalloyed austenite will occur in between 0.1-0.5 seconds whereas the precipitation start times may vary between 10-100 seconds in the same temperature interval. Although they concluded that precipitation could not act rapidly enough to prevent recrystallisation and that solute-drag was the predominant mechanism, they however acknowledged that perhaps no experimental technique was sensitive enough to detect the real start of precipitation. Explanation of the inhibition phenomenon are of three types:

(i) Modification of the driving force for recrystallisation through effects which modify the extent of static recovery preceding recrystallisation. These recovery effects may be influenced by precipitation, solute segregation or changes in stacking fault energy[72].

(ii) Retardation of the migrating interfaces by solute atoms segregated to the interfaces, the so called solute drag models[73].

(ii) Retardation of the migrating interfaces by fine precipitates of a size and/or in a concentration sufficient to pin the boundaries[74].

2.5.4 Strain induced precipitation

The kinetics of precipitation have been studied in both undeformed and deformed austenite by a number of workers. These studies have all shown that deformation greatly accelerates precipitation. A wide range of techniques has been used to follow the progress of precipitation. These include chemical and electro-chemical extraction[75,76], extraction replication[77], transmission electron microscopy[78], microhardness[79] and electrical resistivity measurements[80].

A critical assessment of strain induced precipitation kinetics led Dutta and Sellars to propose the following equation for 5% precipitation in Nb steel:

$$t_{0.05P} = A_{PPT} \cdot [Nb]^{-1} \cdot \varepsilon^{-1} \cdot Z^{-0.5} \cdot \exp\frac{Q_{diff}}{RT} \cdot \exp\frac{B_P}{T^3 (\ln k_S)^2} \qquad (2.5)$$

where $t_{0.05P}$ is the time (s) for 5% strain induced precipitation, ε is the strain, Q_{diff} is the apparent activation energy for diffusion , [Nb] is the concentration in wt% taken into solution during reheating, R is the gas constant, Z is the Zener-Holloman parameter and T is the absolute temperature of holding after deformation. ε is defined as:

$$\varepsilon = -\ln(1 - r) \qquad (2.6)$$

where r is the rolling reduction.

Dutta and Sellars arrived at best values of the constants, $A_{PPT} = 3 \times 10^{-6}$, and $B_{PPT} = 2.5 \times 10^{10}$ after reviewing a considerable amount of data.

The supersaturation ratio, k_S, is the ratio of the product of concentrations of the precipitant species that were in solution due to solution treatment at a higher temperature, over the

equilibrium solubility product at the temperature of holding after the deformation. For Nb steels, this ratio is defined as :

$$k_S = \frac{[Nb][C+{}^{12}N/_{14}]_{soln}}{10^{2.26-6770/T}} \qquad (2.7)$$

This supersaturation ratio determines the 'driving force', that is, the free enthalpy change for precipitation to occur. The critical supersaturation level for nucleation in the case of undeformed austenite is expected to be high. However, the introduction of strain provides sites for nucleation and then precipitation is observed at lower supersaturations. Cohen and Hansen[81] observed precipitation in a single pass rolling experiment with the ratio between 5 and 7.5 and Chilton and Roberts[82] observed precipitation when k_s = 7.7 in their six pass rolling schedule.

The flux of solute to the nucleation sites is controlled by diffusion of Nb, which leads to the term $[Nb]^{-1} \cdot \exp Q_{diff}/RT$. In deformed austenite, the density of preferential nucleation sites is expected to be sensitive to the dislocation density and dislocation arrangement, and therefore to the conditions of prior deformation. In practice, nucleation of carbonitrides in austenite takes place heterogeneously on preferential sites such as grain boundaries and dislocations, or more probably dislocation nodes formed by interaction of individual dislocations inside grains or in subgrain boundaries in the case of deformed austenite.

Dutta and Sellars compared the results of Le Bon *et al*[75] and Watanabe *et al*[76] for 5% precipitation of Nb(C,N) in undeformed austenite with curves calculated from equation (2.3) using the mean value of $B_p = 2.5 \times 10^{10}$ K^3 found for strain induced precipitation. The shape of the curves were in reasonable agreement with both sets of observed results, suggesting that the nature of the precipitation sites is the same as in deformed austenite. However, the longer times for precipitation in undeformed austenite indicate that the density of such sites is much lower than in deformed austenite.

In equation (2.3) therefore, the dependence of nucleation kinetics on strain and on Zener-Hollomon parameter were considered to arise solely from their effects on the density of

nucleation sites, and the specific dependencies were derived empirically from limited experimental observations.

2.6 Recrystallisation-stop temperature (RST)

The principle by which the precipitation of microalloying elements causes recrystallisation to be inhibited[83] is illustrated in Fig. 2.11. The start of recrystallisation in the absence of precipitation is represented by the line ABC, recrystallisation taking longer as the temperature decreases. The start of precipitation of microalloy carbonitrides in undeformed matrix is represented by the C-curve DEF. It is well known that most precipitation processes are nucleated heterogeneously, and are accelerated by deformation. This effect of deformation is represented by the C-curve GHJ. If the start of recrystallisation intersects the start of strain induced precipitation at the temperature Tc, the possibility exists that the recrystallisation maybe inhibited, the horizontal line, BC'. Thus above the point of intersection, B, precipitation occurs in recrystallised austenite, curve DE, and below B precipitation occurs in strained austenite, curve BHJ. Tc is the recrystallisation stop-temperature (RST).

Dutta and Sellars' model proposed that if strain induced precipitation went to 5% completion before recrystallisation went to 5% completion, then recrystallisation would be inhibited, that is, the RST occurs when $t_{0.05RX}$ and $t_{0.05P}$ become equal. The appropriateness of this criterion has been considered in some detail by Dutta, Valdes and Sellars[84]. Comparison of their equations for $t_{0.05RX}$ and $t_{0.05P}$ (equations 2.1 and 2.5) shows that solute content retards recrystallisation, but accelerates strain induced precipitation so that retardation of recrystallisation by strain induced precipitation occurs at higher temperatures with increase in microalloy content, Fig 2.12.

In deformed austenite an effect of the initial austenite grain size is expected on the recrystallisation time as indicated in equation (2.1) but not on strain induced precipitation (equation (2.5)). This is shown schematically in Fig 2.13. The equations also indicate that the RST decreases with increasing strain, as illustrated schematically in Fig 2.14.

The RST is controlled by the amount and type of microalloying elements dissolved during reheating. Cuddy's[85] work on microalloyed steels containing ranges of Nb, V, Ti or Al were reheated to different temperatures to vary the initial solute content, and then deformed in

multipass simulation of plate rolling to investigate the RST. He defined the RST as the temperature at which, after a particular rolling sequence, recrystallisation was incomplete in ~15 s. His results confirmed that the RST increases with increase in initial solute levels, but at markedly different rates. The increase in the RST per gram atom of solute increased in the order V,Al,Ti and Nb, Table 1.3. The measure of the strength, α, of the solute's effect on the RST based on the experimental results shown in Fig 2.15 was quantified. Niobium as solute was 6.75 times more effective than V. Clearly the effectiveness of Nb, Ti, and V differ widely, partly due to differences in precipitation kinetics of Nb(C,N), TiC and VN and partly due to differences in the effects of the microalloy elements in solution on the recrystallisation kinetics.

2.7 Hot Direct Rolling

In conventional steel processing, continuously cast slabs are allowed to cool to room temperature before being reheated for soaking and hot rolling. The reheating has been estimated at an energy cost of 1.2 MJ/tonne, to soak at 1200 - 1250 °C for several hours. Potentially, the economics of the processing could be enhanced by avoiding this loss of heat energy. Several studies [86-90] have been made of the possibilities of rolling the concast slab without allowing the temperature to fall below that required at the mill. This has been achieved by rolling the casting directly as its temperature falls to an appropriate rolling temperature, or by charging it into a high temperature soaking furnace when its temperature has dropped to some lower level. These variants are depicted schematically in Fig 2.16, and have been termed Hot Direct Rolling (HDR) and Hot Charge Rolling (HCR). One variant of HCR is gamma-HCR, in which the minimum temperature reached before recharging is in the austenite phase field. A second variant is α-HCR, in which the minimum temperature is low enough to allow transformation to ferrite before recharging. Both these variants are schematically illustrated in Fig 2.17.

The term CCR, 'conventional' controlled rolling was used by Priestner *et al* [91] ,which referred specifically to controlled rolling of continuously cast slab that had been conventionally cooled to ambient temperature after casting, and then reheated to a soaking temperature before rolling. This is different from that of Jonas and Sellars, who use the term CCR to describe the controlled rolling processes in which microalloying is used to inhibit recrystallisation of austenite at temperatures below the RST in Nb-microalloyed steel. Unlike

reheated austenite in controlled rolling, the as-cast austenite at the start of HDR differs in several ways. As-cast austenite has a very coarse grain size, is dendritic. and its alloy content is segregated interdendritically both on a micro and macro scale. Reheated austenite on the other hand, will be strongly conditioned by the gamma-alpha and alpha-gamma transformations during cooling and reheating. The austenite grain size is therefore refined and results in a degree of chemical homogenisation. This also leads to microalloy carbonitrides to precipitate in both austenite and ferrite during cooling, and to redissolve according to their respective equilibrium solubilities at the reheating temperature. In as-cast austenite, the concentration of the microalloy elements in solution may well depend on the kinetics of precipitation rather than on equilibrium solubilities. Given these factors, it is expected that both the precipitation and recrystallisation kinetics would be dissimilar to that of reheated austenite, and therefore it would be of interest to investigate the applicability of a conventional RST model to HDR.

TABLE 1.0

Value of constant A and B in equation (1.6) used by different authors.

COMPOUND	Constant A in equation (1.1)	Constant B in equation (1.1)	REFERENCE
VC	9500	6.72	K.Narita [29]
VN	8700	3.63	K.Narita [29]
VN	8330	3.46	Irvine *et al* [30]
VN	7070	2.27	R.W.Fountain [31]

TABLE 1.1

Results of calculations based on thermodynamic model for VCN in austenite, after Speer *et al* [39].

ANNEALING TEMP °C (STEEL)	EQUILIBRIUM PRECIPITATE COMPOSITION	EQUILIBRIUM PRECIPITATE MOLE FRACTION	EQUILIBRIUM MATRIX COMPOSITION (wt%)		
			V	C	N
800 (A)	$VC_{0.66}N_{0.34}$	0.0011	0.092	0.0003	0.050
900 (A)	$VC_{0.26}N_{0.74}$	0.00034	0.099	0.002	0.085
900 (B)	$VC_{0.21}N_{0.79}$	0.00075	0.098	0.003	0.066
900 (C)	$VC_{0.39}N_{0.61}$	0.0012	0.095	0.001	0.146
900 (D)	$VC_{0.01}N_{0.99}$	0.0021	0.100	0.074	0.003
900 (E)	$VC_{0.06}N_{0.94}$	0.00023	0.020	0.002	0.089

STEEL	wt%C	wt%N	wt%V
(A)	0.10	0.005	0.10
(B)	0.10	0.01	0.10
(C)	0.10	0.01	0.20
(D)	0.10	0.10	0.10
(E)	0.02	0.005	0.10

TABLE 1.2

Solute retardation parameter (SRP) at a strain rate of $2s^{-1}$ after Ackben and Jonas[68].

ELEMENT	SRP - atomic %		SRP - wt %	
	Static	Dynamic	Static	Dynamic
Mo				
Mo steel	33	25	20	42
Mo-Nb steel	-	15	-	10
Mo-V steel	-	-	-	-
Mo-Nb-V steel	26	20	16	13
Nb				
Nb steel	-	135	-	92
Mn-Nb steel	401	-	272	-
Mo-Nb steel	390	79	265	54
Mo-Nb-V steel	-	107	-	73
V				
V steel	12	8.4	13	9.2
Mo-V steel	-	3.3	-	3.6
Nb-V steel	11	-	12	-
Mo-Nb-V steel	-	5.1	-	5.6
Ti				
Ti-1.6Mn steel	-	35	-	42

TABLE 1.3

Measure of the strength of solute's effect, α, on the RST, after Cuddy[85].

SOLUTE	Nb	Ti	Al	V
α $^{o}C/(atom\ \%)^{1/2}$	1350	410	200	200

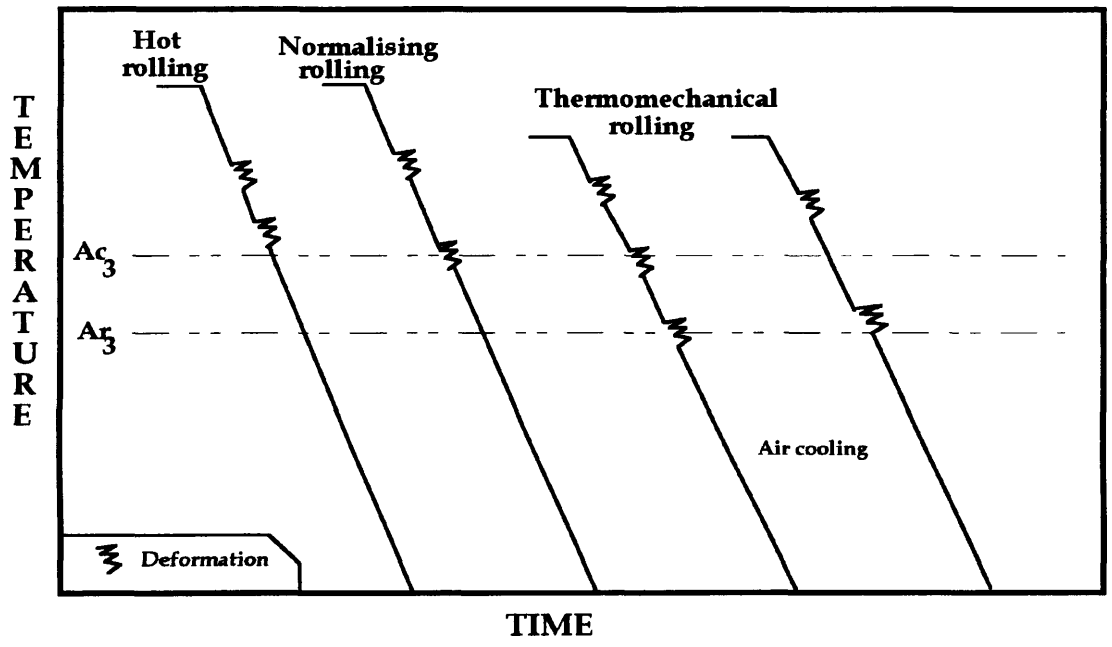

Fig. 2.0 **Relative difference between TMP and other deformation processes, after Kern *et al* [15].**

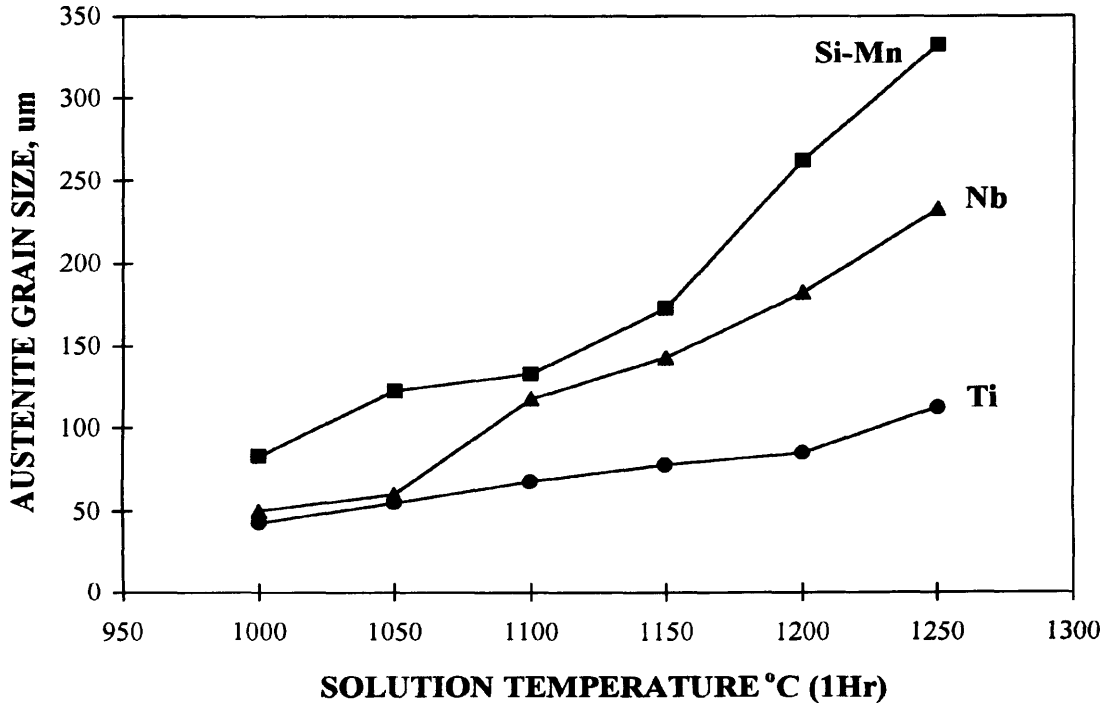

Fig. 2.1 Grain growth of various microalloyed steels, after Kozasu[20].

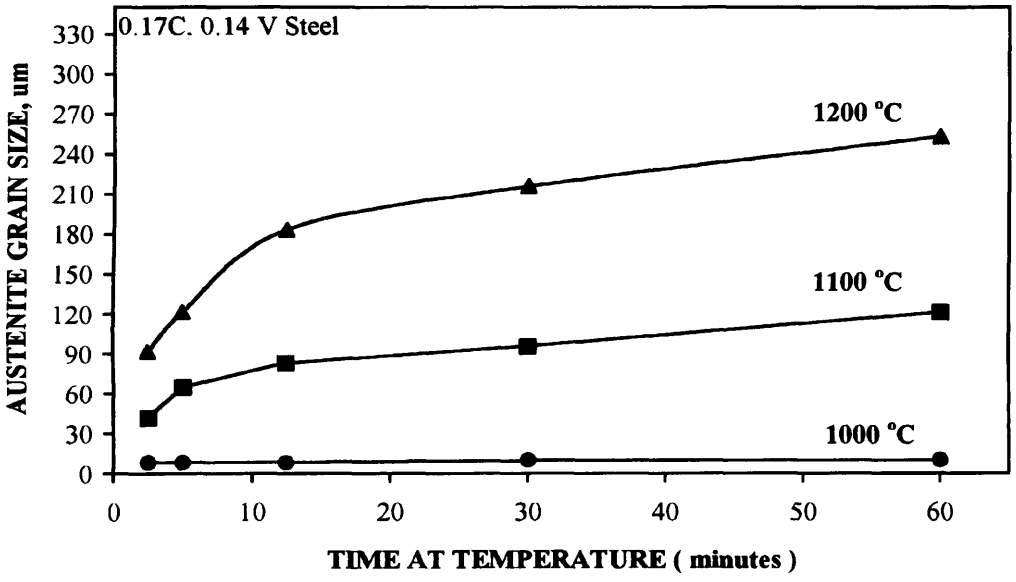

Fig. 2.2 Variation of austenite grain size with time, after Mazzare *et al* [24].

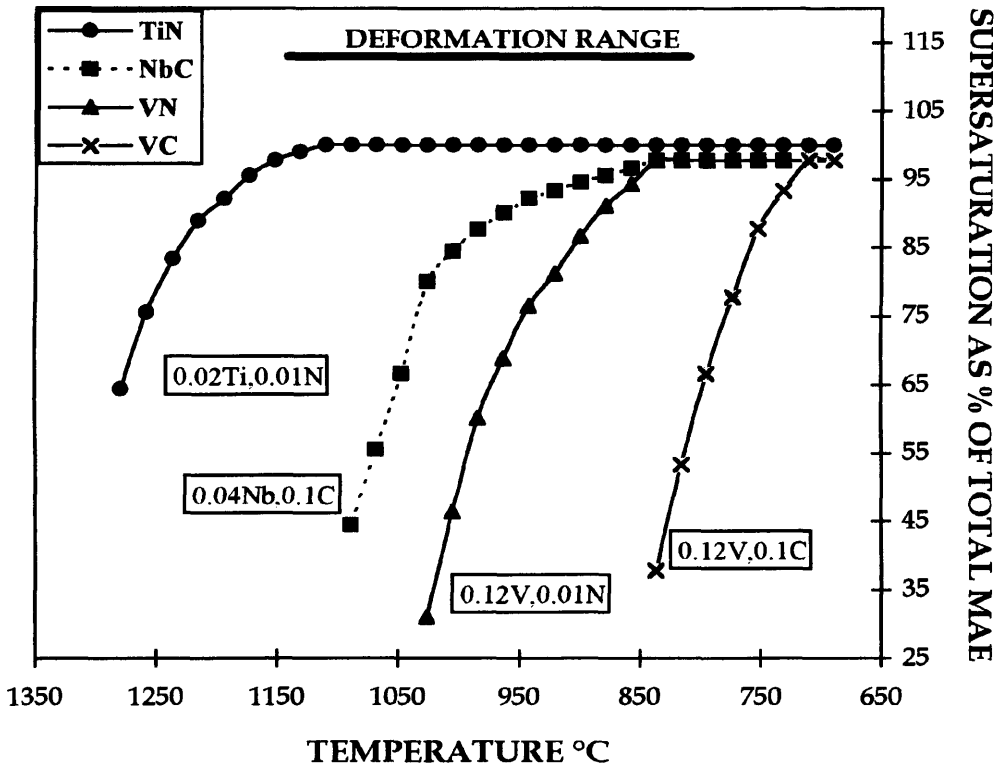

Fig. 2.3 **Precipitation potential of various microalloying element (MAE) systems[32] .**

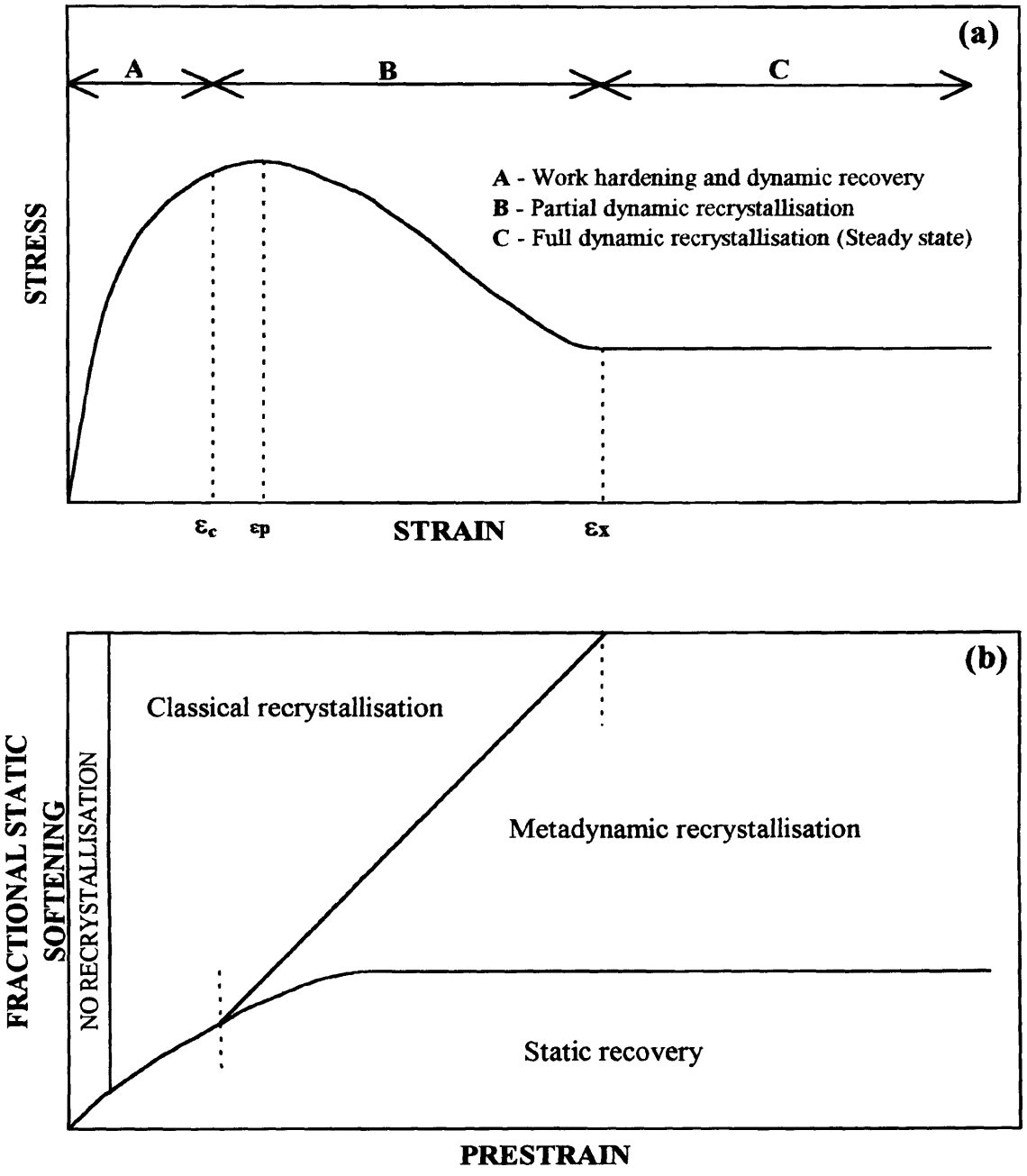

Fig. 2.4 **Schematic representation of:**

(a) **relationship between stress/strain behaviour during deformation;**

(b) **mechanisms of static softening that takes place after deformation.**

After Djaic and Jonas [44].

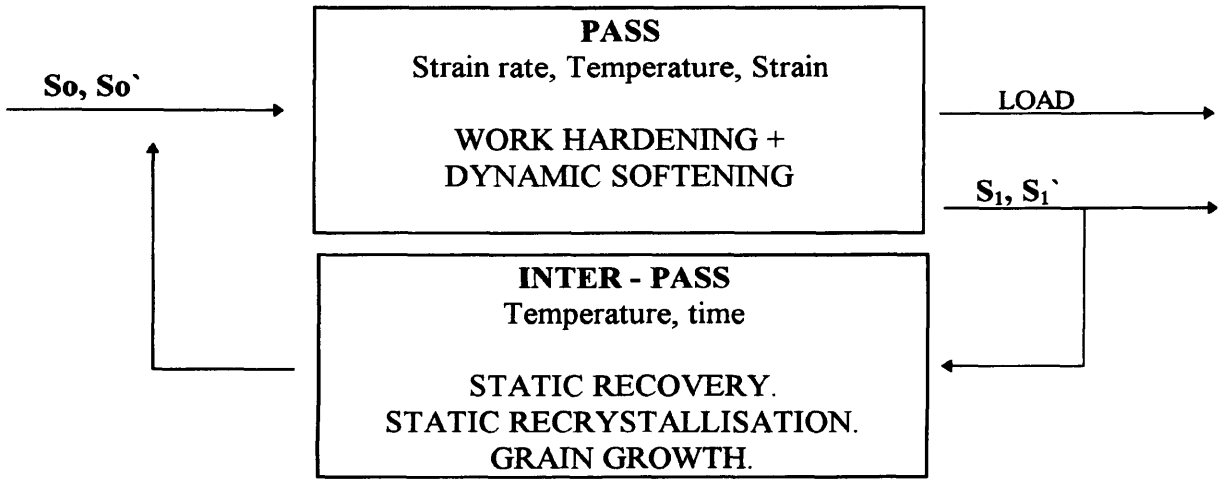

S - grain structure
S` - second phase structure

Fig. 2.5 Schematic diagram of principles of modelling microstructural development in multipass rolling [45].

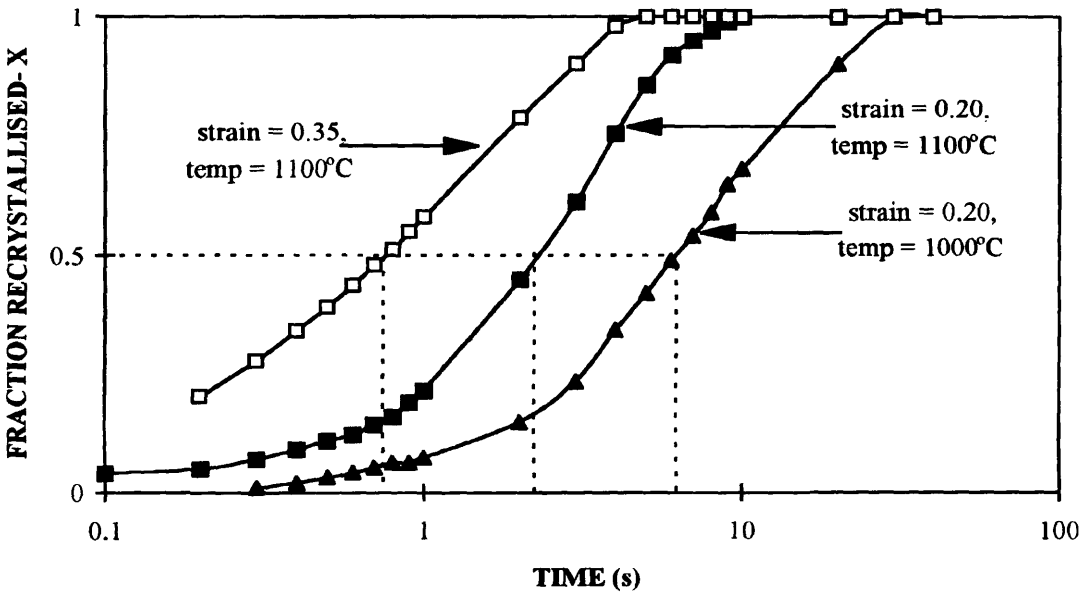

Fig. 2.6 **Dependence of temperature and strain on $t_{0.5RX}$ of 0.095 wt% V steel (d_0 = 165 μm), after Medina and Mancilla[50].**

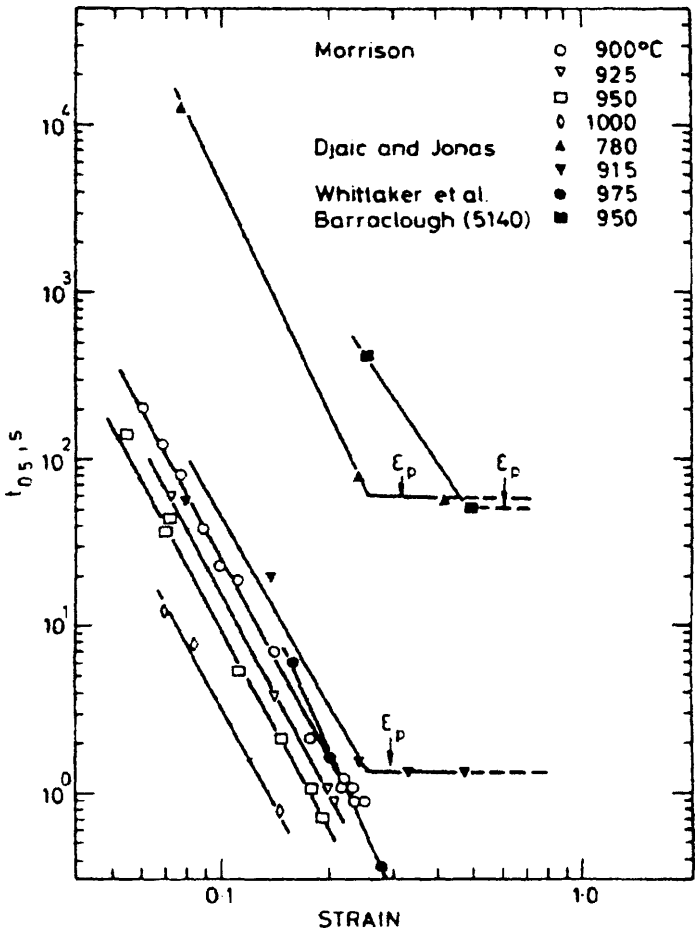

Fig. 2.7 **Sellars[51] literature data relating $t_{0.5RX}$ to applied strain for C-Mn (data of Morrison and Whittaker *et al*) and low-alloy steels.**

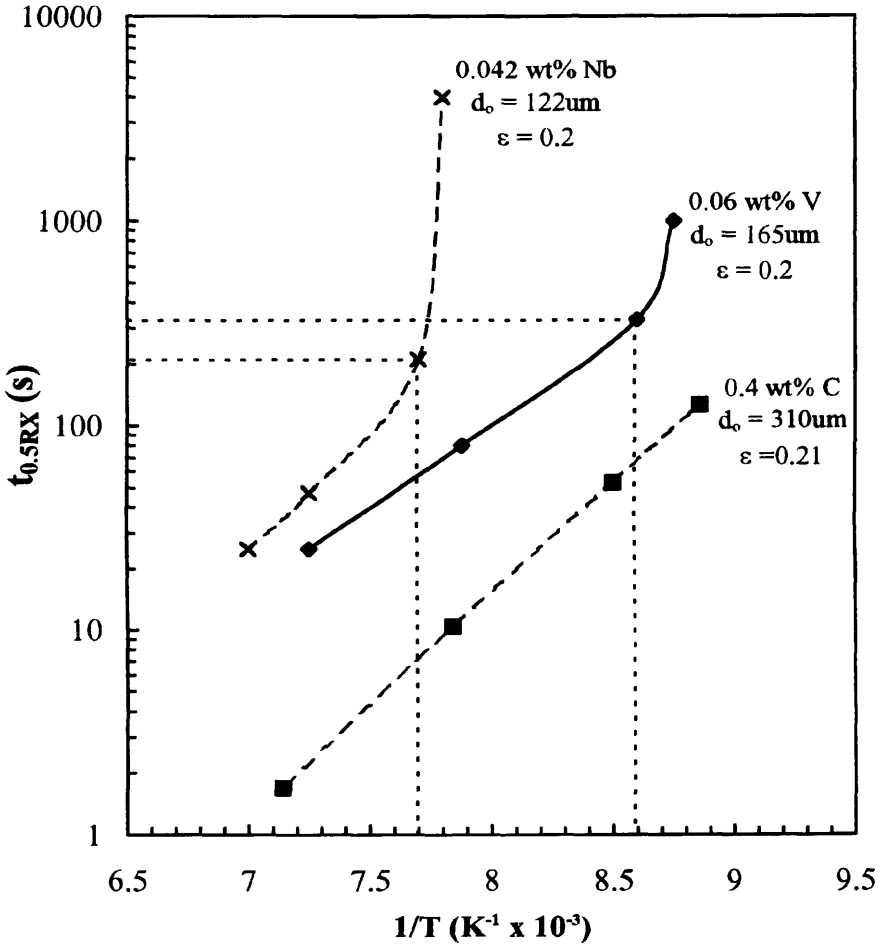

Fig. 2.8 Effect of temperature on $t_{0.5RX}$, after Medina and Fabregue[54].

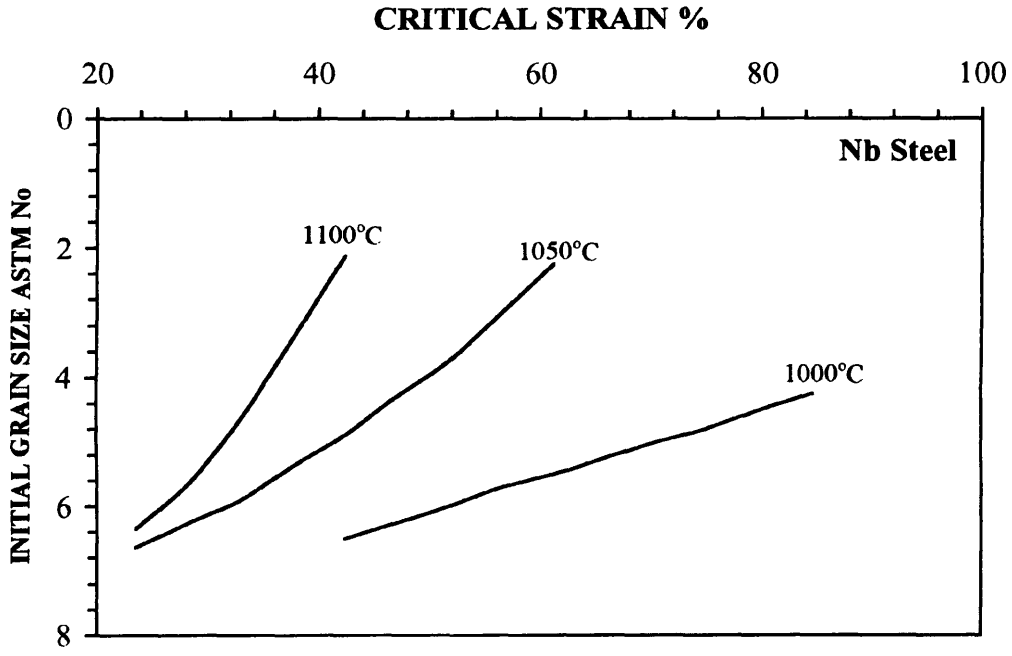

Fig. 2.9 **Effect of deformation temperature and initial austenite grain size on the critical amount of deformation required for complete recrystallisation (3 secs isothermal hold) in a Nb steel, after Tanaka *et al* [61].**

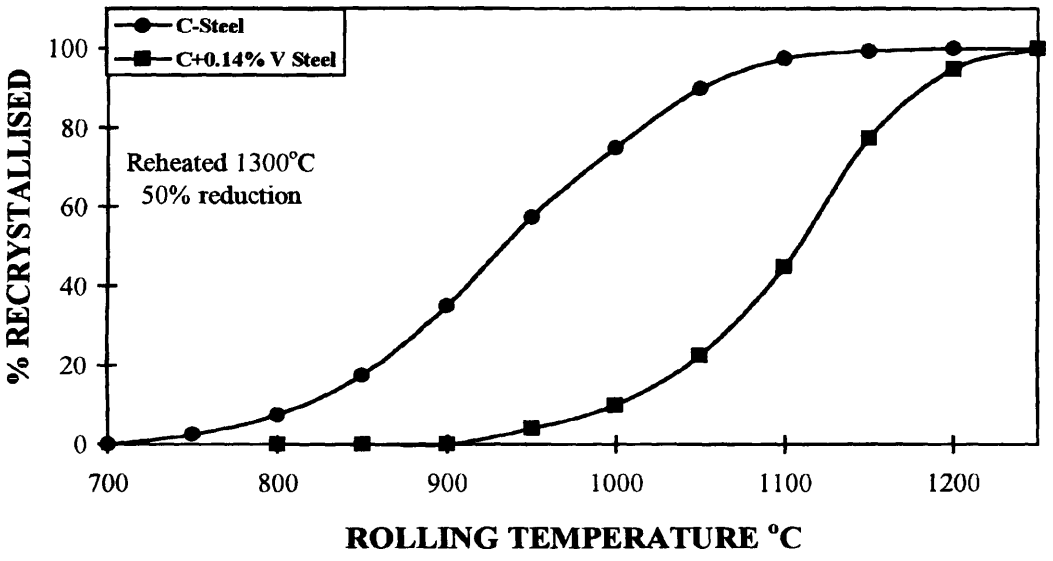

Fig. 2.10 **Effect of rolling temperature on recrystallisation in plain carbon and 0.14% V steel, after Amin and Pickering [62]. Isothermally held for 1s at the rolling temperature and quenched in iced brine after 50% reduction.**

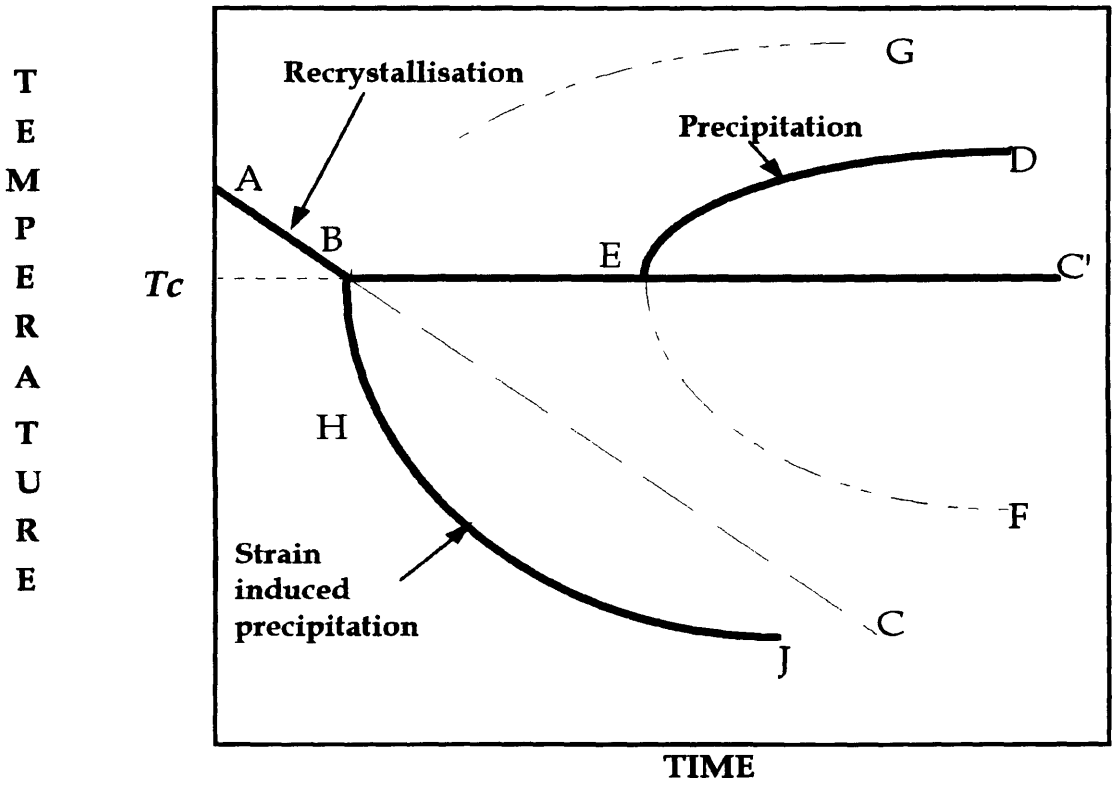

Fig. 2.11 **Schematic representation of the inhibition of recrystallisation by strain induced precipitation[83].**

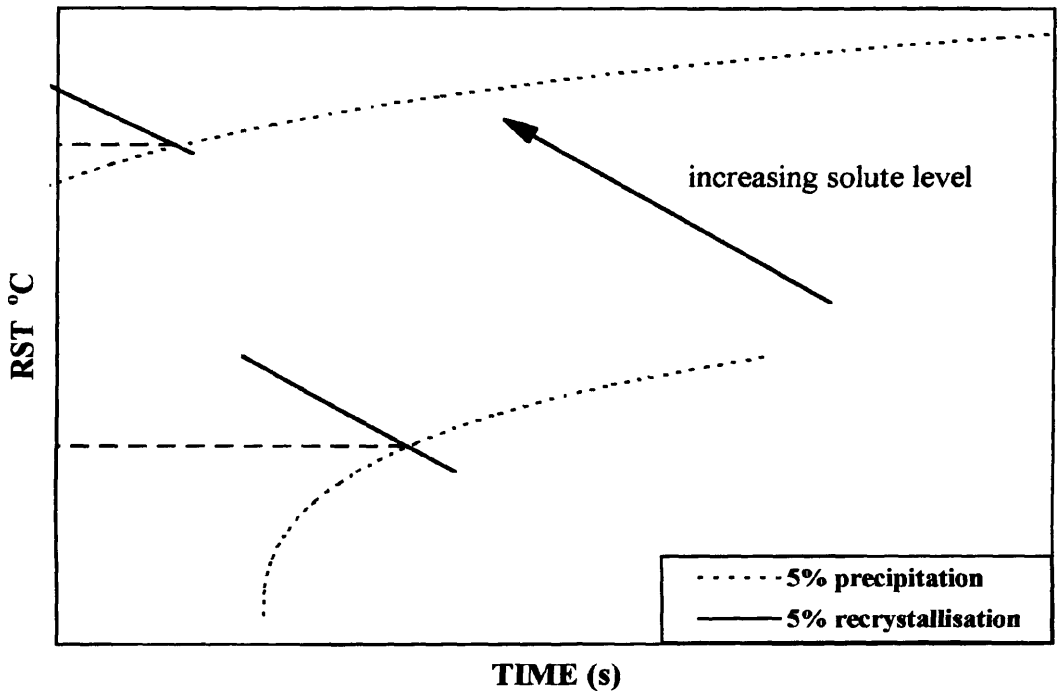

Fig. 2.12 Schematic of the effect of increasing solute on the RST.

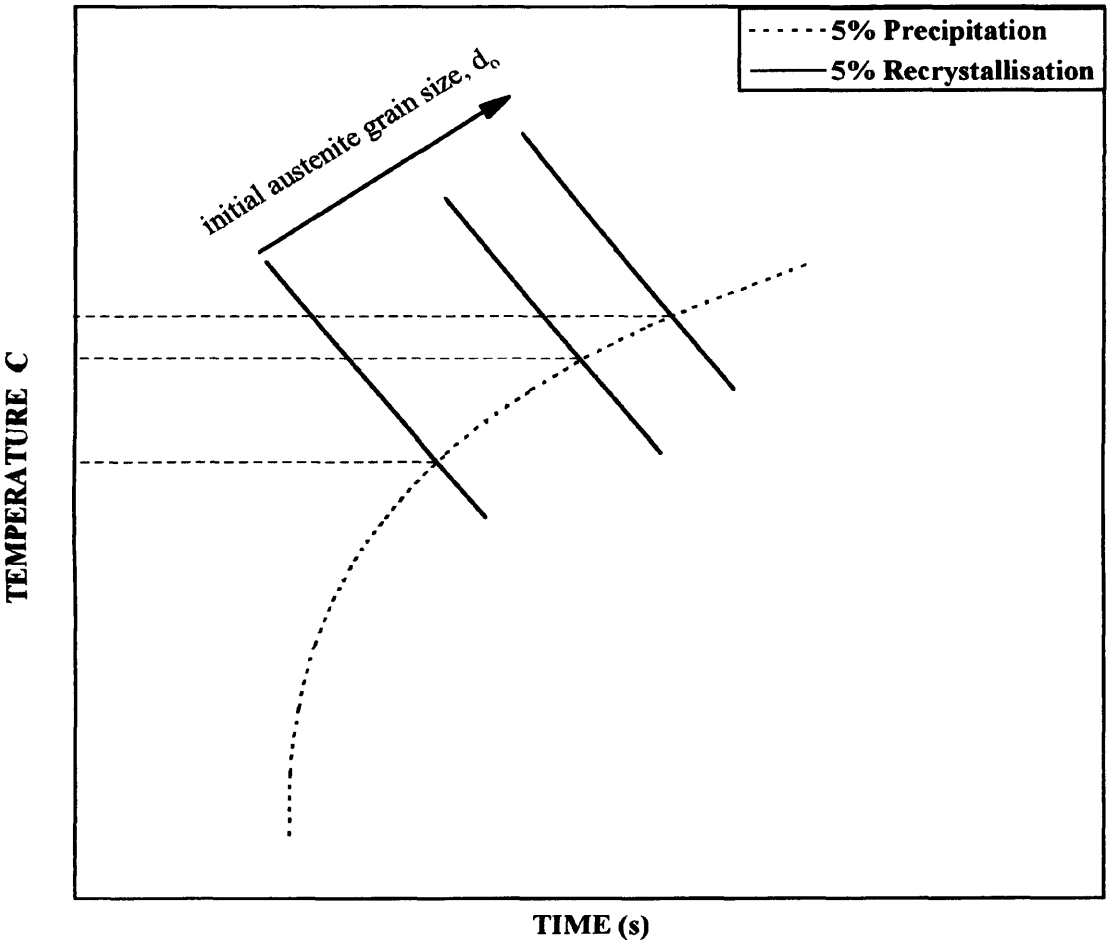

Fig. 2.13 **Schematic of the effect of increasing initial austenite grain size on the RST.**

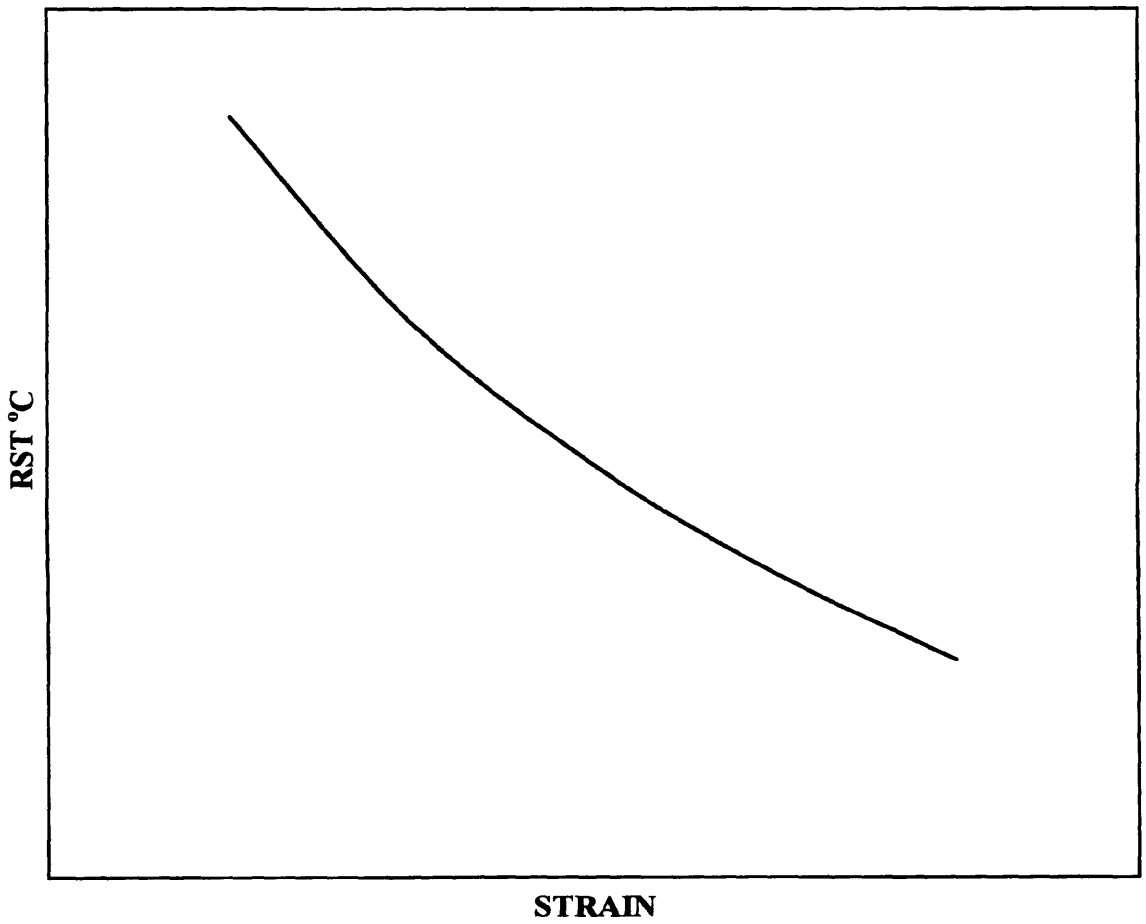

Fig. 2.14 Dependence of RST on strain.

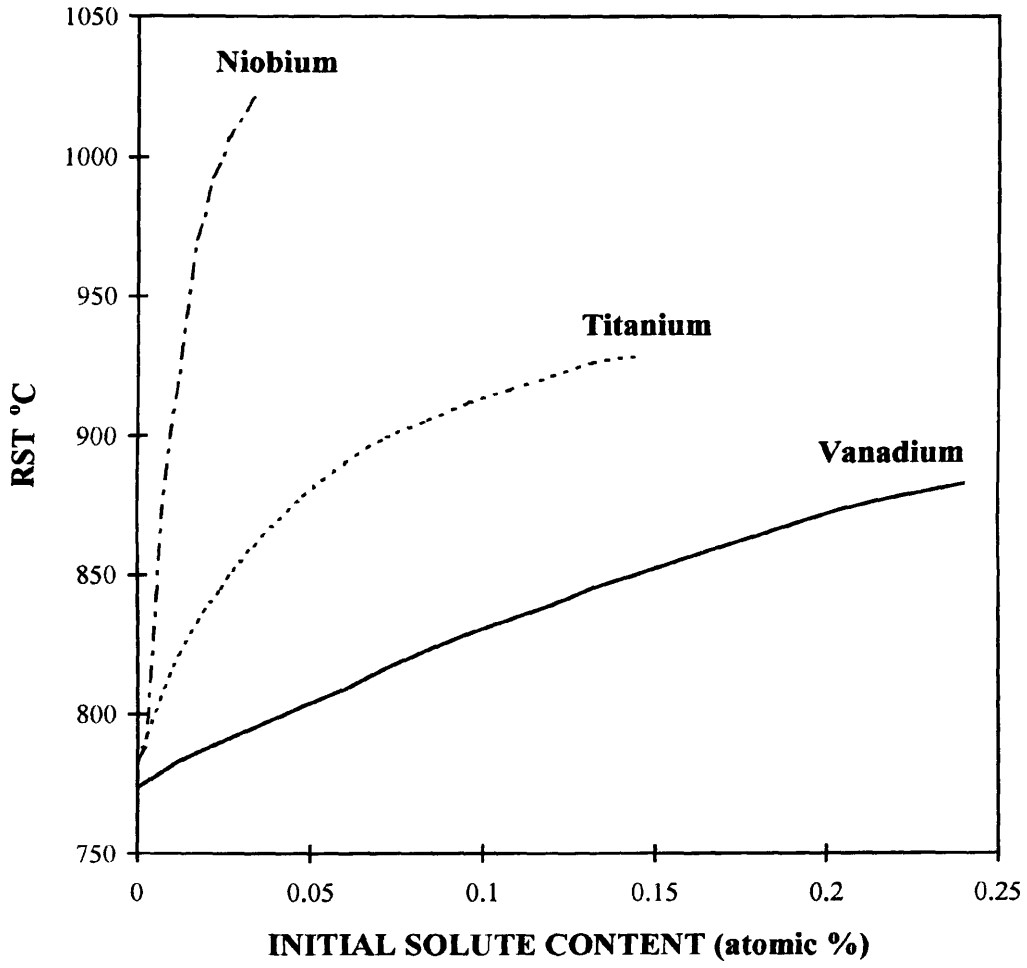

Fig. 2.15 **Effect of microalloying additions on the recrystallisation stop temperature in 0.07 wt% C, 1.40 wt% Mn, 0.25 wt% Si steel, after Cuddy[85].**

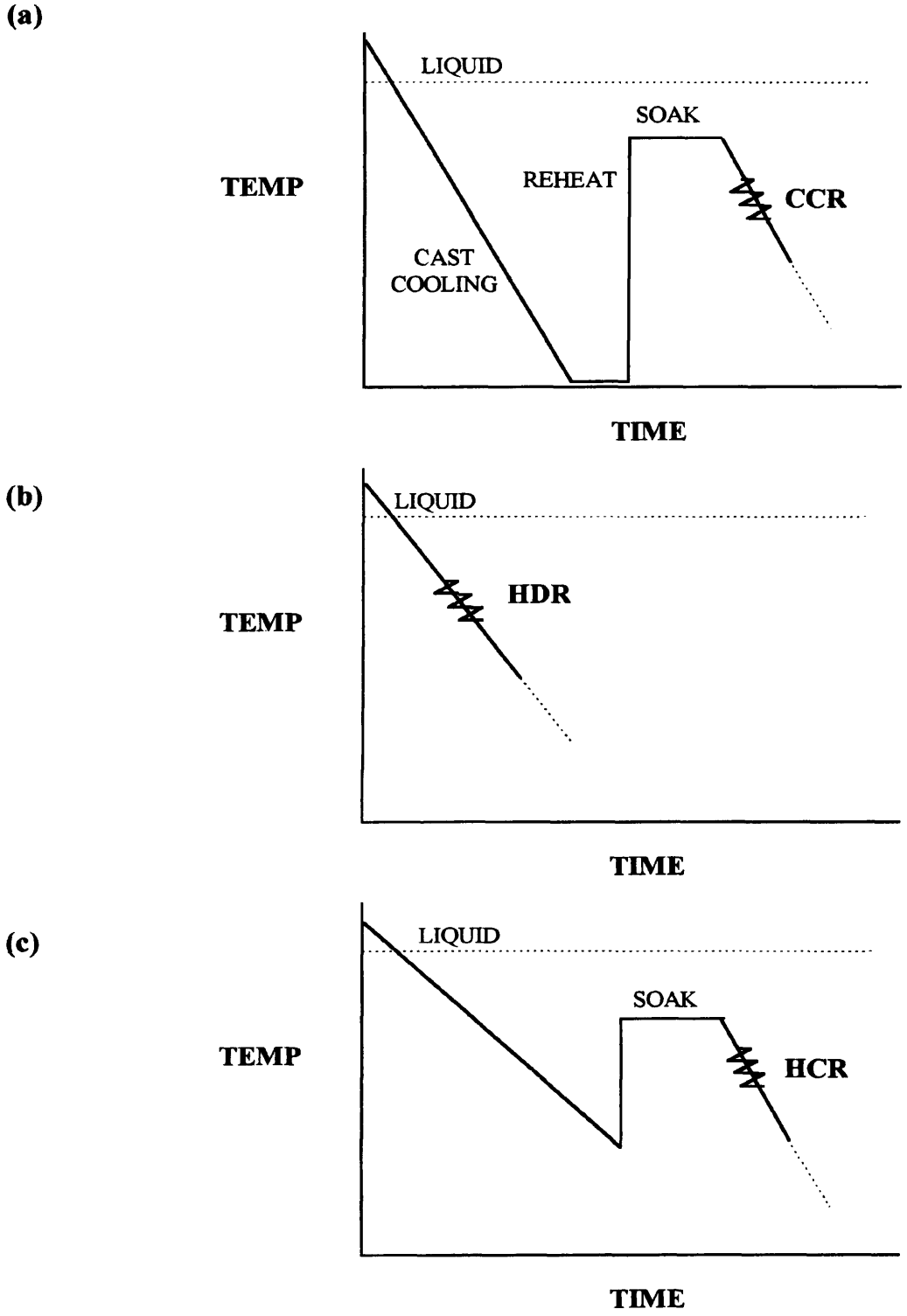

Fig. 2.16 **Schematic representation of :**
(a) conventional controlled rolling - CCR;
(b) hot direct rolling - HDR;
(c) hot charge rolling - HCR.

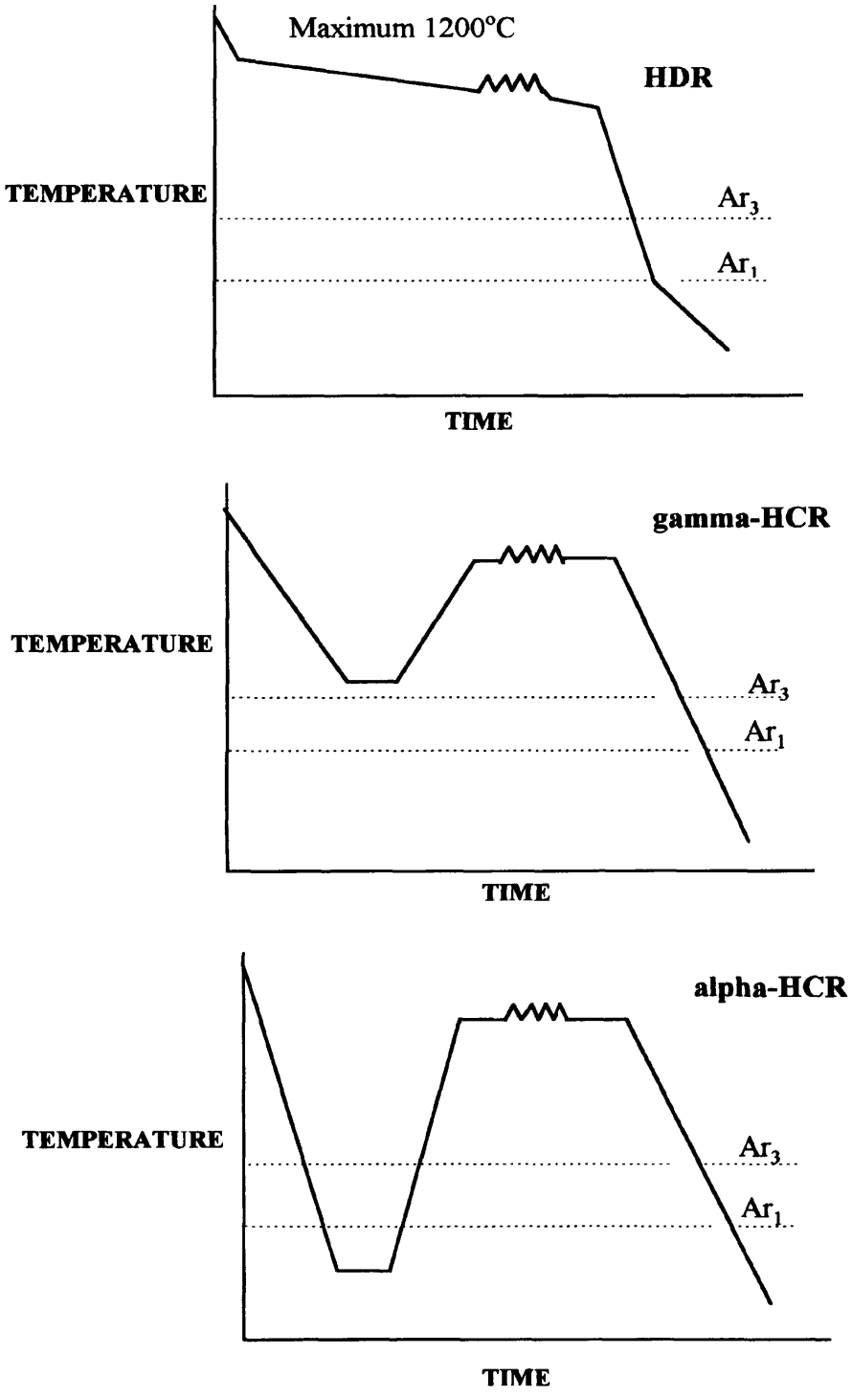

Fig. 2.17 Schematic of Hot Direct Rolling and variants of Hot Charge Rolling.

CHAPTER 3

EXPERIMENTAL PROCEDURES

3.1 Materials for Controlled Rolling

The material for this investigation was received as hot rolled 25mm thick plates, each of the same base composition except for the vanadium content, and of the composition given in Table 3.1. The microstructure of both the plates in the 'as received' condition consisted of banded fine grain ferrite and pearlite; that of 4V is shown in Fig. 3.1. For discussion purposes, the steels will be referred to as 2V and 4V for the steels containing 0.20 and 0.43 wt% V respectively.

3.2 Material for Hot Direct Rolling

Steel castings of 1 kg weight were made by vacuum/ argon induction melting. A flow diagram of the HDR process is shown in Fig. 3.2., and the nominal composition in Table 3.2. Two kinds of mould systems were designed to obtain two different casting structures. In one situation, the ceramic mould was preheated to 1050°C and was itself insulated with a ceramic fibre blanket, in order to simulate the cooling rate of thin slab casting. The macrostructure of the ingots in this mould system consisted of an outer layer of between 1.5 - 2mm deep of columnar grains, the remainder consisted of equiaxed grains having a mean linear intercept grain size of 1150μm. In the other mould system, a cast iron chill block was placed at the bottom of the ceramic mould to obtain a longer length (about 12mm) of columnar layer from the chill, the remainder consisting of a 1.5-3mm deep outer layer of columnar grains and equiaxed grains in the centre of the ingot. In the present experiments, observations were confined to the equiaxed grain region.

The ingots were in the shape of plates measuring approximately 100×75×15mm, and bevelled along the bottom edge for entry into the rolling mill. A thermocouple in a quartz tube was located in the lower third of the ingot. This part of the ingot cooled at approx. 1.9 Ks^{-1} from 1400-1200°C. For discussion purposes, this steel for hot direct rolling will be referred to as 2V - HDR.

3.3 Grain coarsening studies for Controlled Rolling

Small sections, measuring approximately half inch cube, were extracted from both the steel plates. Two sections, one of each composition, were held tightly together by a thin metal wire with the junction of a chromel-alumel thermocouple situated between the two. These were then placed in a muffle furnace, with the leads of the thermocouple connected to a digital temperature readout instrument. The sections were held for 30 minutes at the required temperature. The temperatures selected were in increments of 50°C, from 850 to a maximum of 1250 °C. Immediately after this time, the assembly was withdrawn from the furnace and rapidly agitated in iced brine.

The metallographic procedure described here also applied to slabs and ingots following rolling. Each section was then individually prepared by standard metallographic techniques. To reveal the prior austenite grains of the quenched out microstructures, an etchant consisting of saturated picric acid with 10% Teepol and six drops of HCL acid at between 50-70 °C was used. Frequently, to facilitate etching, a repeat polish-etch technique was necessary.

Grain sizes were measured by the linear intercept technique[92,93] with sufficient counts made to ensure a relative error of < 5% of the measured values. Where necessary, the grain size expressed in microns was converted to ASTM grain size number using the relationship[94] :

$$\text{ASTM No G} = 10 - 6.6439\ \text{Log}_{10}\left(\frac{l}{10}\right) \qquad \textbf{(3.0)}$$

where l is the mean intercept distance in μm.

The mean linear intercept, $\overline{L}_L$ (longitudinal) and $\overline{L}_T$ (transverse) were calculated as:

$$\overline{L}_L = \frac{L_{LT}}{N_{GB}} \qquad \textbf{(3.1)}$$

$$\overline{L}_T = \frac{L_{TT}}{N_{GB}} \qquad \textbf{(3.2)}$$

where L_{LT} is the total length of traverse in the longitudinal direction and L_{TT} is the total length of traverse in the transverse direction. N_{GB} is the number of grain boundaries intersecting the line of traverse.

The aspect ratio of austenite grain was taken as the ratio of:

$$\bar{L}_{\gamma L} \; / \; \bar{L}_{\gamma T} \qquad (3.3)$$

The theoretical austenite aspect ratios (AR_{calc}) were calculated from the following equation:

$$AR_{calc} = \frac{1}{(1-r)^2} \qquad (3.4)$$

where $r = \frac{H-h}{H}$, and $r < 1$. H and h are the slab thicknesses before and after the reduction.

The variation of the theoretical aspect ratios with reduction is shown in Fig. 3.3.

3.4 Slab preparation for rolling

The requisite number of specimens were machined from each of the 25mm thick plates to allow for various reductions during the rolling experiments. In all instances, the longitudinal axis of the slabs was parallel to the original rolling direction of the plates. The thickness of specimens after machining were so planned, that after rolling reduction, the final exit thickness of each slab would be the same, 5mm. This ensured consistency in post rolling treatments of the slabs. The initial specimen thickness for the aim rolling reductions are given in Table 3.3.

The leading edge of each of the finish machined slab was tapered to facilitate entry into the roll gap. To accurately monitor the temperature, a 2.5mm transverse hole was drilled on the centre line extending half the width of the slab. After insertion of the thermocouple junction into the prepared hole in the slab, it was then packed tightly with alumina wool. The leads of the thermocouple were then connected to a digital temperature readout and a chart recorder. To

facilitate handling, a rod was mounted on each slab. The general arrangement is schematically shown in Fig. 3.4, which also applied to the HDR experiments.

3.5 Rolling mill

All the rolling experiments were carried out in the Marshall Richard Barcro, two high reversible experimental rolling mill. The rolls were 209.5mm in diameter and the maximum roll separating force was 35 tons on each roll bearing. The rolling speed was servo controlled at up to 0.5 m/sec. The rolling speed used was 0.31 m/s. Hot air from electric fan heaters was directed at each roll to preheat them in order to reduce roll chilling of the slabs and prevent damage to the rolls.

3.6 Rolling procedure for CR and HDR

The procedure described here (single pass rolling), applied to all the experiments carried out in this investigation. A slab containing the thermocouple and mounted on the handling rod, was inserted into a muffle furnace set at the required reheat temperature. This was held for 30 minutes, from the moment the aim reheat temperature was attained. A second 'holding' furnace for isothermal holding the rolled slab was positioned on the exit side of the rolls. It was not possible to accurately predict the temperature of the slab on exit from the rolls, however, from previous experiments a drop of approximately 30°C occurred during a roll pass. This was allowed for in the experiments, and the recorded isothermal hold temperatures during a roll pass is the temperature of the slab while in the furnace, estimated from the chart recorder printout. The 'holding' furnace was therefore set at a temperature 30°C below the aim rolling temperature.

The roll gap was adjusted to 5mm in excess of the thickness of the slab such that the reheated slab could be inserted straight into the 'holding' furnace (through the roll gap) situated on the entry side of the rolls. The roll-gap was then set to obtain the aim reduction and the rolls were set in motion. The slab was withdrawn from the 'holding' furnace at a temperature approximately 10°C above the aim rolling temperature, and then drawn into the rolls at the correct aim rolling temperature. On exit, the rolled slab was immediately inserted into the same 'holding' furnace which was moved to the side of the mill, for a specified time, and, finally quenched by rapid agitation in iced brine. Final slab thickness was measured and the

true reduction determined. A typical rolling schedule, for CCR is schematically illustrated in Fig. 3.5.

To simulate HDR, ingots were allowed to cool in the mould to a few degrees above the aim rolling temperature. The slab was stripped from the mould, inserted into the roll gap, and rolled directly into another furnace which was preset at the aim isothermal holding temperature.

The nominal strain rate was different for each slab, which and was taken into account in estimating the strain rate. Tamura *et al* [95] gave the following relationship for evaluating the equivalent mean strain rate throughout a reduction:

$$\bar{\varepsilon} = \frac{2}{\sqrt{3}} \times \frac{\pi}{30} \times N\sqrt{\frac{R_D}{H}} \times \frac{1}{\sqrt{r}} \times \ln\frac{1}{1-r} \qquad (3.5)$$

N and R are the rotating speed in revolutions per minute and the radii of the rolls respectively. Typical strain rates for the reductions applied in this investigation are given in Table 3.4.

3.7 Determination of recrystallisation

A longitudinal section from the mid-width of the rolled and quenched slab was extracted, mounted and prepared (as described earlier) for microscopical examination, Fig. 3.6. The presence, absence or extent of recrystallisation was evaluated by examination of the microstructures. The occurrence of recrystallisation was ascertained by measuring the austenite grain size, the grain aspect ratio and by scrutiny of the etched, quenched out microstructures for evidence of new grains. The extent of recrystallisation, where appropriate, was determined by standard point counting technique[96].

TABLE 3.1

Nominal composition of the materials for CCR.

ELEMENT wt %	C	Si	Mn	P	S	Al	N	V
2V STEEL	0.14	0.31	1.41	0.011	0.009	0.026	0.0053	0.20
4V STEEL	0.15	0.32	1.40	0.014	0.009	0.040	0.0066	0.43

TABLE 3.2

Nominal composition of the material for HDR

ELEMENT wt %	C	Si	Mn	P	S	Al	N	V
2V - HDR	0.12-0.141	0.30-0.35	1.32-1.41	0.005-0.008	0.0035-0.006	0.01-0.03	0.005	0.20-0.22

TABLE 3.3

Machined slab dimensions (CCR) for the appropriate level of reductions

REDUCTION %	INITIAL THICKNESS mm
20	6.25
30	7.14
40	8.33
50	10.00

TABLE 3.4

Calculated strain rates for roll speed of 0.31m/s.

REDUCTION	STRAIN RATE S^{-1}	
%	CCR	HDR
20	6.86	4.43
30	8.38	5.78
40	9.62	7.17
50	10.66	8.70

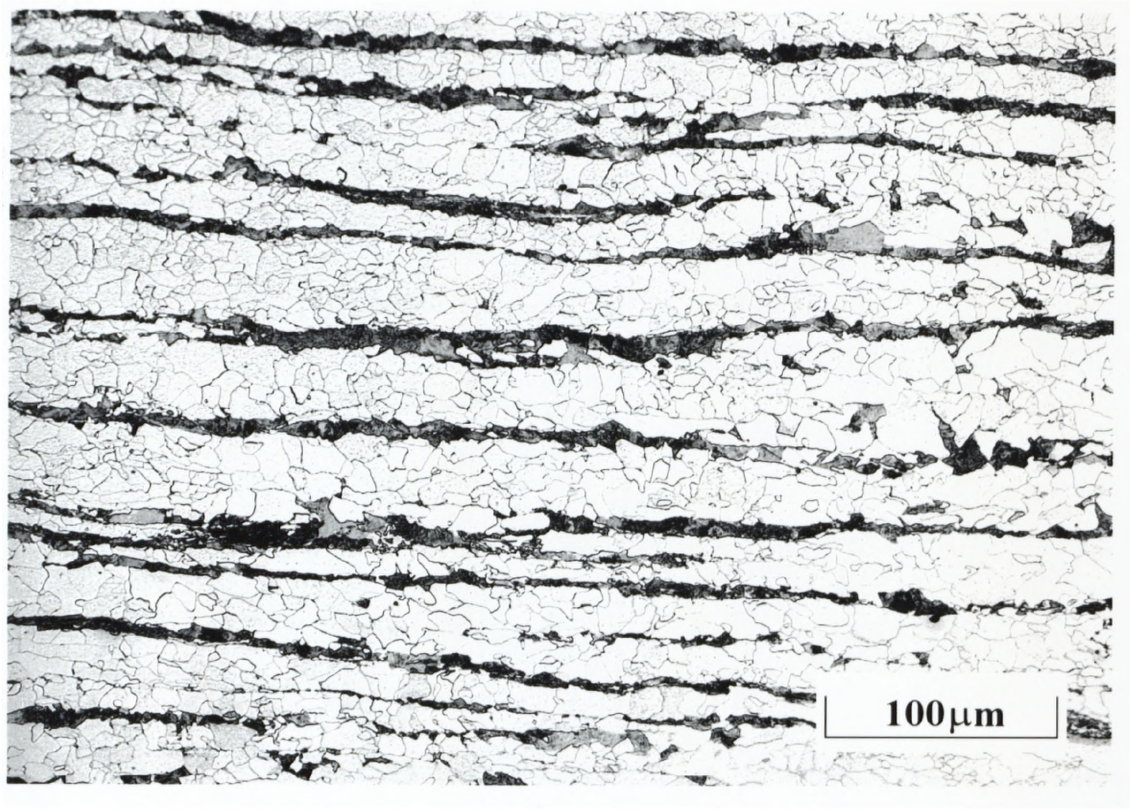

Fig. 3.1 Microstructure of the 0.43% vanadium steel (4V) in the 'as received' condition.

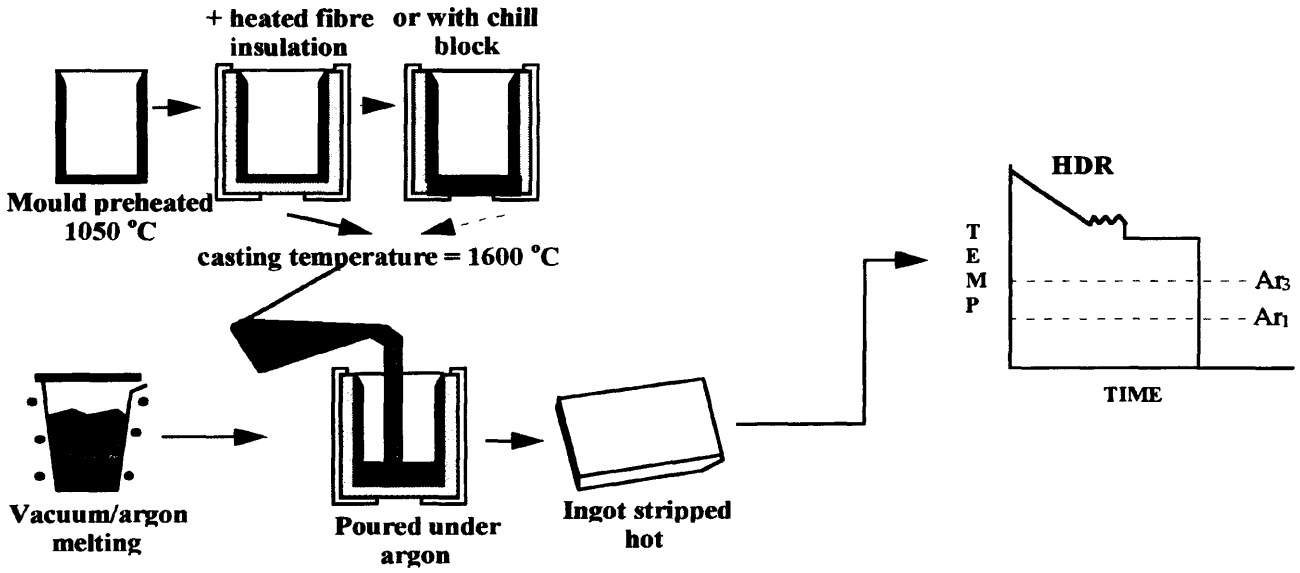

Fig. 3.2 Flow diagram of HDR simulation.

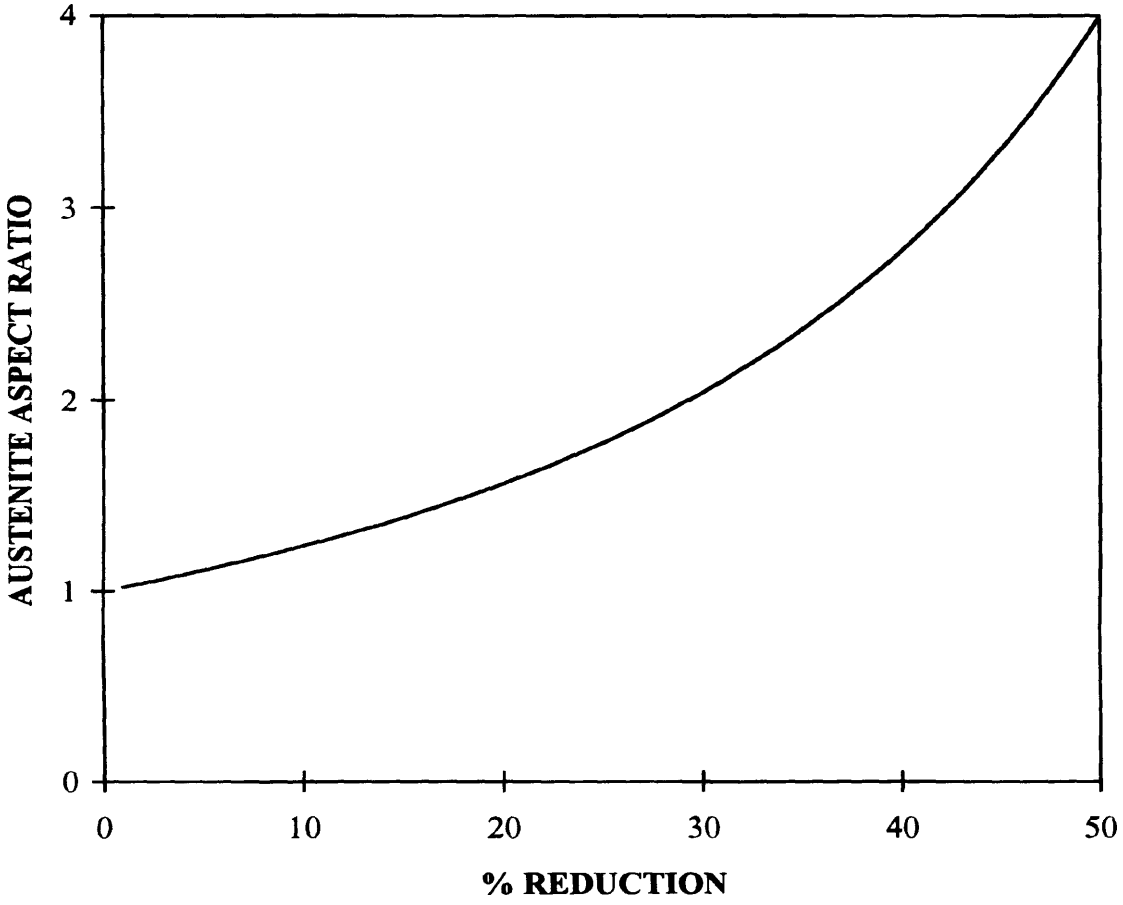

Fig. 3.3 **Dependence of theoretical austenite aspect ratios on applied reduction.**

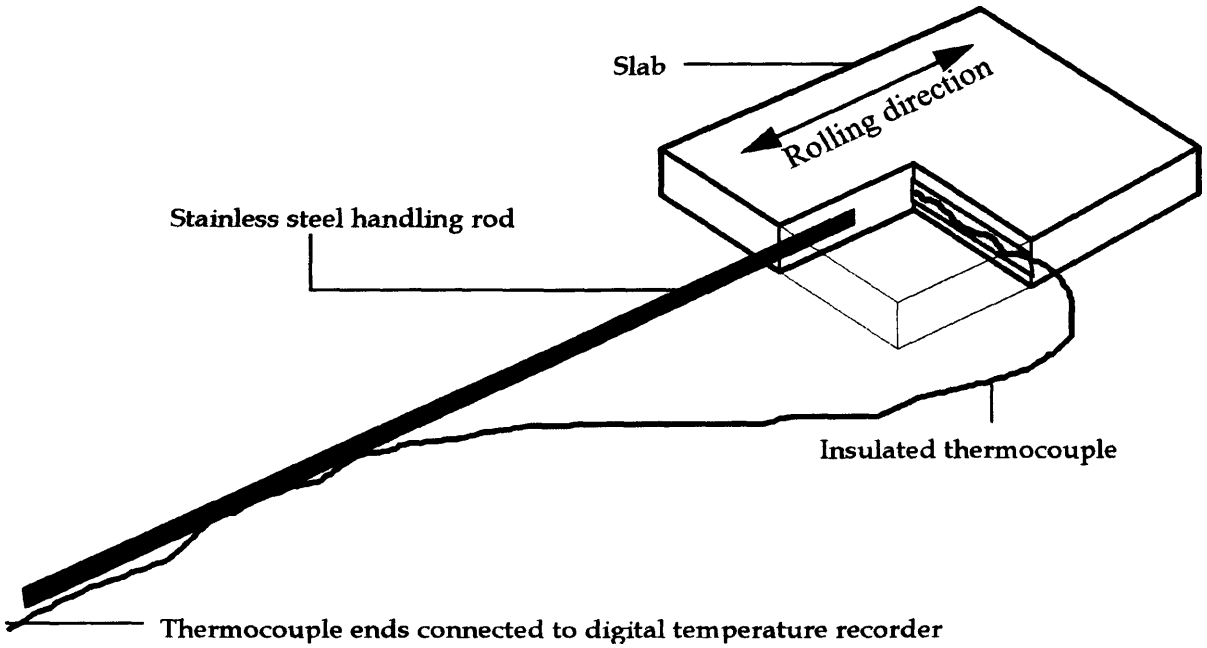

Fig. 3.4 Schematic illustration of a typical slab prepared for rolling.

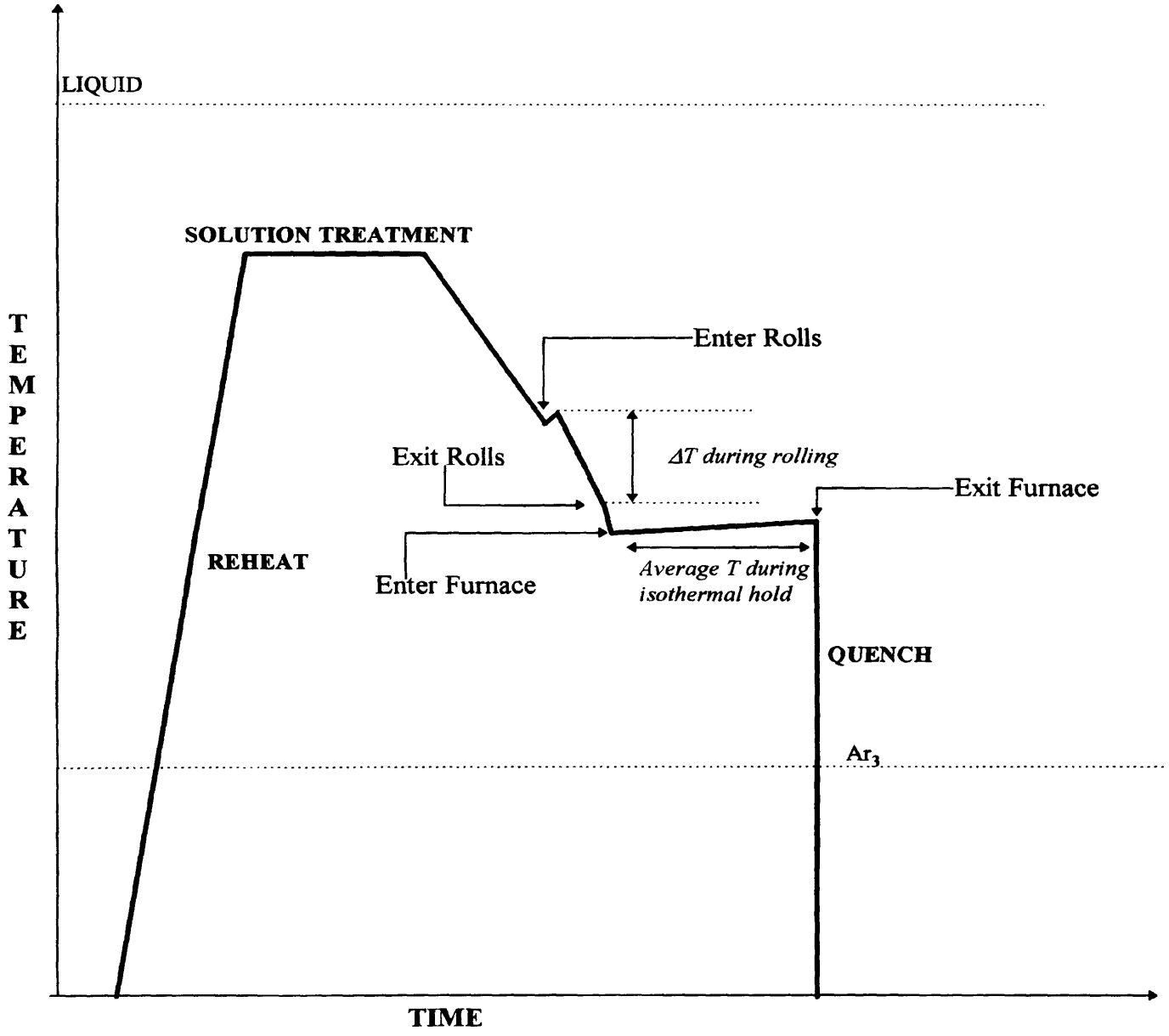

Fig. 3.5 **Schematic illustration of a typical rolling schedule for CCR slabs.**

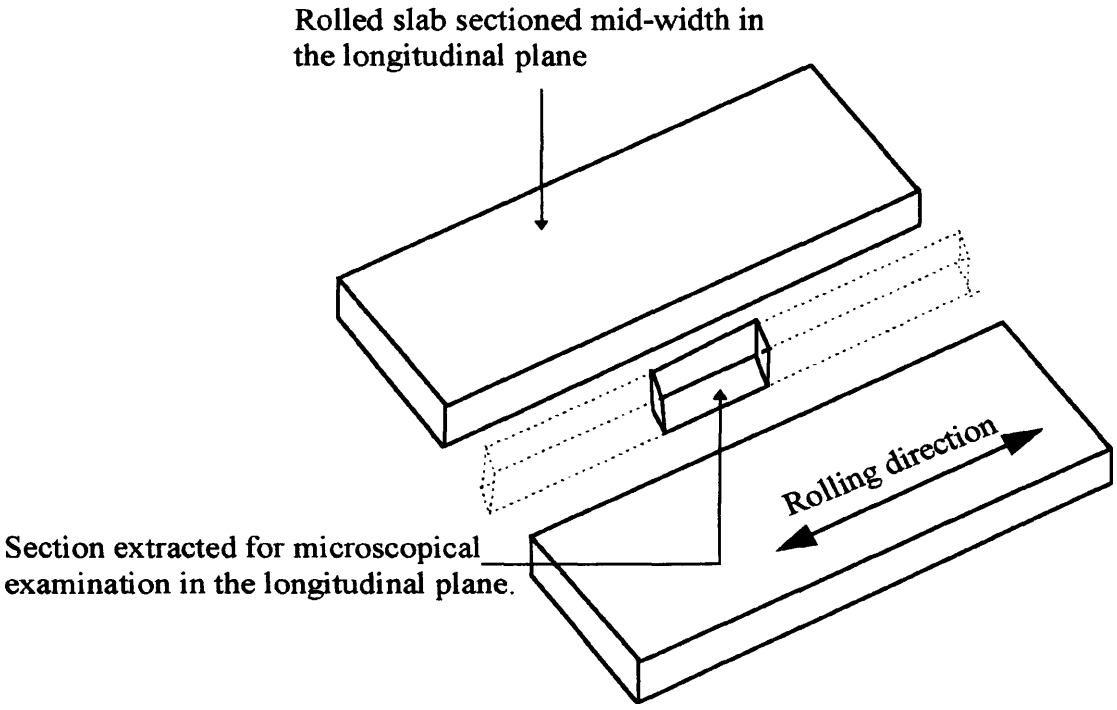

Fig. 3.6 Schematic illustration showing the location of section extracted for microscopical examination for both CCR and HDR.

CHAPTER 4

RESULTS

4.1 Reheated austenite grain size

The purpose of this experiment was to establish:

(a) the reheated austenite grain size for input in the Dutta and Sellars model, and;

(b) the grain coarsening characteristics of the two steels.

The results of the grain coarsening experiments are given in Table 4.1 and the measured aspect ratios of the reheated and quenched structures shown in Fig. 4.1. The aspect ratios were all reasonably close to a value of 1.0, indicating an almost equiaxed grain structure.

The dependence of austenite grain size on reheating temperature of the two steels for half hour anneals is shown in Fig. 4.2. The ASTM grain size of the austenite of the 2V steel was approximately linearly dependant upon the temperature, coarsening immediately on reheating, a feature commonly observed in mild and C-Mn steels. On the other hand, the rate of increase of the austenite grain size with temperature of the 4V steel changed discontinuously at a temperature of 990°C (grain coarsening temperature), and thereafter increased with temperature in a manner similar to the 2V austenite. The grain growth features displayed by the austenite of 4V were similar to those observed for C-Mn-Nb steel investigated by Priestner *et al* [97].

4.2 Model inputs

Using Dutta and Sellars' constants and concept, minor modifications were made by substituting the equilibrium solubility product of VN for Nb(C,N) and the particular methodology of the present experiments. In the VCN system, the precipitate nucleus is assumed to be predominantly VN due to the high solubility of VC in austenite. The equilibrium solubility product was defined by Speer *et als* [39] relationship,

$$\mathrm{Log}[V][N] = 3.02 - \frac{7840}{T} \qquad \textbf{(4.0)}$$

Using equation (4.0), the solution temperatures were calculated for the two compositions. These were 1050 °C and 1140 °C for 0.2 and 0.43 wt% V respectively, Fig. 4.3. From Fig. 4.2, the grain coarsening temperature, T_{GC}, of the two compositions are approximately 900°C and 990°C for 2V and 4V respectively. The T_{GC} can be considered to be where an equilibrium exists between the driving force for grain coarsening and the pinning force opposing boundary motion. It has been shown by Erasmus[98] that the grain coarsening temperature is always less than the VN solvus temperature, due to the temperature dependent growth of VN. The grain coarsening temperatures of 2V and 4V are both 150°C below their respective calculated VN solvus, Fig. 4.4, confirming the observations of Erasmus.

To aid microscopical examination of recrystallised grains following deformation, a sufficiently large initial reheated austenite grain size was chosen. As the RST is a function of a number of metallurgical and processing variables and is expected to be different for 2V and 4V, it was advantageous to make comparisons at constant grain size. The reheated grain size selected was therefore the same, 92 μm for 2V and 4V. The reheat temperatures for this grain size, determined from Fig. 4.2 were 1200 and 1228 °C for 2V and 4V respectively. These reheat temperatures are 150 and 88 °C above the estimated solution temperatures, Fig. 4.5. Typical reheated austenite grain structure of 4V is shown in Fig. 4.6.

For HDR, the average austenite grain size was 1150 μm established from a sample quenched from 1000 °C and from those slabs which were rolled but exhibited nil recrystallisation. The grain size of elongated austenite grains was taken to be equal to:

$$\bar{L}_{\gamma} = \sqrt{\bar{L}_{\gamma L} \cdot \bar{L}_{\gamma T}} \qquad \textbf{(4.1)}$$

Fig. 4.7 shows the reheated austenite grain structures of 2V and 2V-HDR and clearly illustrates the large difference in the austenite grain size. It was not possible to vary the grain size of the HDR material such that the RST for the two conditions could be compared at constant grain size.

The reheated grain sizes established for the three compositions were to be input into the model.

4.3 Modelling the RST

Data in the literature indicated that the solute drag effect exerted by V solute is smaller than that due to Nb, resulting in relatively faster recrystallisation kinetics of V austenite for comparable testing conditions. Jonas *et al* [66] reported the effect of Mo, Nb, and V on the occurrence of static recovery and recrystallisation after high temperature deformations. The steels had a base composition of 0.05% C and 1.40% Mn. To this, single additions of 0.30% Mo, 0.035% Nb and 0.115% V were made. Interrupted hot compression tests were performed at 900 and 1000 °C and at a constant strain rate of 2 s^{-1}. The greatest solute retardation of static recovery and recrystallisation was produced by the Nb addition, followed by that of Mo, V leading to the smallest delay. Fractional softening associated with static recovery was approximately 12%. From their data at 1000 °C, for fractional softening of 20% (assumed to be approximately the start of recrystallisation), the Nb steel took ~ 3.5 seconds and the V steel ~ 1.05 seconds. At this temperature, all the solute was expected to be in solution. Even though the V content was almost three times that of Nb, the time to the onset of recrystallisation of the V steel is approximately a third of the Nb steel. As an approximation, it is assumed that by reducing the Nb content by a third, the solute drag is reduced and the time to the start of recrystallisation is therefore reduced to almost that of V steel in this example.

In order to model the RST's so that variables in an experimental campaign could be estimated, Dutta and Sellar's equation (2.1) for $t_{0.05RX}$ was modified* to include a factor of 0.3 to allow for a reduced solute drag effect of V compared to that of Nb. The equation for $t_{0.05RX}$ to take this effect into account is now as follows:

$$t_{0.05RX} = A_{RX} \cdot d_o^{\,2} \cdot \varepsilon^{-4} \cdot \exp\frac{Q_{RX}}{RT} \cdot \exp\left\{\left(\frac{B_{RX}}{T} - 185\right) \cdot [V] \cdot 0.3\right\} \qquad \textbf{(4.2)}$$

Equation (2.5) for $t_{0.05P}$, by substituting V instead of Nb, now becomes:

$$t_{0.05P} = A_{PPT} \cdot [V]^{-1} \cdot \varepsilon^{-1} \cdot Z^{-0.5} \cdot \exp\frac{Q_{diff}}{RT} \cdot \exp\frac{B_P}{T^3 (\ln K_S)^2} \qquad \textbf{(4.3)}$$

* This was an initial approximation (F=0.3) prior to the start of the experimental campaign. This was later modified to F=0.1 (Chapter 5, p98) when data for the same wt% of Nb and V was compared.

A programme was written to determine the intersection of the 5% precipitation and recrystallisation plots calculated from equations (4.2) and (4.3). A typical graphical representation of these two calculations is shown in Fig. 4.8 for the conditions stated.

In this figure, rolling at 1000°C after solution treatment at 1200°C, and then isothermally holding at 860°C following deformation, the model predicts that 5% precipitation occurs in 4.2 seconds and 5% recrystallisation in 76.4 seconds. Precipitation, therefore, will have occurred in unrecrystallised austenite. On the other hand, 5% precipitation and recrystallisation occurs in 139.3 and 3.6 seconds respectively when isothermally held at 940°C following deformation. Precipitation, here, would not have occurred as recrystallisation would have preceded strain induced (SIP) precipitation. When held at ~910°C, the possibility exists that recrystallisation will have been inhibited, that is when 5% precipitation and recrystallisation occurred simultaneously.

4.3.1 Determining the model RST

To determine the RST predicted by the model, a range of rolling and holding temperatures for reductions of 0.1, 0.2, 0.3, 0.4 and 0.5 were input into the model. The strain rates were calculated for a roll speed of 0.31 m/sec. Rolling temperatures that were initially input into the model were in increments of 25°C from 850 to 950°C for each reduction. The isothermal holding temperatures were estimated at 30°C below the appropriate rolling temperatures. For each condition, if the time to 5% recrystallisation was less than the time to 5% precipitation, then recrystallisation would precede precipitation and the slab would be expected to be either fully or partially recrystallised. If on the other hand, precipitation preceded recrystallisation, then the slabs would be expected to exhibit a 'pancaked' microstructure indicative of strained, unrecrystallised austenite. A typical graph that was generated is shown in Fig. 4.9. Here it can be estimated that the RST for 0.2 reduction is between 900 - 925°C and between 875 - 900°C for 0.4 reduction. Once this was determined for all the aim reductions, the analysis was repeated with increments of either 1 or 5°C of the rolling temperature within this range, such that it was possible to evaluate the temperature at which the time to 5%recrystallisation and precipitation were almost equal. The model RST was then determined by separating the fully/partially and non-recrystallised regions. The graph in Fig. 4.10 shows the model RST of the three steels.

4.3.2 Determining the post deformation hold times

To investigate the experimental RST, the rolling temperature, isothermal hold temperatures and the reductions were selected on either side of the predicted RST, Fig. 4.11. Those to the right of the RST would be expected to be fully or partially recrystallised and those to the left, unrecrystallised.

In order to generate sufficient static recrystallisation (to aid microscopical examination) where applicable during the isothermal hold following deformation, the slabs were held for the calculated times for 50% recrystallisation ($t_{0.5RX}$), which were calculated using the Avrami equation (1.8) for static recrystallisation, when X was equated to 0.5, $t_{0.05RX}$ was determined from the model and the value of the exponent, k, was assumed to be 2.

In summary therefore, the model RST was used as an approximate guide to select rolling reductions and temperatures for a reheated austenite grain size of 92μm for steels 2V and 4V and , 1150μm for 2V-HDR. The time to 5% recrystallisation for the selected reductions was derived from the model. Using the Avrami equation with an exponent k = 2, the estimated time to 50% recrystallisation was then calculated. Having established these parameters, the experimental campaign was begun, and the results are described in the following sections.

5.0 Steel 2V - Recrystallisation results

The rolling reductions, isothermal hold times, temperatures, and the results of microscopical examination are tabulated in Table 4.2.

Fig. 4.12 shows the results of single pass recrystallisation experiments on reheated austenite of steel 2V. The results show the presence of three distinct regions in this figure:

(i) combinations of rolling reductions and temperature which failed to cause any recrystallisation, represented by the open squares. In these specimens, the measured austenite grain aspect ratio was very close to that calculated from the applied rolling reduction. Fig. 4.13;

(ii) combinations which resulted in partial recrystallisation, represented by the half open squares. The amount of recrystallisation is indicated by the values adjacent to these data points;

(iii) combinations, at high temperatures which caused complete recrystallisation, represented by the solid squares and in which the austenite grain aspect ratio was close to 1 and the grain size had been significantly reduced.

A typical example of a fully recrystallised refined austenite grain structure is shown in Fig. 4.14 compared to the as-reheated grain structure prior to deformation.

The results here show that the model overestimates the experimental RST of steel 2V as shown Fig. 4.15.

5.1 Recrystallisation results - Steels 4V and 2V-HDR

As with steel 2V, the results of the single pass recrystallisation experiments on reheated austenite of 4V also exhibited three distinct regions as shown in Fig. 4.16, consisting of fully recrystallised, partial and nil recrystallisation zones. A typical partially recrystallised austenite grain structure is shown in Fig. 4.17. Figure 4.18 (a) illustrates an unrecrystallised grain structure whilst new grains initiating at triple points of the austenite grains are evident in Fig. 4.18 (b) from the specimen which exhibited 6.5 % recrystallisation. In specimens in which there was no or little evidence of any recrystallisation, the measured aspect ratios were reasonably close to the calculated ratios, Fig. 4.19.

Comparison of the model and experimental RST shows that as with steel 2V, the model overestimates the experimental RST, Fig 4.20. The difference between the model and experimental RST increased with increasing rolling reduction.

The recrystallisation results for the 2V-HDR are summarised in Fig. 4.21. As with the other two steels, the model again overestimates the RST as shown in Fig. 4.22.

6.0 Summary of the results

The experimentally determined RST's of the three steels are summarised in Fig. 4.23. The RST decreases with reduction, as predicted by the model, and in the order 4V, 2V-HDR and 2V for the three steels. The differences in the RST arise from the differences in solute levels and the process route, which in turn influence both the recrystallisation and precipitation kinetics.

The Dutta and Sellar's model was initially modified to take into account the equilibrium solubility product of VN instead of Nb(C,N). In addition, the faster recrystallisation kinetics in the V steel, due to a reduced solute drag effect compared to Nb, was also taken into account in equation (4.2) for $t_{0.05RX}$. This was in the form of a factor, whose value as a first approximation was taken to be equal to 0.3.

The single pass recrystallisation results of the three steel compositions has shown the presence of three distinct regions comprising a fully recrystallised, partially recrystallised and non recrystallised zones. Even with the initial modifications to the model described above, the model overestimates the experimentally determined RST's, summarised in Fig. 4.24.

In the two steels of similar composition but different processing route, the RST is marginally higher for HDR than for CCR. Although the model proposes a quadratic dependence of $t_{0.05RX}$ on d_o, and given the large range in grain size (92 and 1150 μm), the differences between the experimental RST's for the two processes is much smaller than would be expected on the basis of the original model. For the CCR processed steels, both the experimental and model RST is relatively higher, as predicted by the model, for the higher solute (0.43 wt% V) containing steel.

Clearly, analysis and manipulation of experimental data as is possible, and modifications to the original model are necessary to provide reasonable agreement between the experimental and predicted RST's.

Table 4.1

Results of grain coarsening, 0.5hr anneal at temperature.

SLAB REHEAT TEMPERATURE °C	STEEL 2V		STEEL 4V	
	GRAIN SIZE μm (ASTM)	ASPECT RATIO	GRAIN SIZE μm (ASTM)	ASPECT RATIO
900	13.3 (9.18)	0.93	10.50 (9.86)	1.08
950	15.5 (8.74)	1.05	11.30 (9.65)	0.97
1000	25.0 (7.36)	0.89	12.75 (9.30)	1.08
1050	28.9 (6.93)	1.05	22.17 (7.69)	1.06
1100	43.4 (5.76)	0.89	33.5 (6.51)	1.09
1150	71.25 (4.33)	1.09	51.0 (5.30)	1.08
1200	92.0 (3.60)	1.06	67.0 (4.51)	1.08
1250	145 (2.28)	0.98	105 (3.22)	0.99

TABLE 4.2

STEEL: 2V-CCR. Results of the CCR experiments.

Roll speed: 0.31 m/sec; Reheat temperature; 1200 °C (0.5 hr); Reheated grain size; 92 μm.

REDUCTION	ROLL TEMP (Hold Temp) °C	RECRYSTALLISATION %	GRAIN SIZE μm (Aspect ratio)	HOLD TIME seconds
0.21	1000 (970)	100	38.75 (1.10)	60
0.22	980 (945)	100	42.4 (1.01)	125
0.29	1000 (910)	100	32.5 (1.09)	10
0.27	950 (910)	100	34.5 (0.97)	60
0.41	1000 (970)	100	24.8 (0.98)	10
0.47	1005 (950)	100	20 (1.0)	1
0.48	950 (930)	100	19 (1.05)	4
0.46	930 (905)	100	28 (1.03)	14
0.50	900 (885)	100	20.25 (1.07)	13
0.48	930 (900)	100	19.25 (1.13)	5
0.49	880 (850)	12.00	-	30
0.47	890 (860)	16.25	-	20
0.36	900 (870)	17.08	-	66
0.29	910 (880)	32.5	-	280
0.18	930 (900)	41.67	-	360
0.27	910 (870)	0	(1.71)	78
0.16	880 (860)	0	(1.35)	348
0.17	900 (870)	0	(1.43)	516

TABLE 4.3

STEEL: 4V-CCR. Results of the CCR experiments.

Roll speed: 0.31 m/sec; Reheat temperature: 1228 °C (0.5 hr); Reheated grain size, 92μm.

REDUCTION	ROLL TEMP (Hold Temp) °C	RECRYSTALLISATION %	GRAIN SIZE μm (Aspect ratio)	HOLD TIME seconds
0.30	1040 (1010)	100	31.75 (1.10)	9.5
0.31	990 (960)	6.46	-	90
0.38	970 (935)	8.25	-	56
0.38	985 (960)	14	-	21
0.50	960 (920)	26.5	-	27
0.17	1030 (1000)	35.25	-	95
0.49	970 (940)	42.75	-	16
0.29	980 (950)	0	(1.96)	145
0.21	1000 (975)	0	(1.44)	360
0.20	980 (950)	0	(1.51)	943
0.19	970 (940)	0	(1.46)	1527

TABLE 4.4

STEEL: 2V-HDR. Results of the HDR expriments.

Roll speed: 0.31 m/sec. Mean austenite grain size is 1150 μm.

CAST No (REDUCTION)	ROLL TEMP (Hold Temp) °C	RECRYSTALLISATION %	GRAIN SIZE μm	HOLD TIME seconds
VMC 81	(quenched from 1000°C)	-	1170	-
VMC 82 (0.335)	927 (900)	8.5	-	100
VMC 83 (0.39)	906 (876)	15.9	-	120
VMC 84 (0.40)	880 (860)	5.03	-	240
VMC 85 (0.27)	958 (928)	25.8	-	480
VMC 86 (0.22)	960 (930)	14.7	-	300
VMC 87 (0.21)	929 (900)	0	1190	120
VMC 88 (0.31)	903 (873)	0	1160	180
VMC 89 (0.39)	880 (850)	0	1180	180

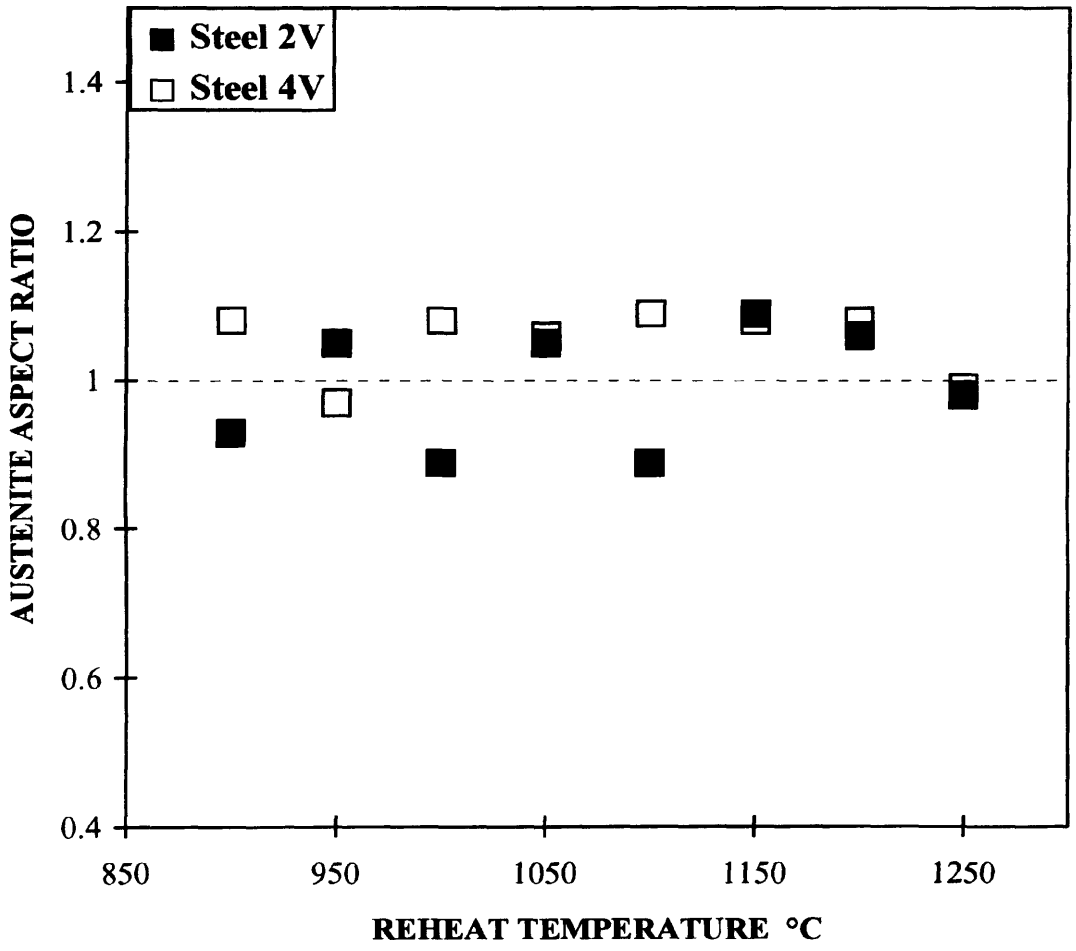

Fig. 4.1 **Measured austenite aspect ratios of slabs reheated to the appropriate temperature. 0.5 hr anneals.**

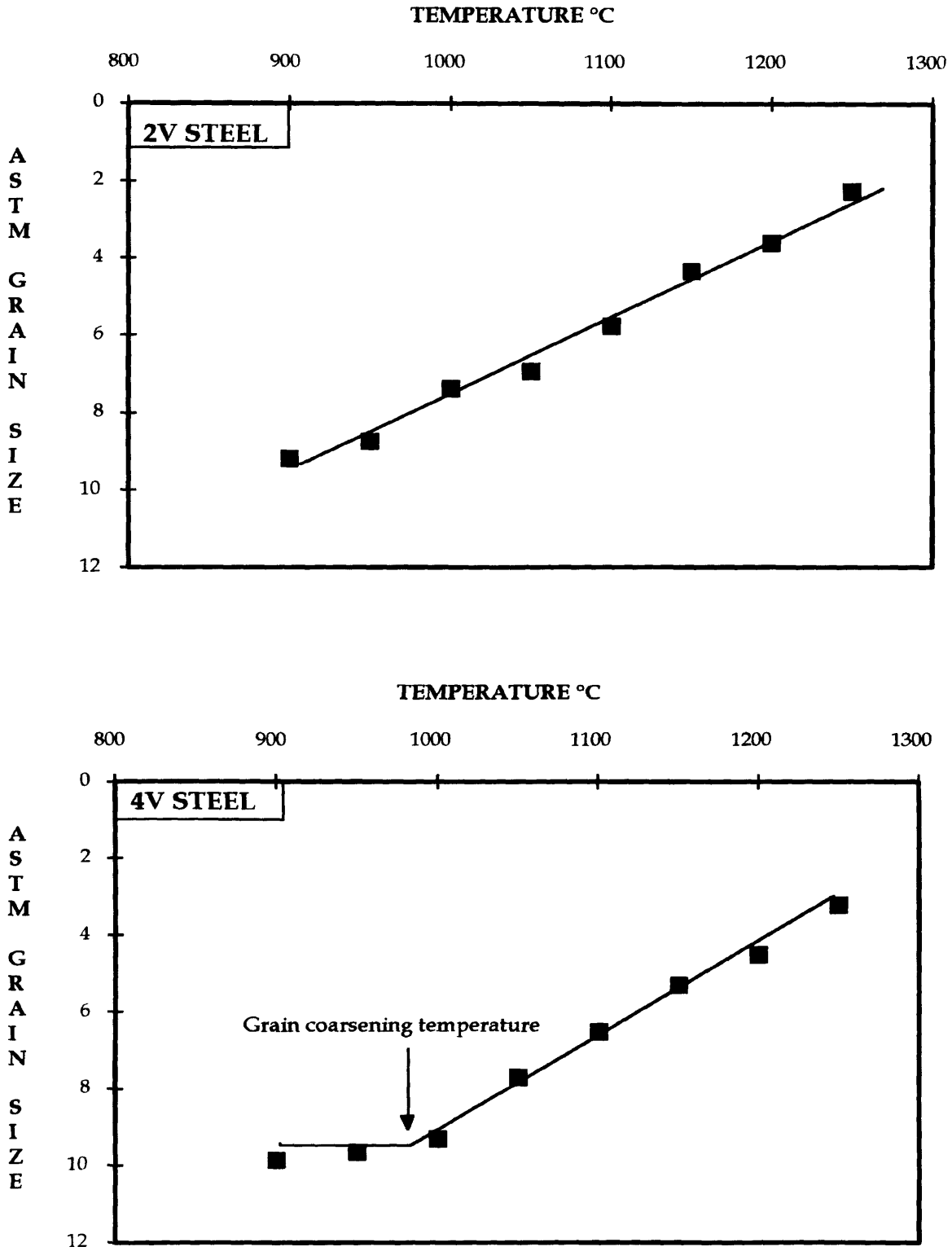

Fig. 4.2 **Dependence of reheated austenite grain size of the two steels on reheating temperature. 0.5hr anneals.**

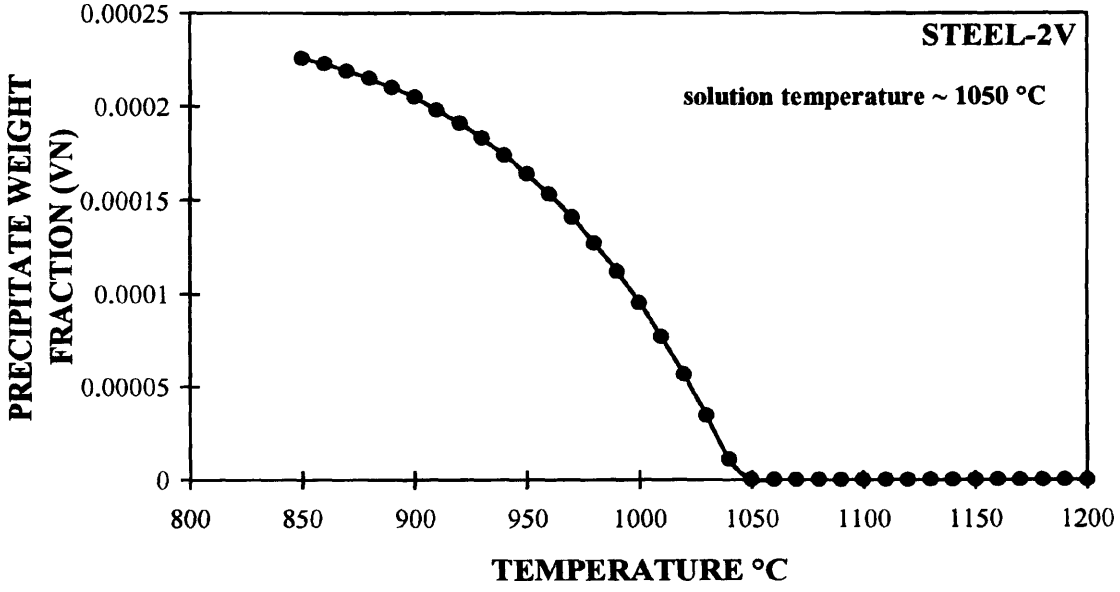

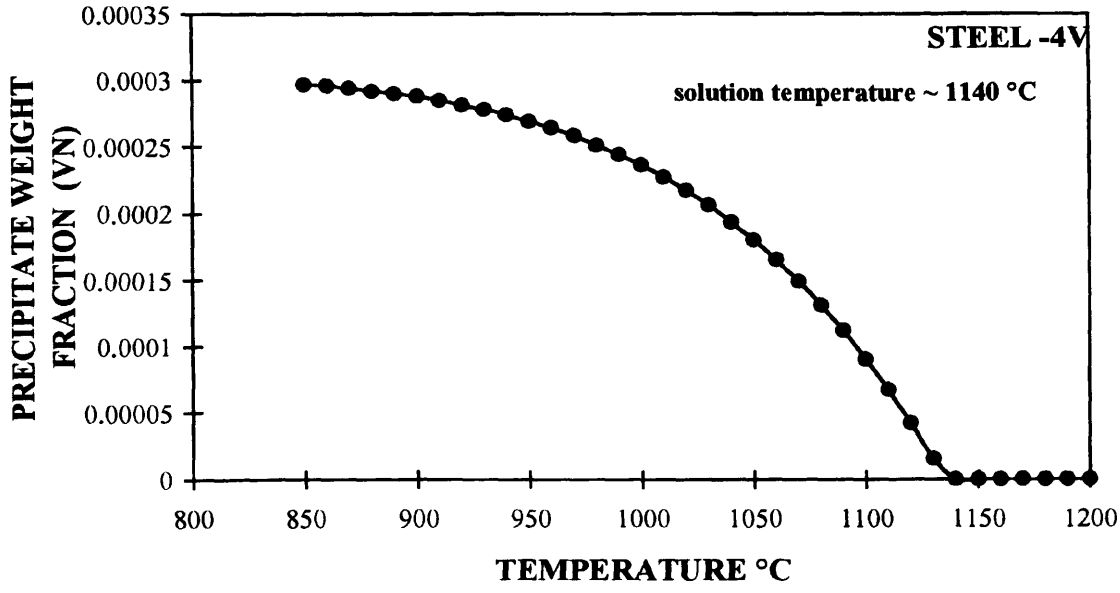

Fig. 4.3 **Calculated dependance of weight fraction precipitate (VN) on reheating temperature of the two steels.**

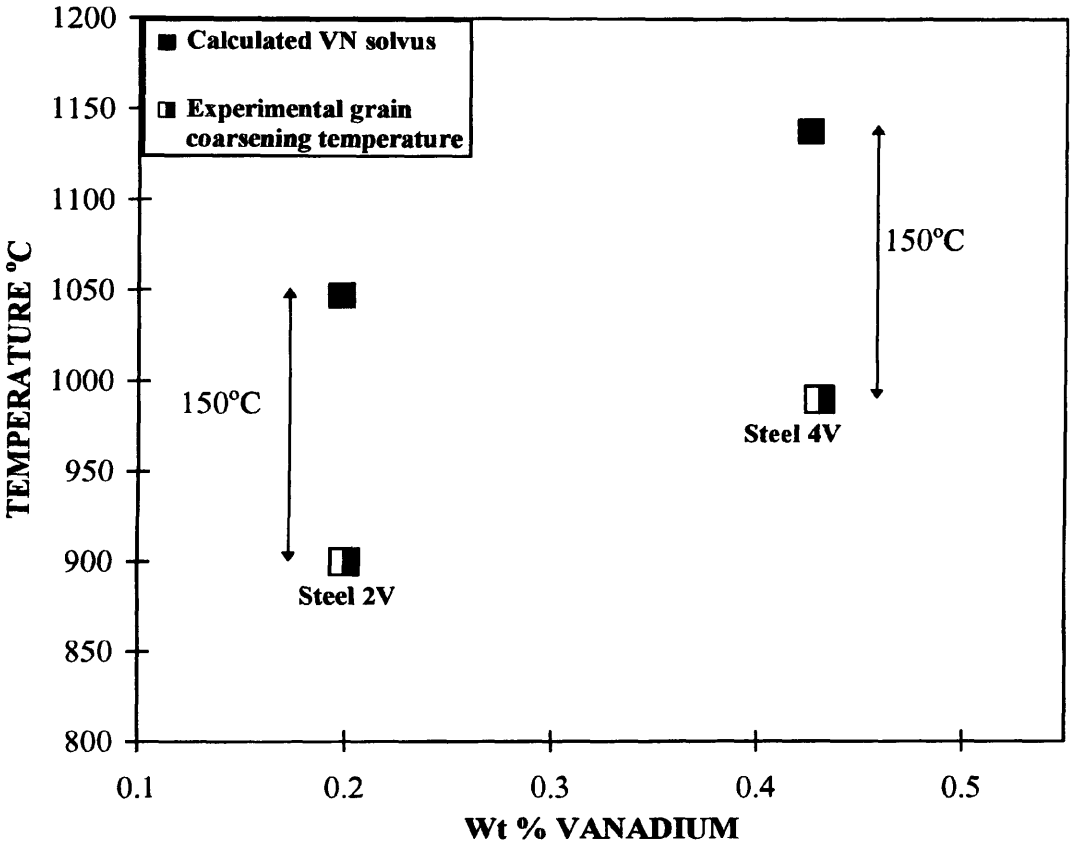

Fig. 4.4 **Relationship between the grain coarsening and VN solvus temperature of the two steels.**

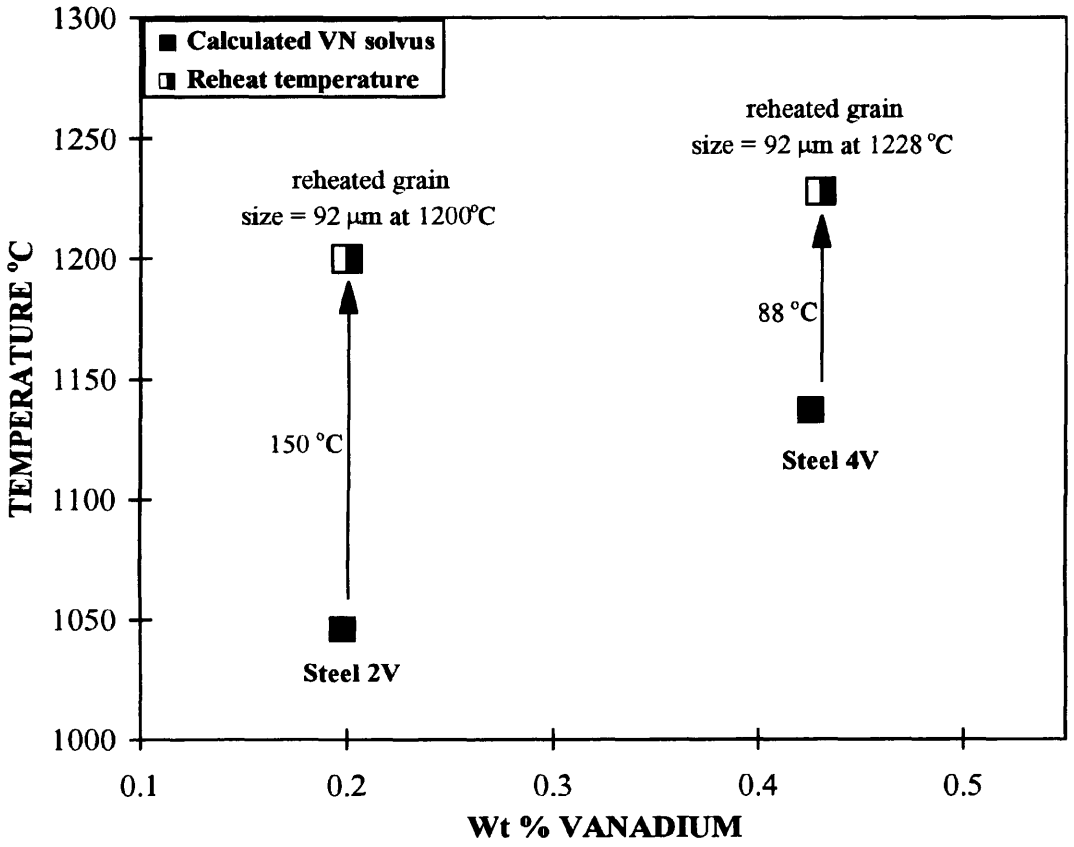

Fig. 4.5 **Relationship between the VN solvus and reheat temperature to yield a reheated grain size of 92 μm for both the steels.**

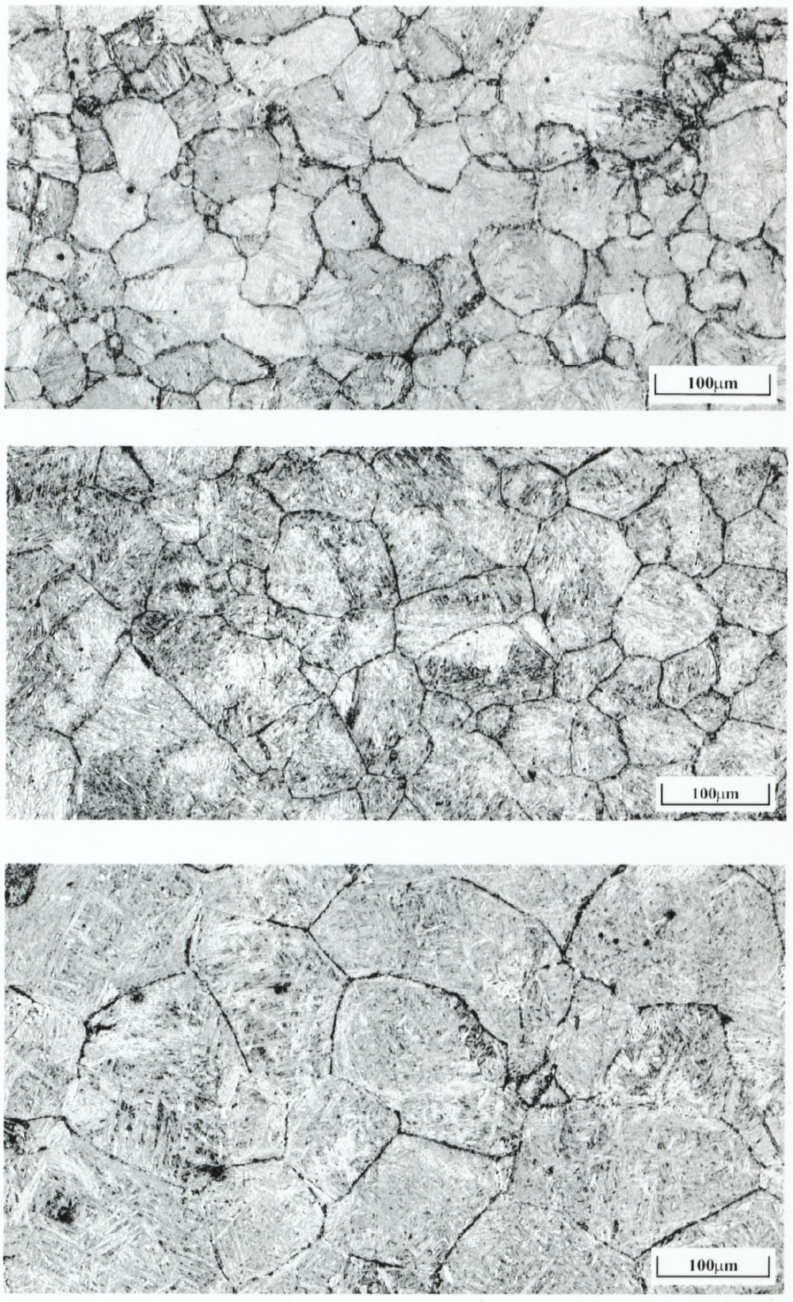

Fig. 4.6 Reheated austenite grain structure of 0.43% vanadium steel (4V).

(a) Reheated at 1150°C - average austenite grain size of 51μm

(b) Reheated at 1200°C - average austenite grain size of 67μm

(c) Reheated at 1250°C - average austenite grain size of 105μm

(a)

(b)

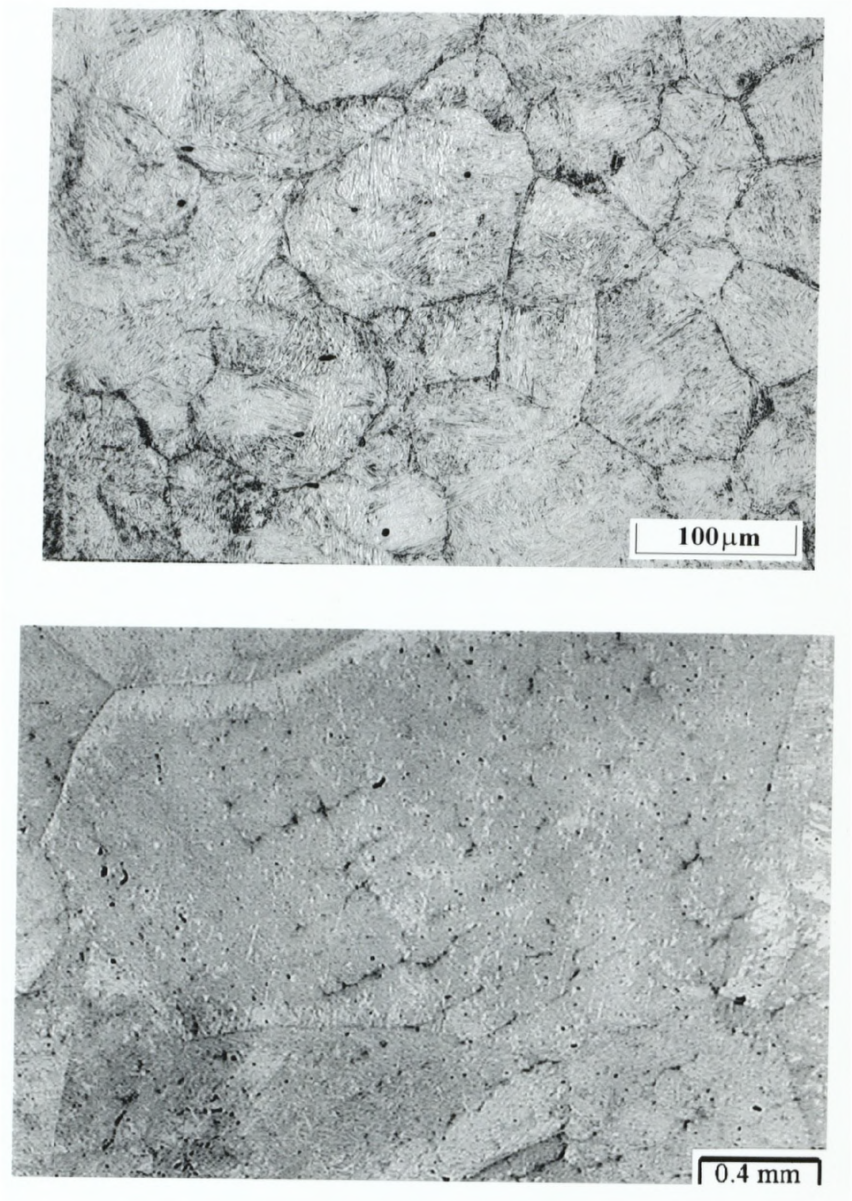

Fig. 4.7 **Reheated and as-cast austenite grain structures.**

(a) 2V reheated to 1200°C for 0.5hr. Mean grain size is 92 μm.

(b) 2V-HDR quenched from 1000°C. Mean grain size is 1170 μm.

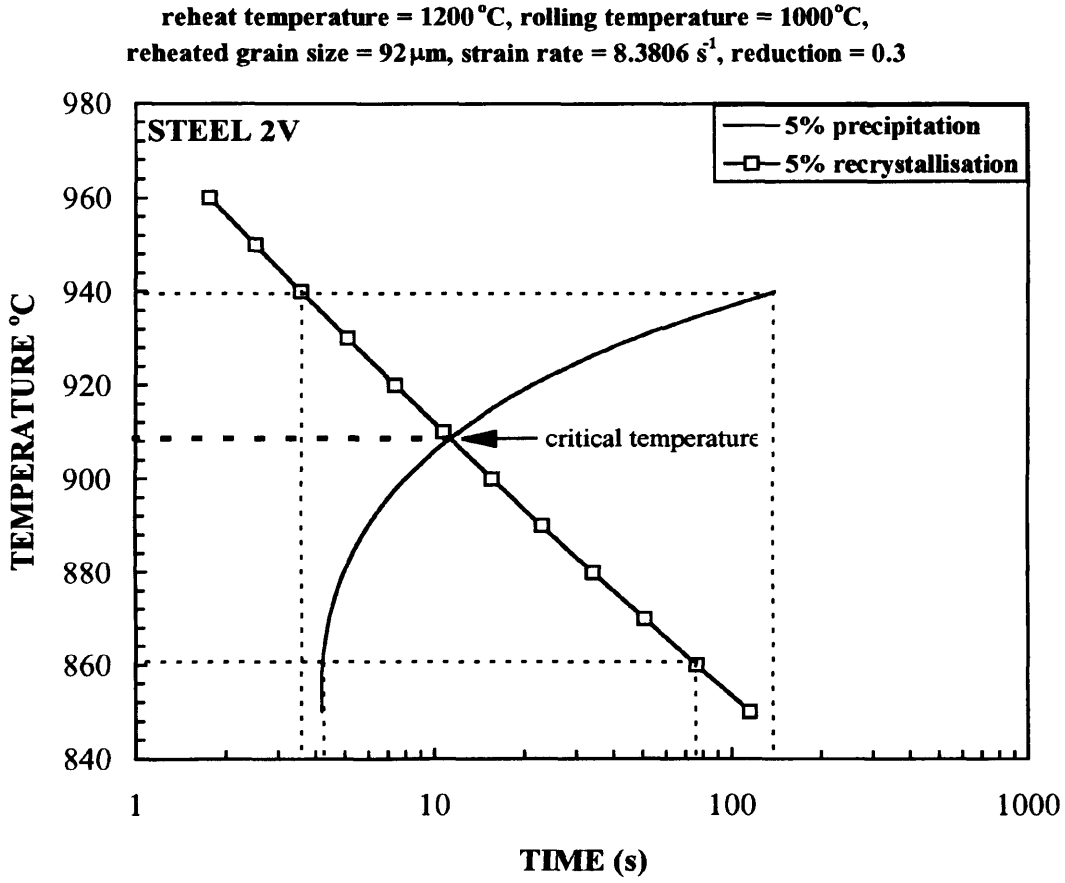

Fig. 4.8 **Calculated times to 5% precipitation and recrystallisation of 2V for the stated conditions.**

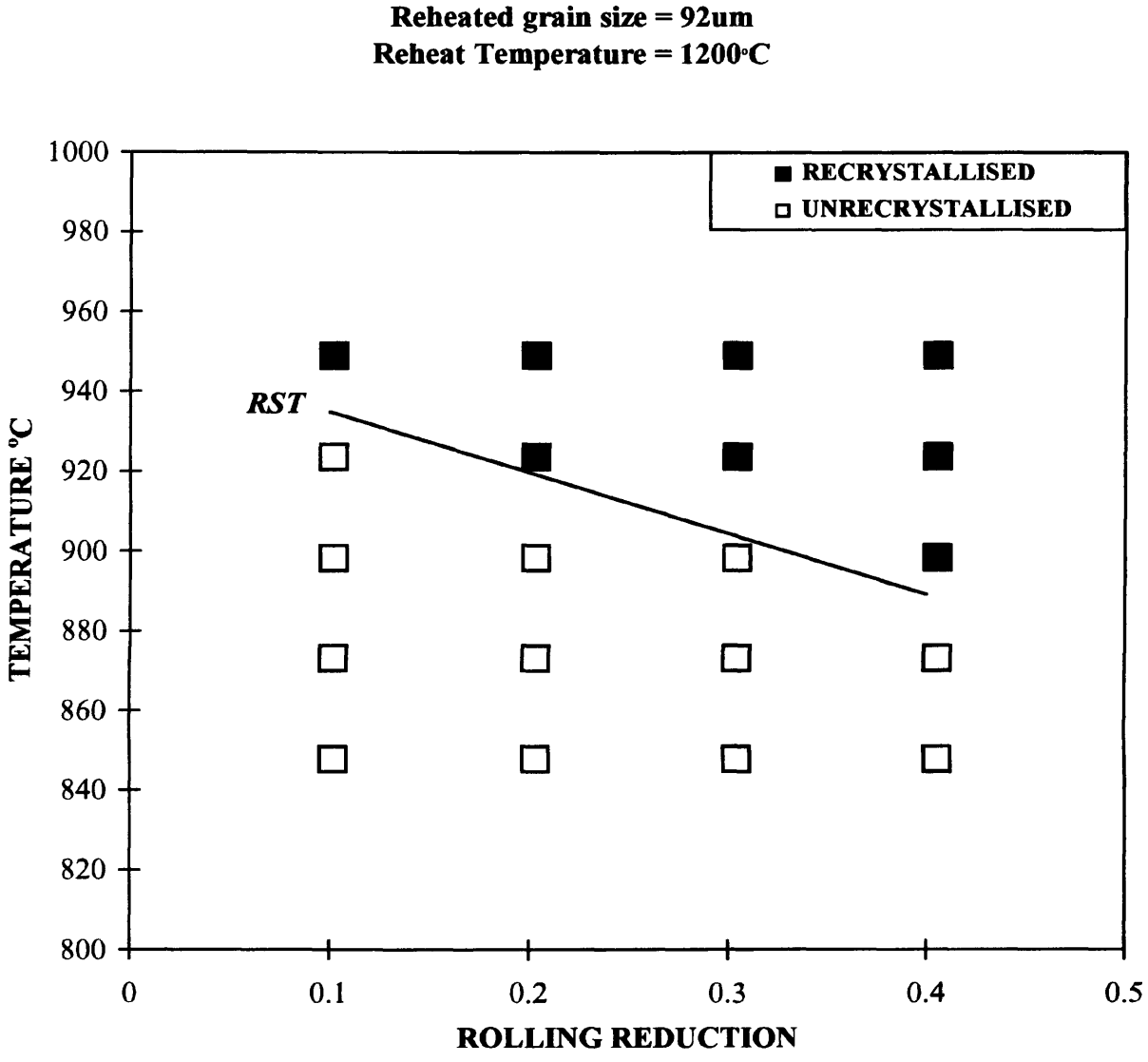

Fig. 4.9 **Method for determining the model RST, separating regions of recrystallised and unrecrystallised austenite.**

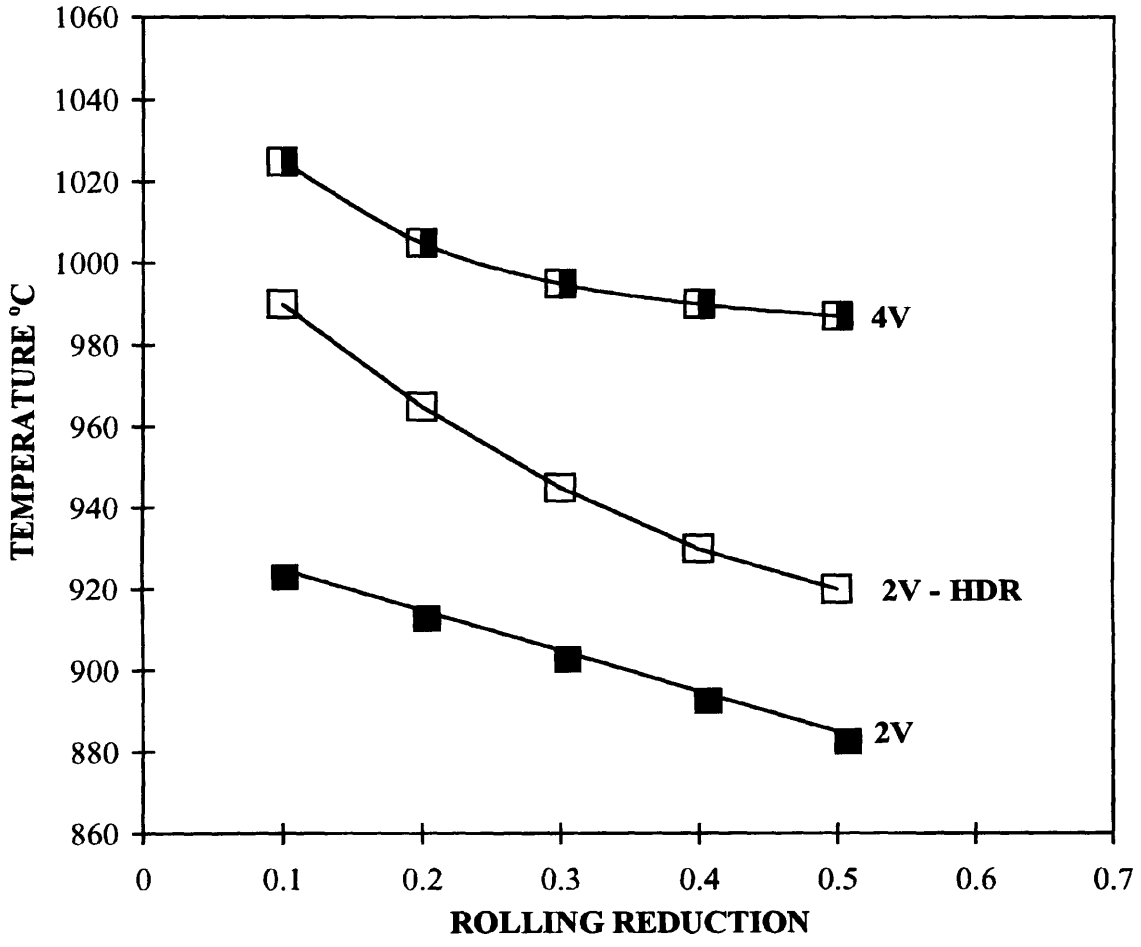

Fig. 4.10 **Predicted dependence of model RST's of steels 2V, 2V-HDR and 4V on rolling reduction for reheated austenite grain size of 92 μm for CCR and 1150 μm for HDR.**

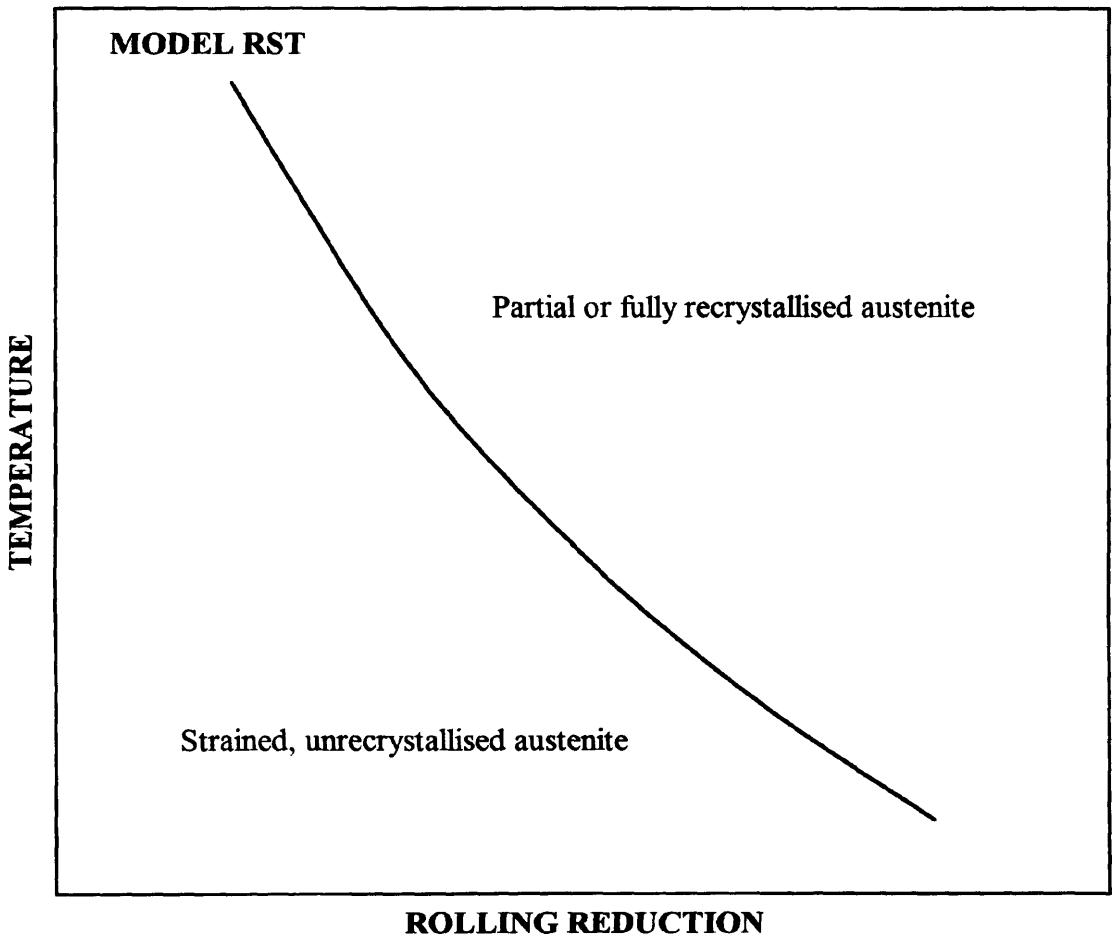

Fig. 4.11 Schematic of the unrecrystallised and fully recrystallised austenite regions relative to the RST.

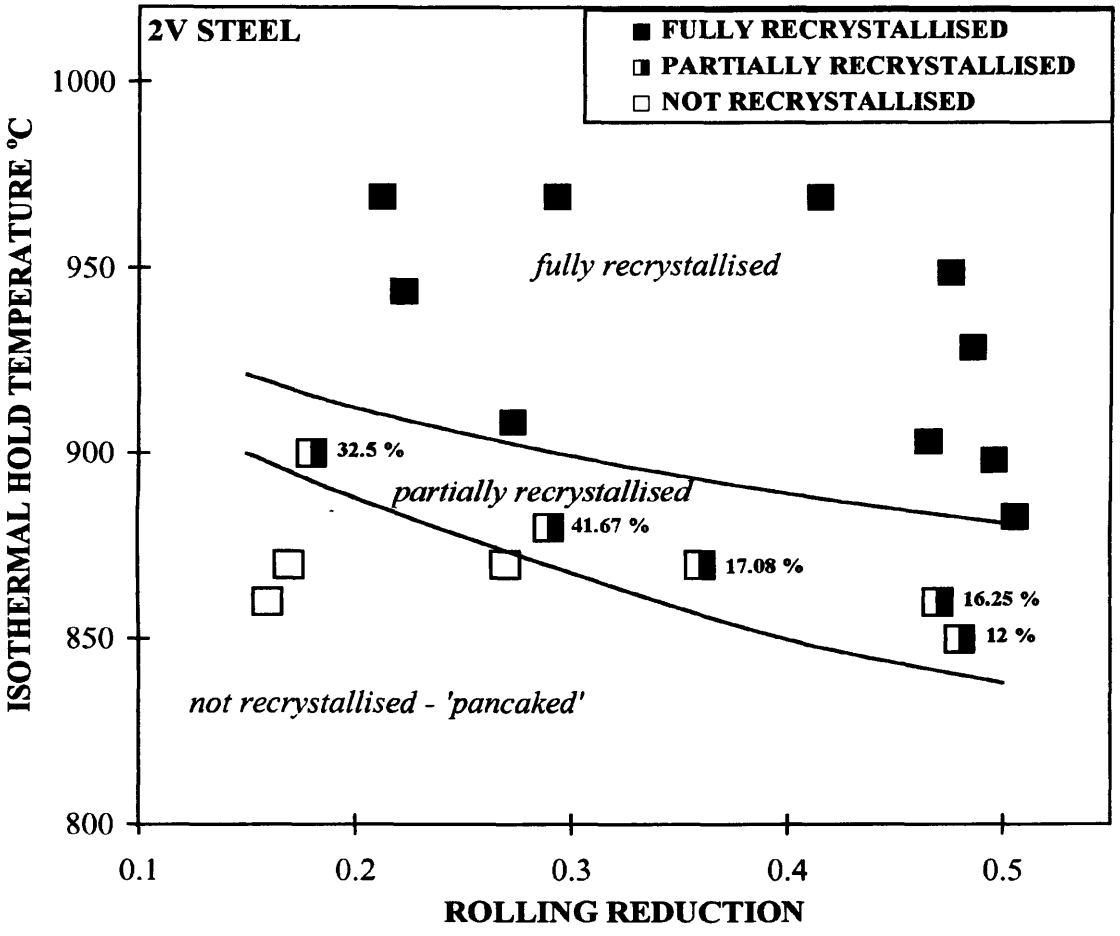

Fig 4.12 **Results of recrystallisation experiments on reheated austenite of steel 2V. The figures adjacent to the data points in the partially recrystallised region is the percent recrystallisation.**

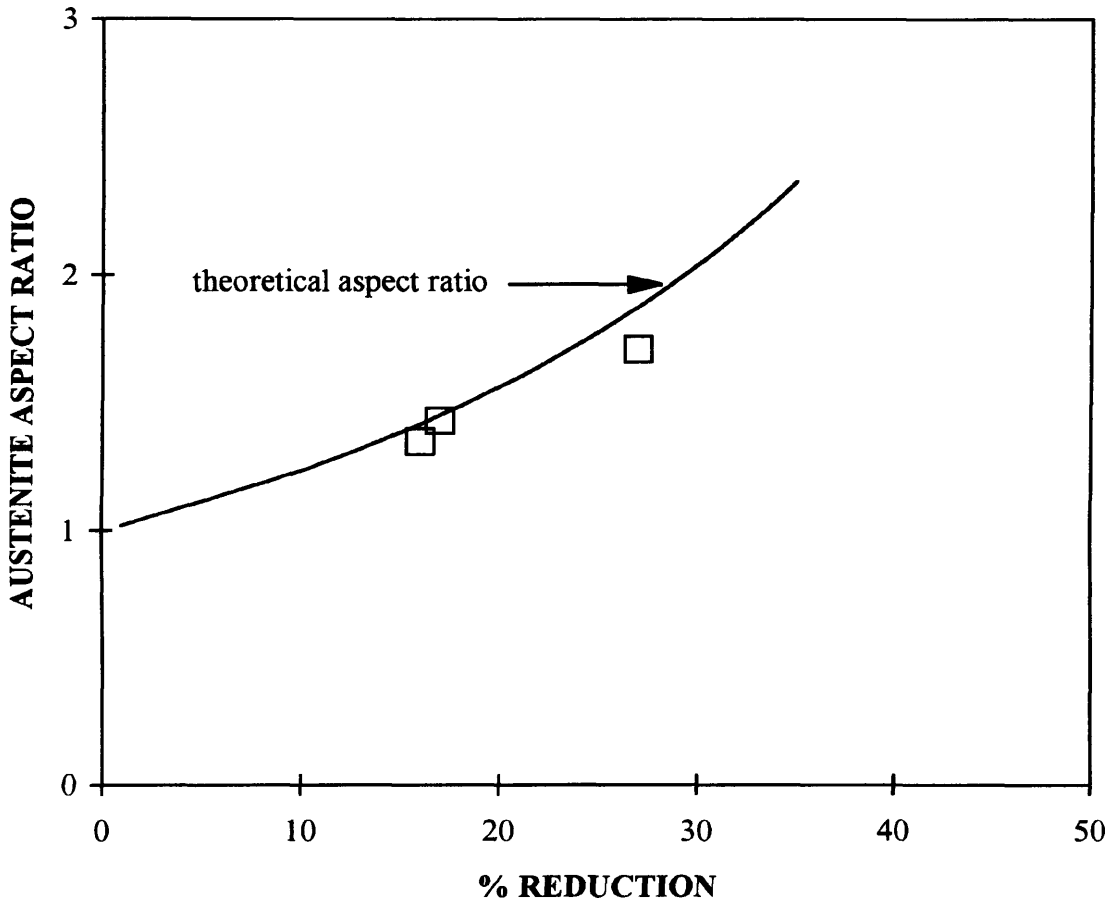

Fig. 4.13 **Relationship between the theoretical and measured aspect ratios of specimens exhibiting nil recrystallisation - steel 2V.**

(a)

(b)

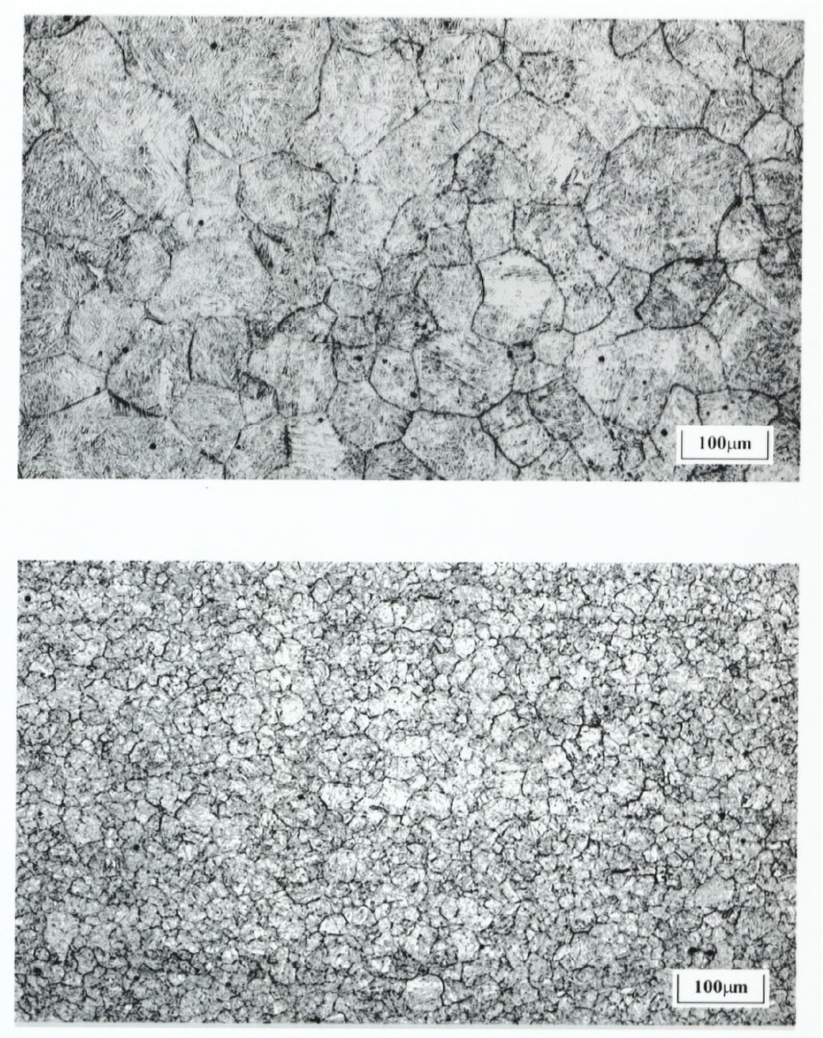

Fig. 4.14. Reheated and fully recrystallised grain structure of the 0.20% vanadium steel (2V).

(a) Reheated to 1200°C for 0.5hr. Average austenite grain size of 92μm.

(b) Reheated to 1200°C, rolled to 50% reduction at 900°C, held at 885°C for 13 seconds and quenched. Fully recrystallised average austenite grain size of 20.25μm.

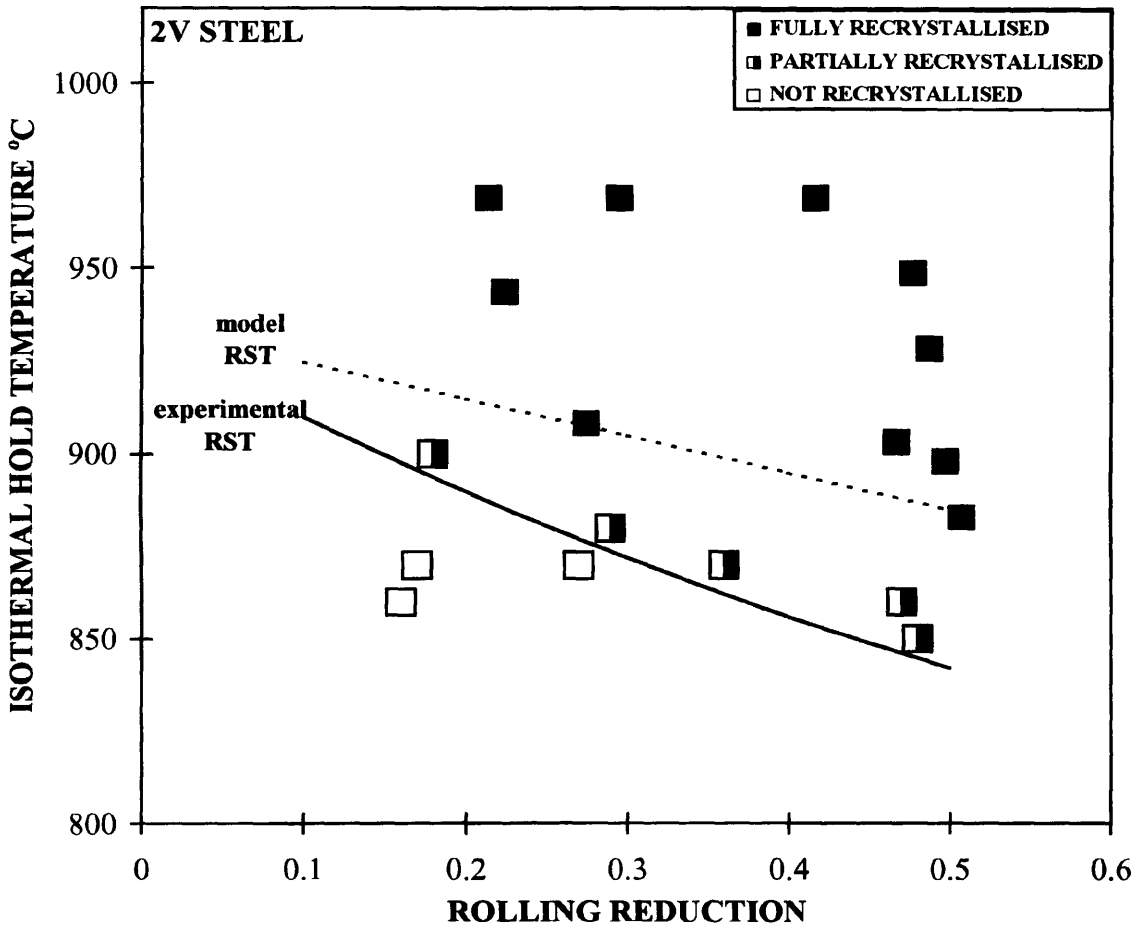

Fig. 4.15 Comparison of the experimental and model RST of steel 2V.

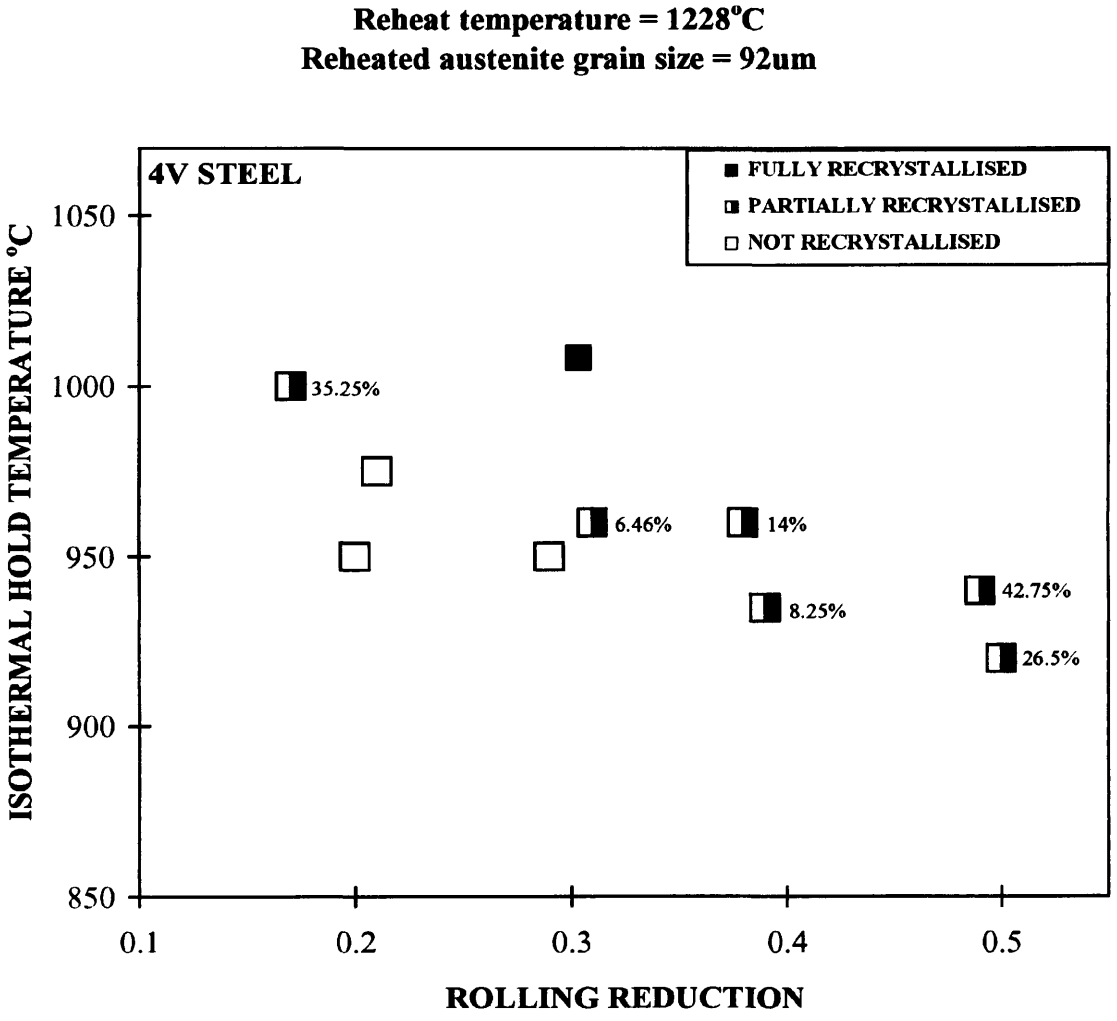

Fig. 4.16 **Results of recrystallisation experiments on reheated austenite of steel 4V.**

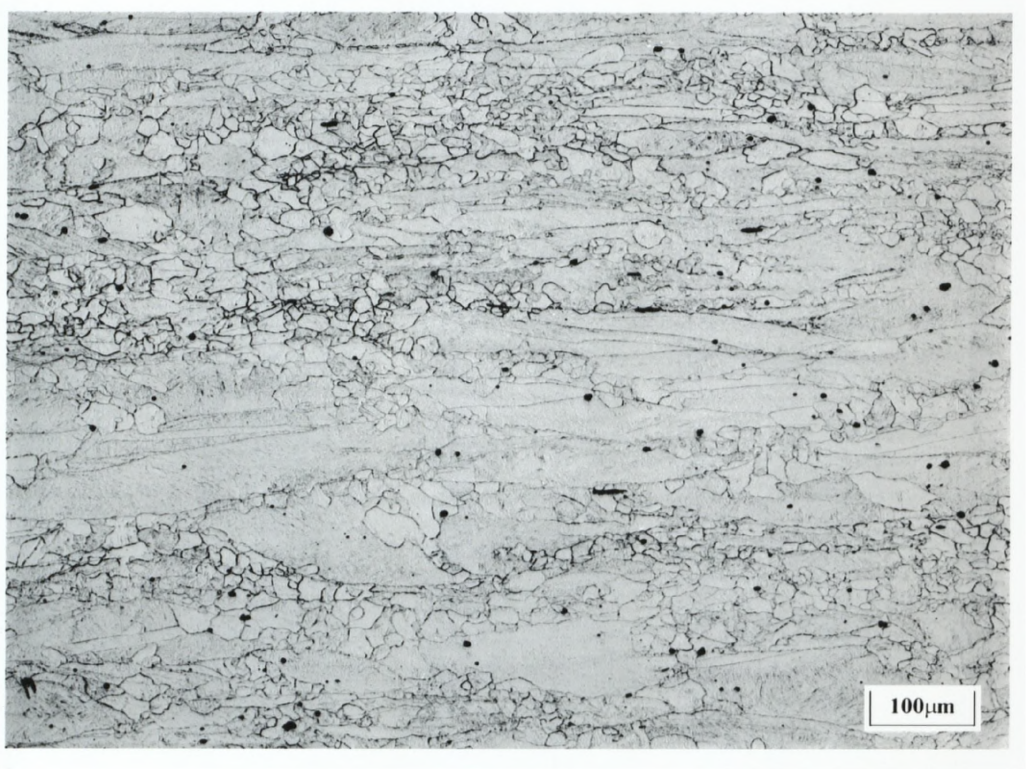

Fig. 4.17 Partially recrystallised (26.5%) microstructure of steel 4V; Reheated 1230°C, 50% reduction at 960°C, isothermally held at 920°C for 27 seconds and quenched.

(a)

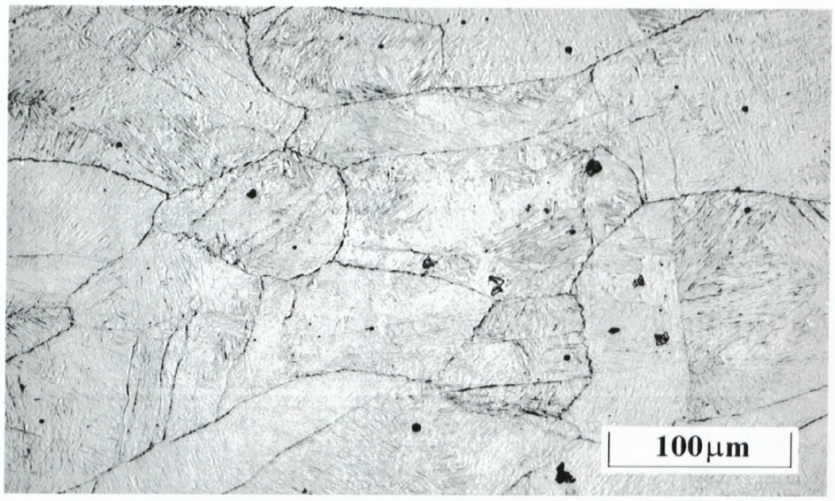

(b)

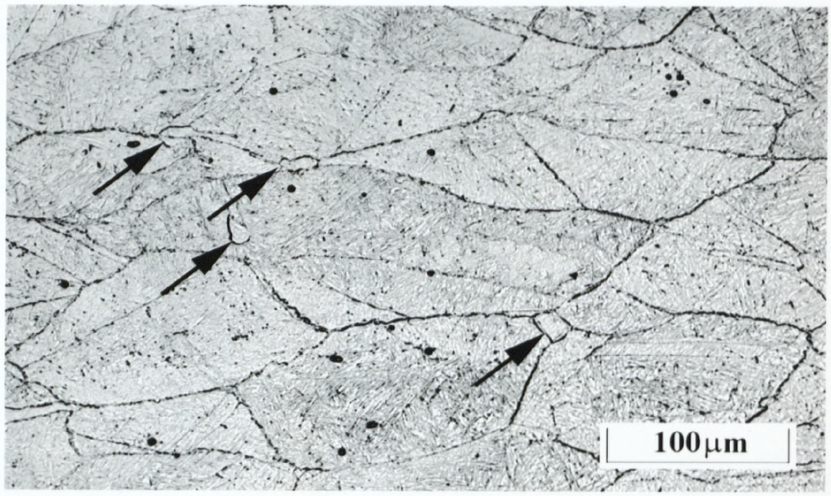

Fig. 4.18 Typical microstructures following single pass rolling of the 0.43% vanadium steel (4V).

(a) Reheated 1228°C, rolled to 21% reduction at 1000°C, isothermally held at 975°C for 360 seconds and quenched. Unrecrystallised grain structure.

(b) Reheated 1228°C, rolled to 31% reduction at 990°C, isothermally held at 960°C for 90 seconds and quenched. New grains initiating.

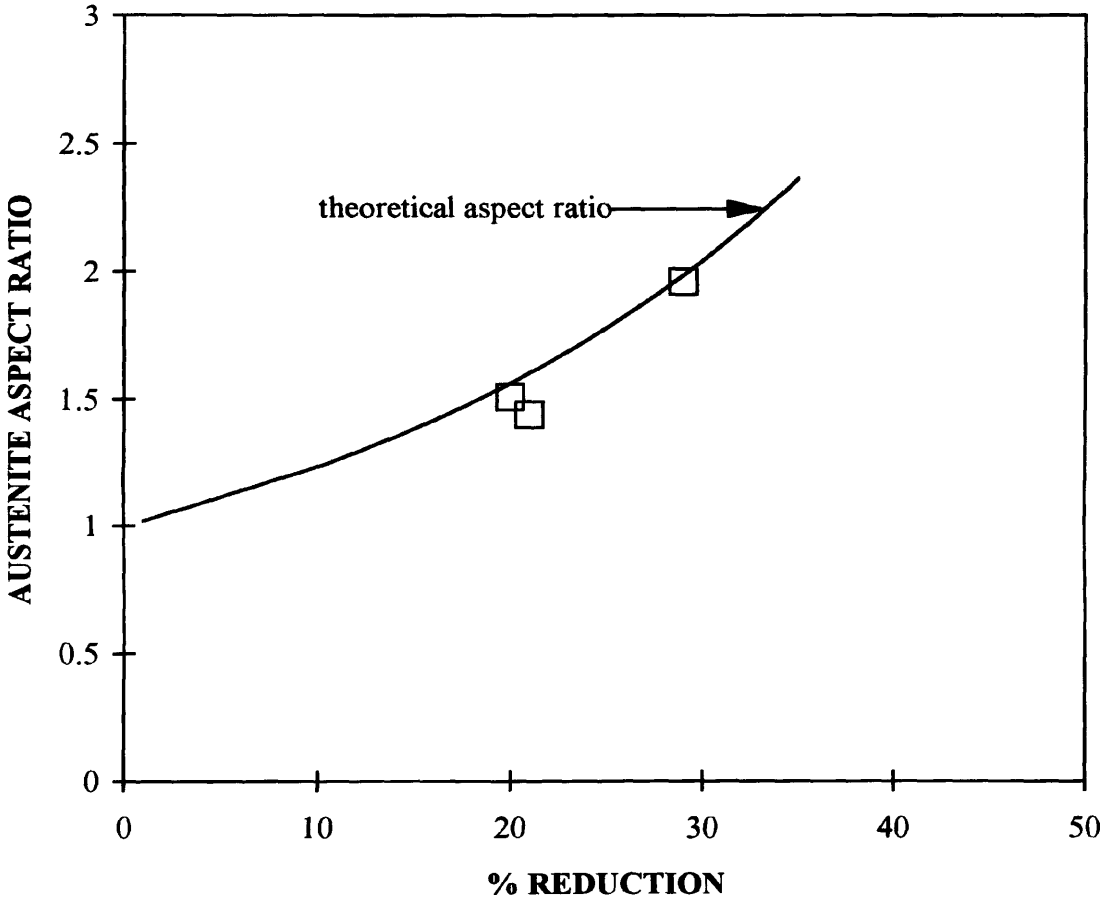

Fig. 4.19 **Relationship between the theoretical and measured aspect ratios of specimens exhibiting nil recrystallisation - steel 4V.**

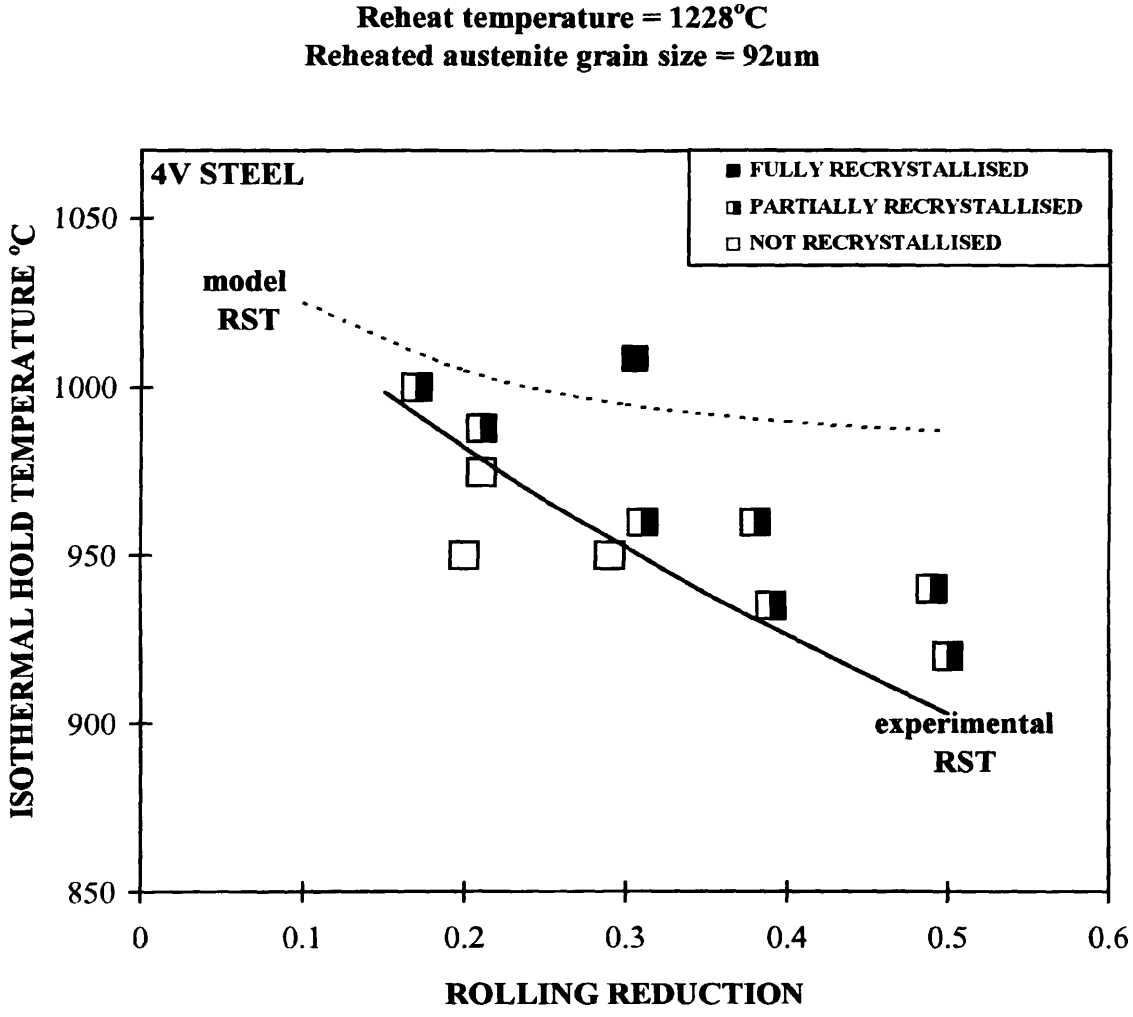

Fig. 4.20 Comparison of the experimental and model RST of steel 4V.

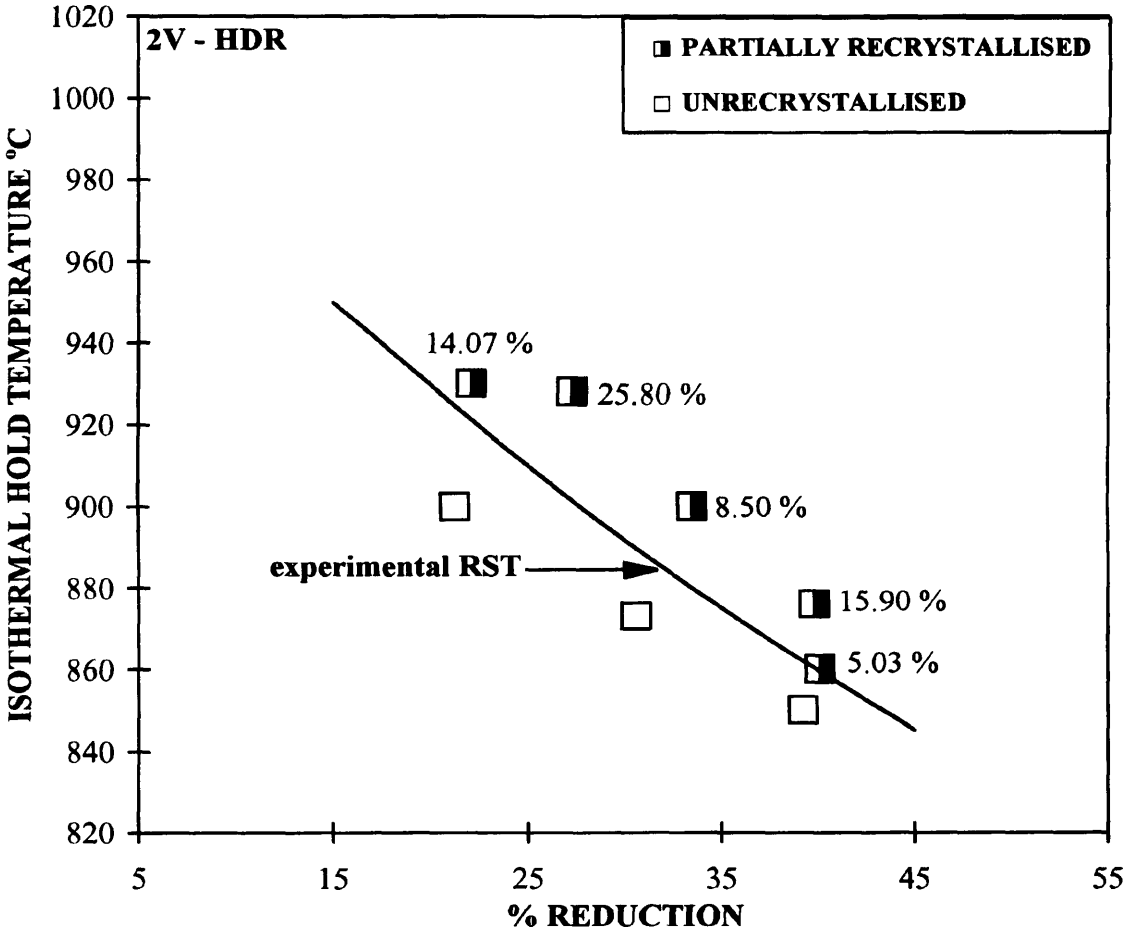

Fig. 4.21 **Experimental RST of 2V-HDR. The figures adjacent to the data points are the percentage values of recrystallisation.**

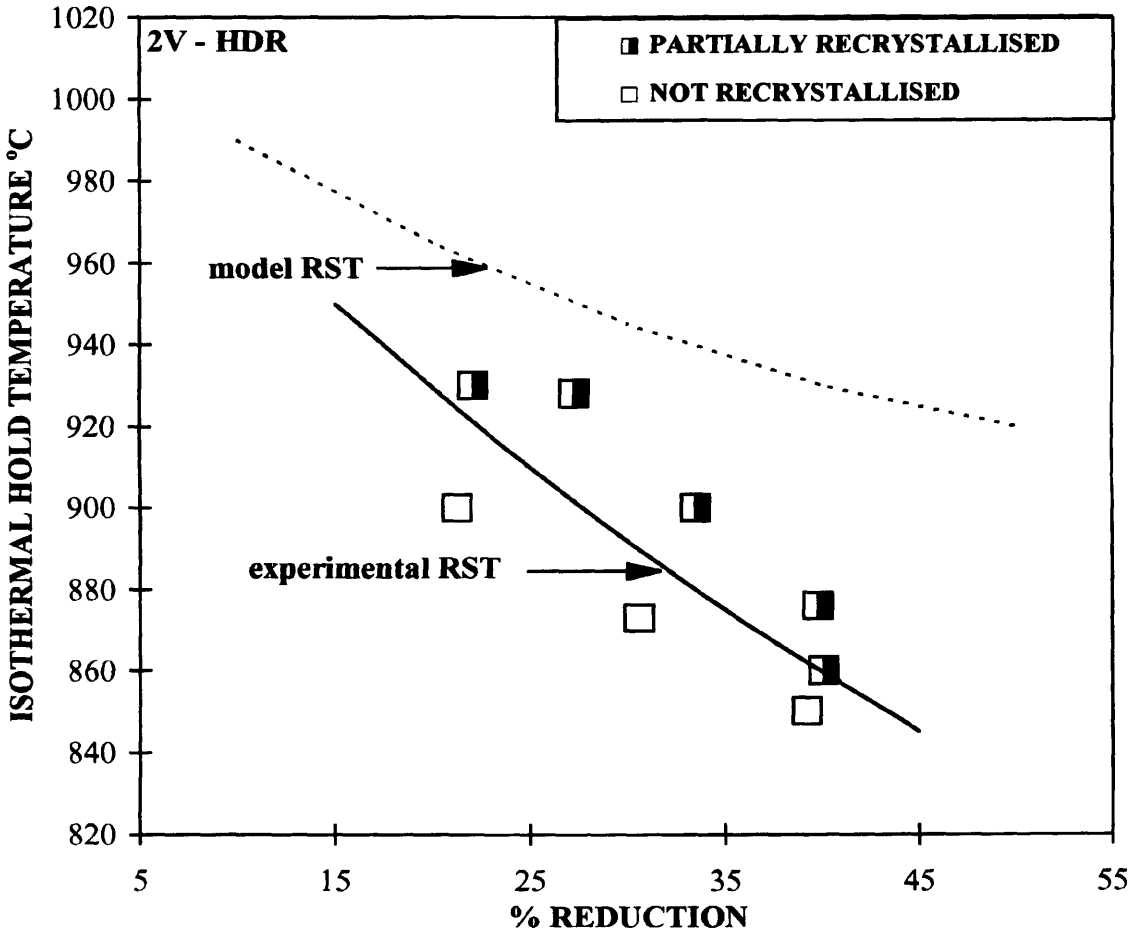

Fig. 4.22 Comparison of the experimental and model RST of steel 2V - HDR.

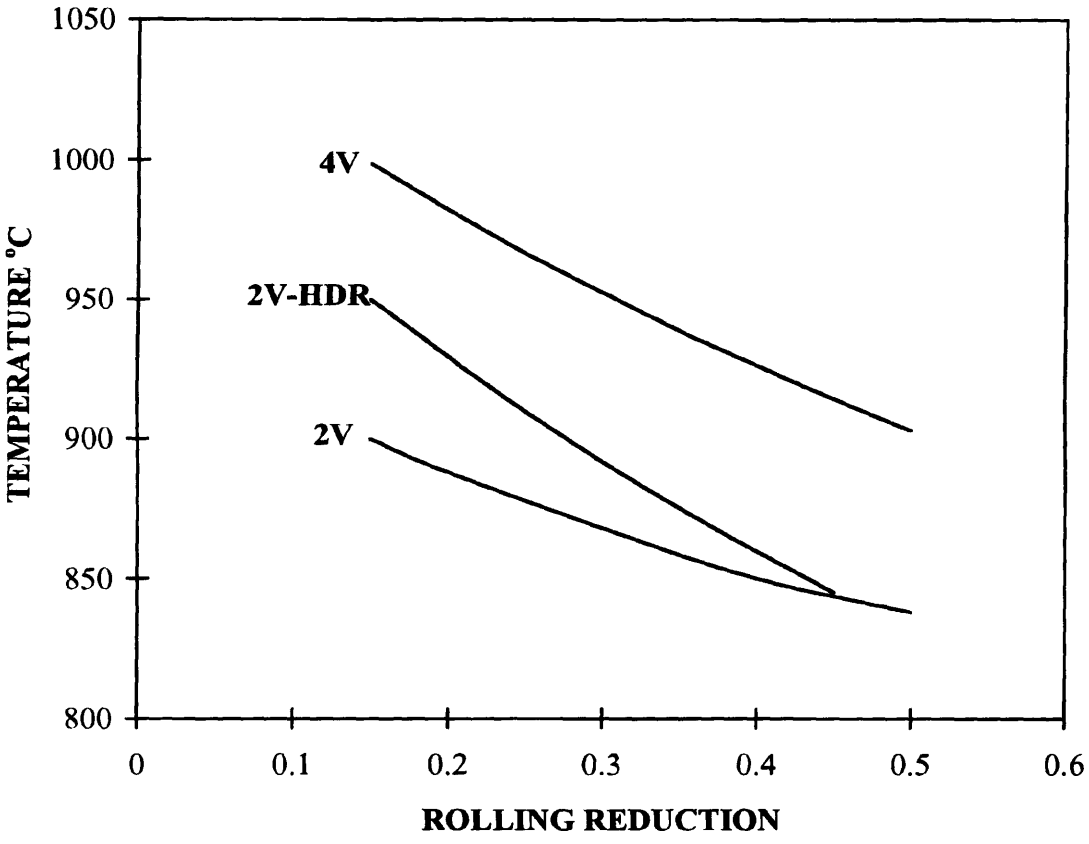

Fig. 4.23 Experimental RST's of the three steels.

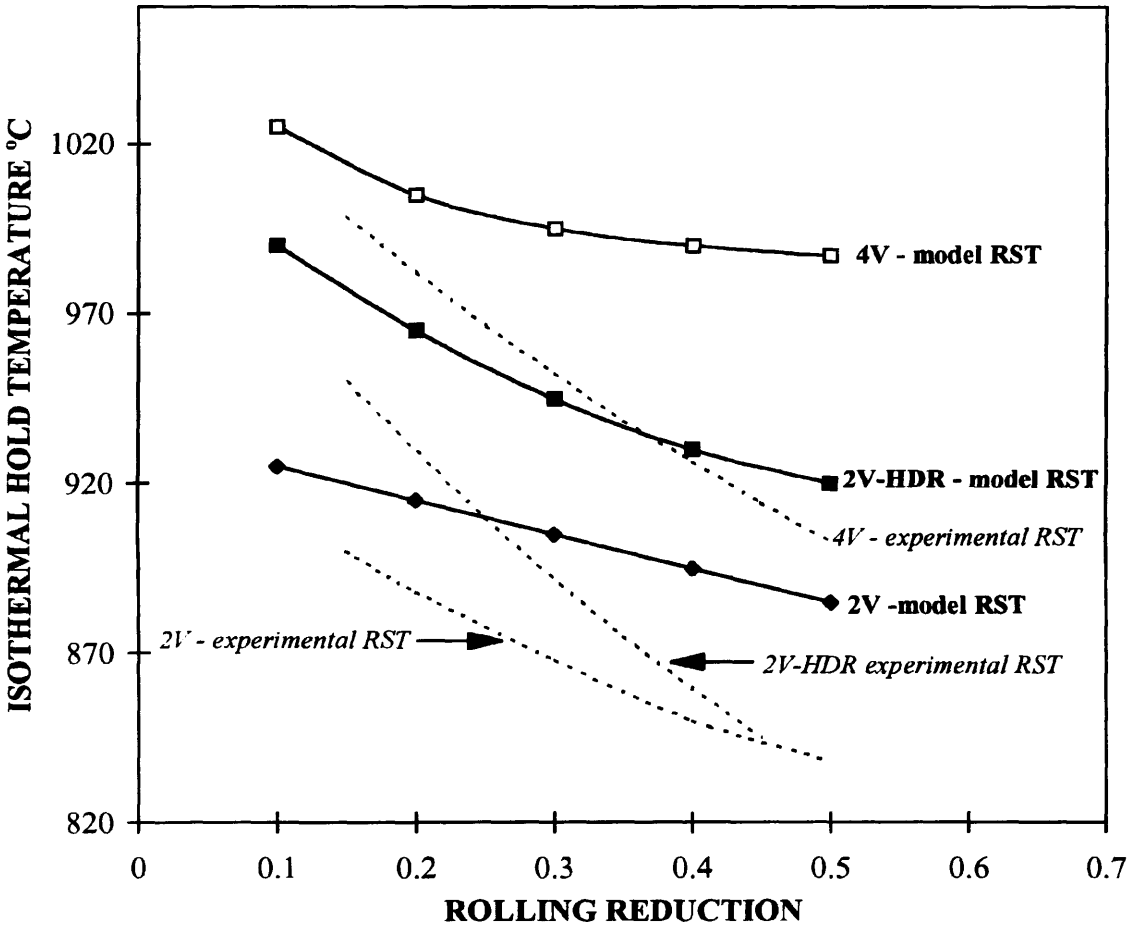

Fig. 4.24 Model and experimental RSTs of the three steels.

CHAPTER 5

MODIFICATIONS TO THE MODEL

5.1 Effect of solute drag on $t_{0.05RX}$

It is known that solute atoms of microalloying elements retard recovery and the onset of recrystallisation in deformed austenite. From experimental data in the literature [64-71], the retarding effect of various solutes increases in the following ascending order:
Ni < Cr < Mn < V < Mo < Ti < Nb.

Yamamoto *et al* [99] investigated the role of V and Nb solute atoms in the retardation of static recovery and the onset of recrystallisation in deformed extra-low carbon (0.002 wt%) austenite. Most microalloying elements were expected to remain dissolved in the steel, and the amount of stoichoimetric precipitates was expected to be low. It was therefore assumed that the retardation of recrystallisation was due to solute drag.

For an equal amount of solute V or Nb (0.10 wt%) deformed at 900 and 1000 °C (d_o = 140 μm, ε = 0.693), they found that the recrystallisation of V austenite was much faster than the corresponding Nb austenite, as shown in Fig. 5.0.

As has been explained earlier that, to initiate this experimental campaign, a solute drag factor F was incorporated in the equation for $t_{0.05RX}$ as a first approximation based on the data of Jonas *et al* [66]. However, his data related to 0.05 wt% C steel containing single additions of 0.115 wt% V and 0.035 wt% Nb tested at 1000 °C and from solubility considerations, it was assumed that strain induced precipitation did not occur at the test conditions. In contrast, the data of Ouchi is for the same wt % addition of V and Nb in ultra low carbon steels in which the amount of precipitates is expected to be very low. This data is therefore more appropriate in comparing the relative solute drag effect.

To assess these effects in terms of the Dutta and Sellars' model, the factor F in the term " F · [V] " in equation (5.0) was varied to fit the equation to Ouchi's data.

$$t_{0.05RX} = A_{RX} \cdot d_o^{\,2} \cdot \varepsilon^{-4} \cdot \exp\frac{Q_{RX}}{RT} \cdot \exp\left\{\left(\frac{B_{RX}}{T} - 185\right) \cdot F \cdot [V]\right\} \qquad \textbf{(5.0)}$$

Such comparison as was possible is shown in Fig. 5.1. For the Nb steel, equation (5.0) when F = 1.0, fits Ouchi's data reasonably well. For the V steel, it was necessary to reduce F from 1.0 to 0.1 in order to obtain the same degree of agreement between equation (5.0) and Ouchi's data. Also plotted in this figure is the original approximation, that is when F = 0.3. It is clear that this original approximation overestimates the solute drag effect of V, that is, the estimated time to the onset of recrystallisation is too long. Substituting for Q_{RX}, B_{RX} and F, the time to 5% recrystallisation, equation (5.0) becomes:

$$t_{0.05RX} = A_{RX} \cdot d_o^{\,2} \cdot \varepsilon^{-4} \cdot \exp\frac{300{,}000}{RT} \cdot \exp\left\{\left(\frac{2.75 \cdot 10^5}{T} - 185\right) \cdot [V] \cdot 0.1\right\} \qquad \textbf{(5.1)}$$

5.12 Effect of grain size on $t_{0.05RX}$

Dutta and Sellars reviewed a large amount of literature data and found a quadratic dependence of $t_{0.05RX}$ on the initial austenite grain size, d_o, as :

$$t_{0.05RX} \propto d_o^{\,2} \qquad \textbf{(5.2)}$$

The grain sizes were in the range 25 - 250 μm. Medina [100] reported the results of deformations on three steels microalloyed with 0.043, 0.060 and 0.093 wt% V. The initial austenite grain sizes when reheated at 1260 °C for 30 minutes were 172, 167 and 165 μm respectively for the three compositions. They found a linear dependency of $t_{0.5RX}$ on d_o for this very small range of grain size. The grain size in the present experiments ranged from 92 μm to 1150 μm, a much greater range than that considered by either Medina or Dutta and Sellars.

A typical value of $t_{0.05RX}$ for HDR, for an ingot rolled to 27.3% reduction at 958 °C and then isothermally held at 928 °C for 480 seconds, is plotted in Fig. 5.2 and compared with the prediction of Dutta and Sellars equation (5.1) fitted to data at grain sizes of 80 and 220 μm. Clearly the quadratic dependence of $t_{0.05RX}$ on d_o is inappropriate to the large grain size applying in the present research.

The results of Priestner *et al* [101] on as-cast and reheated austenite of 0.1%C, 0.04% Nb also shows that, as in this work, the experimental RST was higher for the HDR material than the CCR processed material. Fig. 5.3. The austenite grain sizes in their experiments were 83 and 850 μm for CCR and HDR respectively. The problem with the model, for their experimental materials and conditions was that it predicted too large a dependency of RST on grain size. The model produced good agreement with their experimental results for both as-cast and reheated austenites by reducing the dependence of $t_{0.05RX}$ on d_o from the power of 2 to the power of 1; that is a linear dependence. Also, the pre-exponential constant A_{RX} (equation (5.1)) had to be changed at the same time from 6.75×10^{-20} to 1.23×10^{-17}. In fact, a linear dependence on grain size has also been used by other authors[55].

From the above considerations and the results plotted in Fig. 5.2, the pre-exponential constant A_{RX} is increased from 6.75×10^{-20} to 1.74×10^{-17} such that equation (5.1) can be rewritten for V steels as:

$$t_{0.05RX} = 1.74 \times 10^{-17} \cdot d_o \cdot \varepsilon^{-4} \cdot \exp\frac{300{,}000}{RT} \cdot \exp\left\{\left(\frac{2.75 \times 10^5}{T} - 185\right) \cdot [V] \cdot 0.1\right\} \quad \textbf{(5.3)}$$

5.13 Experimental fraction recrystallised

For all partially recrystallised specimens, the isothermal hold times at temperatures had been calculated for the predicted time to 50% recrystallisation by conversion of the unmodified model $t_{0.05RX}$ using the Avrami equation. Fig. 5.4 shows that for each condition, the expectation from the model was that the specimens would exhibit 50% recrystallisation

whereas the experimental fraction recrystallised was below this by an amount depending on the deformation parameters.

Some data on V steels exists in the literature [54,56,58,60,62,64,68,100,], but very little of this has been directed specifically at a systematic study to evaluate the effect of variables on recrystallisation-precipitation kinetics and particularly on the effect on $t_{0.05RX}$ or $t_{0.05P}$.
The present research, however, yielded value of fraction recrystallised after selected times and deformations at selected temperatures.

The times to 50% recrystallisation ($t_{0.5RX}$) from the experimental isothermal hold times and fraction recrystallised were deduced first and then $t_{0.05RX}$ using the Avrami equation. The choice of the exponent k in the equation is important as it reflects the time interval between $t_{0.05RX}$ and $t_{0.95RX}$. This time interval decreases as k increases from a value of 1 to a value of 2. It was not possible from the experimental data to evaluate the value of the exponent k, which is obtained from plots of log (ln(1/1-x) versus log t (s) for a given set of deformation conditions. However, the experimental results have shown that at comparable composition, the RST for the HDR is higher than for the CCR material. Also the grain size is almost 12.5x that for the reheated austenite. The large grain size raises the temperature for the start of recrystallisation after constant deformation. As the tendency is for recrystallisation to be nucleated on grain boundaries, the initial grain size would therefore play a strong role in determining the number of sites per unit volume available for nucleation, that is, $t_{0.05RX}$ would be higher for a large grain size than a small grained material at comparable deformation conditions. The time to the onset of recrystallisation is delayed to longer times with a large initial grain size. As there would be fewer nucleation sites per unit volume due to a relatively small total grain boundary area of a large grain size, the time interval $t_{0.95RX}$ - $t_{0.05RX}$ is also expected to be longer.

From these considerations, a value of 1 for CCR and 0.8 for HDR has been assumed for deducing $t_{0.05RX}$ from the experimental data using equations (1.8) and (5.3).

These "experimental" values are tabulated in Table 5.1 and compared using the modified model, equation (5.3), in Fig. 5.5. Also plotted in this figure are actual experimental $t_{0.05RX}$

values obtained from the data of Ouchi [99] and Medina [60]. It is seen that the model for the start of recrystallisation is a reasonable predictor of the data that was available.

5.14 Summary relating to $t_{0.05RX}$

The effect of V solute drag, relative to that of Nb, on recrystallisation kinetics has been established by fitting the equation to the data of Ouchi *et al.* This data related to ultra-low carbon steels containing the solutes and in which under the deformation conditions, it was assumed that the retardation of recrystallisation was due to solute drag. Having established the degree of solute drag, the original model was modified by incorporating a term " F· [V] " into the equation where F has been found to have a value of 0.1.

The pre-exponential constant A_{RX} and the exponent m, were varied to fit the experimental data for a typical HDR result to take into account the large range of grain size (92-1150 μm) in this investigation. A linear dependence of $t_{0.05RX}$ on d_o and a value of $1.74 \cdot 10^{-17}$ of A_{RX} were found to be more appropriate.
The model has then been modified by incorporating these parameters into the equation.

Finally, values of $t_{0.05RX}$ were deduced from the experimental value of fraction recrystallised after selected times and deformation at selected temperatures assuming values of the exponent k in the Avrami equation of 1.0 and 0.8 for the CCR and HDR steel respectively.
When these " experimental " results including the data of Ouchi and Medina were compared to the modified model values, it was found that the model for the start of recrystallisation was a reasonable predictor of the data that was available.

Having established the equation for $t_{0.05RX}$, the next stage was to perform a similar analysis to modify as appropriate, the equation for $t_{0.05P}$.

5.2 Start of strain induced precipitation

Dutta and Sellars original equation (2.5) for $t_{0.05P}$ was based on an inversion of the standard equation[102] for steady state nucleation rate, J, of the form:

$$J_S \approx \left(\frac{N^*}{a_\alpha{}^2}\right) \cdot D_{eff} \cdot X_\alpha \cdot \exp\left(\frac{-\Delta G^*}{k_\beta T}\right) \qquad (5.4)$$

where N* is the density of nucleation sites per unit volume, ΔG^* is the critical free energy for nucleation, X_α is solute concentration, T is the temperature, k_β is the Boltzmann's constant and D_{eff} is the diffusion coefficient of the solute.

The diffusion coefficient and activation energy for diffusion of V in austenite are [103]:

$D_{o(V)} = 3.65 \times 10^{-4}\ m^2s^{-1}$ and
$Q_{d(V)} = 293\ kJ\ mol^{-1}$

These values are used to calculate D_{eff} in equation (5.5) using the relationship:

$$D_{eff} = D_o \cdot \exp\left(\frac{Q_d}{RT}\right) \qquad (5.5)$$

The larger D_o for V than for Nb in austenite effectively decreases the value of the constant A_{PPT} in equation (5.3) by a factor $D_{o(Nb)} / D_{o(V)}$, where $D_{o(Nb)}$ is $1.4 \times 10^{-4}\ m^2s^{-1}$, and $Q_{d(Nb)}$ is 270 kJ mol^{-1}[7]. The new value of A_{PPT} equals 1.15×10^{-6}. That is, the more rapid diffusion of V results in a relatively shorter time to the onset of precipitation.

For nucleation of carbonitride particles, ΔG^* in equation (5.4) is of the form[102]:

$$\Delta G^* = \frac{16\pi\gamma^3 f_o}{3(\Delta G_v)^2} \qquad (5.6)$$

where f_o is a modifying factor that arises for nucleation at dislocations or at grain boundaries because of the strain and surface energy, and which is less than unity for homogeneous nucleation. γ is the interfacial energy and ΔG_V is the free energy change per unit volume

arising from the chemical driving force. This chemical driving force is related to k_S (supersaturation ratio) as:

$$\Delta G_V = - (RT/V_m) \ln k_S \qquad \textbf{(5.7)}$$

From these considerations, equation (5.4) can be rewritten for Nb as:

$$J_S = \alpha \cdot [Nb] \cdot \exp\left(-\frac{Q_d}{RT}\right) \cdot \exp\left(\frac{16\pi\gamma^3 V_m^2 N_o f_o}{3RT(-RT\ln k_S)^2}\right) \qquad \textbf{(5.8)}$$

where α is a constant, V_m is the molar volume of Nb(C,N) and N_o is Avagadro's number. The constant, B_P, in Dutta and Sellars equation for $t_{0.05P}$ (4.3) is defined from equation (5.8) as:

$$B_P = \frac{16\pi\gamma^2 V_m^2 N_o f_o}{3R^3} \qquad \textbf{(5.9)}$$

If it is assumed that the modifying factor, f_o, is the same in both V and Nb steel, then the smaller V_m for V(C,N) will reduce the constant B_P by a factor:

$$\frac{B_{P(V)}}{B_{P(Nb)}} = \frac{V_{m(V)}^2}{V_{m(Nb)}^2} \cdot \frac{(a_{V(C,N)}^3)^2}{(a_{Nb(C,N)}^3)^2} \qquad \textbf{(5.10)}$$

Here, 'a' is the lattice parameter whose values[104] are:

$a_{V(C,N)}$ = 0.415 nm, and

$a_{Nb(C,N)}$ = 0.443 nm.

By substitution, $B_{P(V)} / B_{P(Nb)} = 0.656$ and, $B_p = B_{p(V)} = 0.656 \times (2.5 \times 10^{10}) = 1.64 \times 10^{10}$.

From the above considerations, equation (4.3) can then be modified for vanadium steels as:

$$t_{0.05P} = 1.15 \times 10^{-6} \cdot [V]^{-1} \cdot \varepsilon^{-1} \cdot Z^{-0.5} \cdot \exp\frac{293000}{RT} \cdot \exp\frac{1.64 \times 10^{10}}{T^3 (\ln k_S)^2} \qquad \textbf{(5.11)}$$

Fig 5.6 shows reasonable agreement between values calculated by equation (5.11) and Medina's[60] data.

5.3 Summary relating to $t_{0.05P}$

By taking into account the more rapid diffusion of V than of Nb in austenite, the onset of strain induced precipitation in V steels occurs in a shorter time than in Nb steels. The constant A_{PPT} was therefore reduced by a factor which allows for the faster diffusion.

Similarly, the value of the constant B_P is also changed to reflect the differences in both the molar volumes and the lattice parameters. It is seen that the modified model for the time to 5% strain induced precipitation is in reasonable agreement with the data that was available.

Having established the modified model for the time to 5% recrystallisation and strain induced precipitation, the next stage is to quantitatively compare the prediction of this model with the experimental RST's of the three steels.

5.4 Comparison of the modified model and experimental RST's

It is seen in Fig. 5.7 that the agreement between the experimental and predicted RST of reheated austenite of 2V is much better with the modified model.

For 2V-HDR, the model RST using equations (5.3) and (5.11), when $B_P = 1.64 \times 10^{10}$, overestimates the experimental RST. In their original paper, the constant A_{PPT} was selected to give agreement with the observed times for 5% precipitation at 900 °C and the optimum value of B_P was determined by trial-and-error computations using equation (2.5) to give the best fit

of the form of precipitation-time-temperature curve to the observations. They found that the values of B_P were within a factor of 2.5 of the mean value of 2.5 x 10^{10} K^3. Their equation for $t_{0.05P}$ does not take into account the effect of grain size for the range studied, but it is inferred that strain induced precipitation (SIP) may be slower in austenite of extra-ordinarily large grain size and that the constant B_P may be large for large grain sizes.

Unlike reheated austenite, the as-cast austenite at the start of HDR differs with respect to microalloying elements. The as-cast austenite is dendritic, and its alloy content is segregated interdendritically both on a micro and macro scale and the amount of microalloying species in solution is determined by the kinetics of precipitation following the liquid-δ-γ phase changes rather than on equilibrium solubilities. On the other hand, a degree of chemical homogenisation is achieved in reheated austenite by the gamma-alpha and alpha-gamma transformations during cooling and reheating. The complexity of precipitate evolution in as-cast austenite is illustrated by the work done by Priestner *et al* [105] on Nb-Ti steels during solidification and post-solidification. Here, small ingots were cooled slowly to simulate larger castings. Cooling was interrupted at various temperatures in the austenite phase field, either by quenching or by holding isothermally before quenching. Precipitate morphology, distribution, particle size and composition were investigated by TEM and STEM. In certain conditions, no carbonitrides were observed, yet observations in reheated austenite and thermodynamic predictions suggested that carbonitrides should have precipitated. In others, the compositions of the precipitates deviated strongly from equilibrium. It is therefore likely that the sequence, composition and distribution of precipitate particles and hence the driving force k_S, may well deviate from thermodynamic predictions of the as-cast austenite in this investigation.

From these considerations, the value of B_P for the as-cast austenite is increased from 1.64 x 10^{10} to 2.5 x 10^{10} in equation (5.11). There is good agreement between the modified model incorporating the new value of B_P and the experimental RST as shown in Fig. 5.8. Clearly, the RST is very sensitive to the kinetics of SIP, which appears to be slower in the very coarse as-cast austenite of the present HDR experiments.

Comparison of the modified model RST with the experimental RST of the reheated austenite of 4V is shown in Fig. 5.9. The agreement between the modified model and the experimental RST is much better than that predicted by the original model.

5.5 Summary

In summary therefore, the original model proposed by Dutta and Sellars for niobium steels has been modified to suit the materials and experimental methodology in this investigation. Reasonably good agreement has been found between the RST's predicted by the modified model and the experimental data from this investigation. The modified model was also found to be a reasonable predictor of both the onset of recrystallisation and strain induced precipitation of the data that was available in the literature.

TABLE 5.1

Value of $t_{0.05RX}$ (s) converted from experimental values using the Avrami equation.

Model $t_{0.05RX}$ (s) calculated from equation (5.3) when $A_{RX} = 1.74 \times 10^{-17}$, m = 1 and F = 0.1

(% RX)	MODEL $t_{0.05RX}$ (s)	CALCULATED $t_{0.05RX}$ (s)	CALCULATED $t_{0.5RX}$ (s)	AVRAMI EXPONENT
		STEEL 2V		
32.5	63.52	46.98	634.74	1.0
41.67	13.24	26.64	359.96	1.0
17.08	6.3	18.08	244.20	1.0
16.25	2.12	5.78	78.16	1.0
12.0	2.32	12.04	162.63	1.0
		STEEL 2V - HDR		
8.5	41.28	50.33	1303.80	0.8
15.9	39.65	26.22	679.25	0.8
25.8	51.91	53.13	1376.095	0.8
14.7	126.68	72.94	1889.32	0.8
		STEEL 4V		
35.25	10.3	1.32	151.74	1.0
6.46	2.22	53.095	933.95	1.0
14.0	0.81	2.43	96.49	1.0
42.75	0.39	0.14	19.88	1.0
26.5	0.67	0.75	60.77	1.0
8.25	1.8	19.87	450.72	1.0

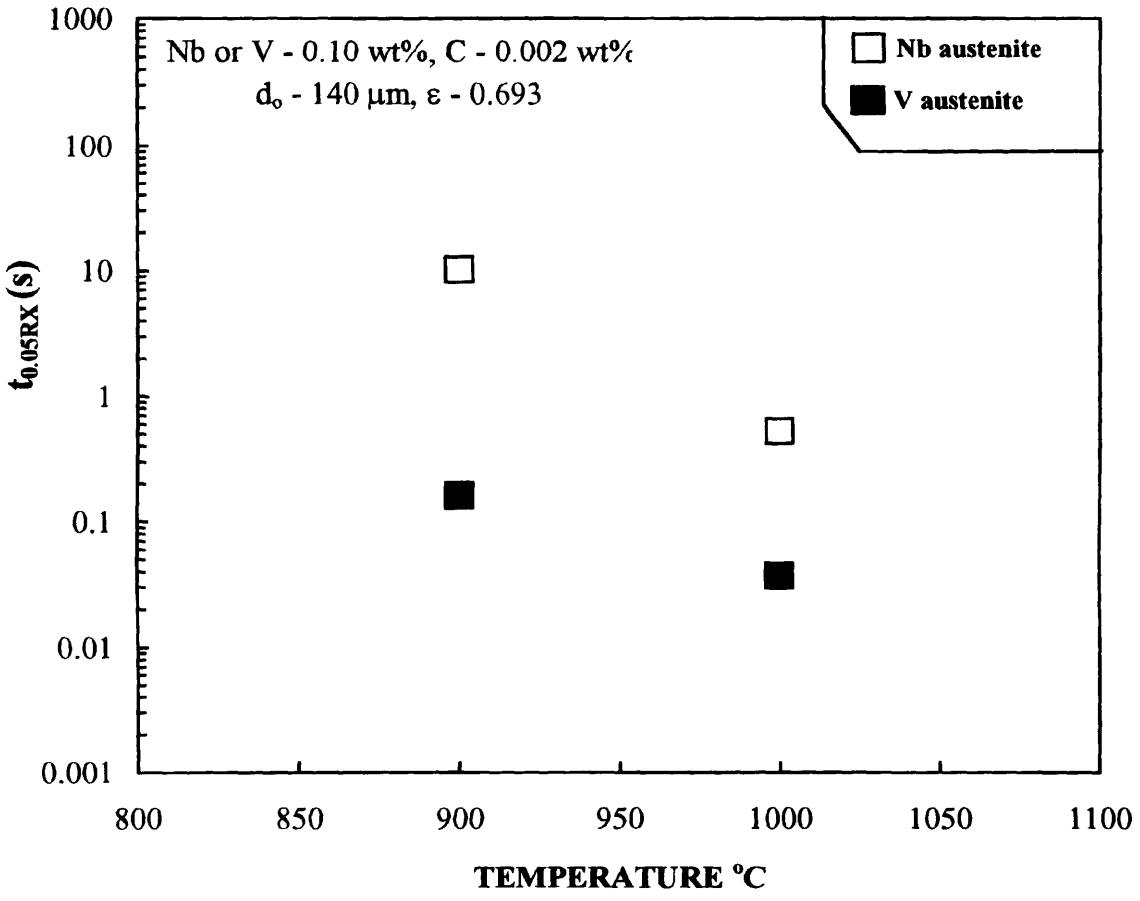

Fig. 5.0 **Effect of vanadium and niobium solute on $t_{0.05RX}$, from the data of Ouchi *et al* [99].**

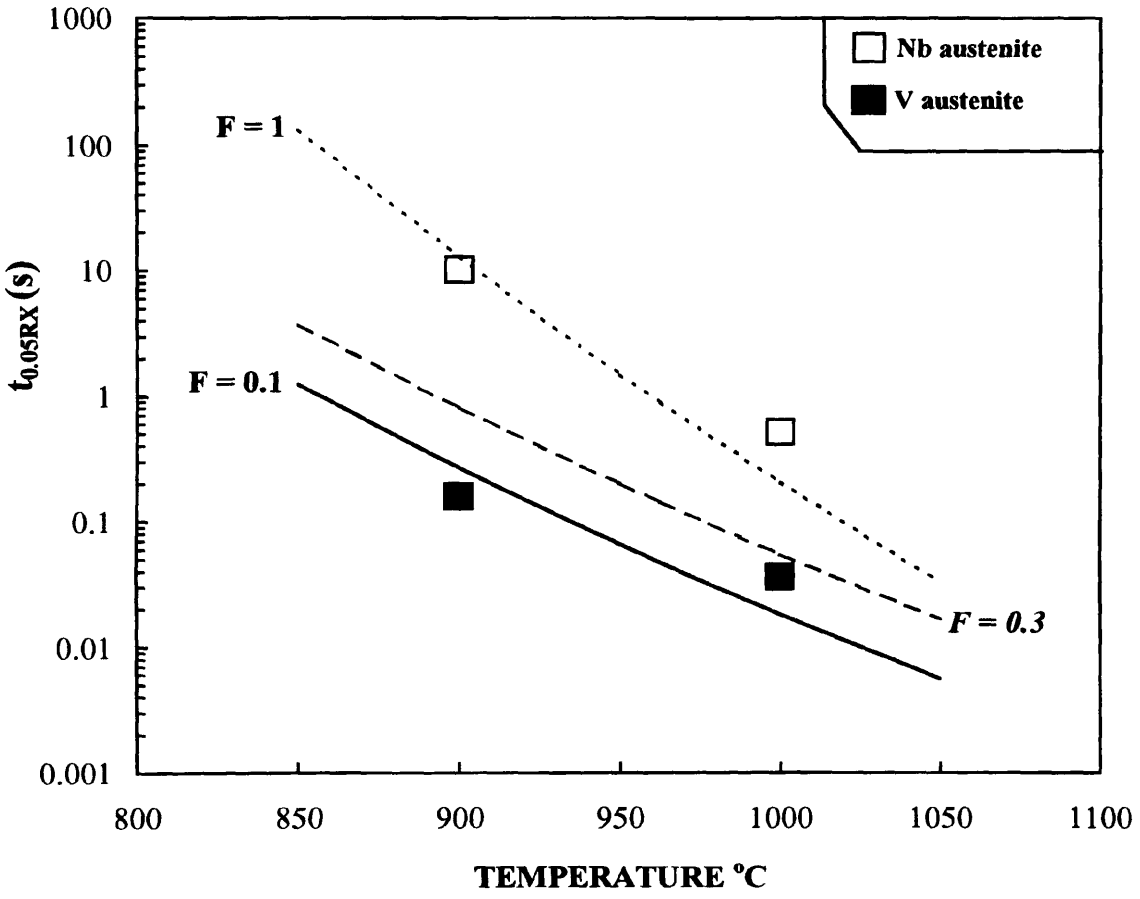

Fig. 5.1 **Effect of solute drag factor F, on $t_{0.05RX}$, from the data of Ouchi *et al* [99].**

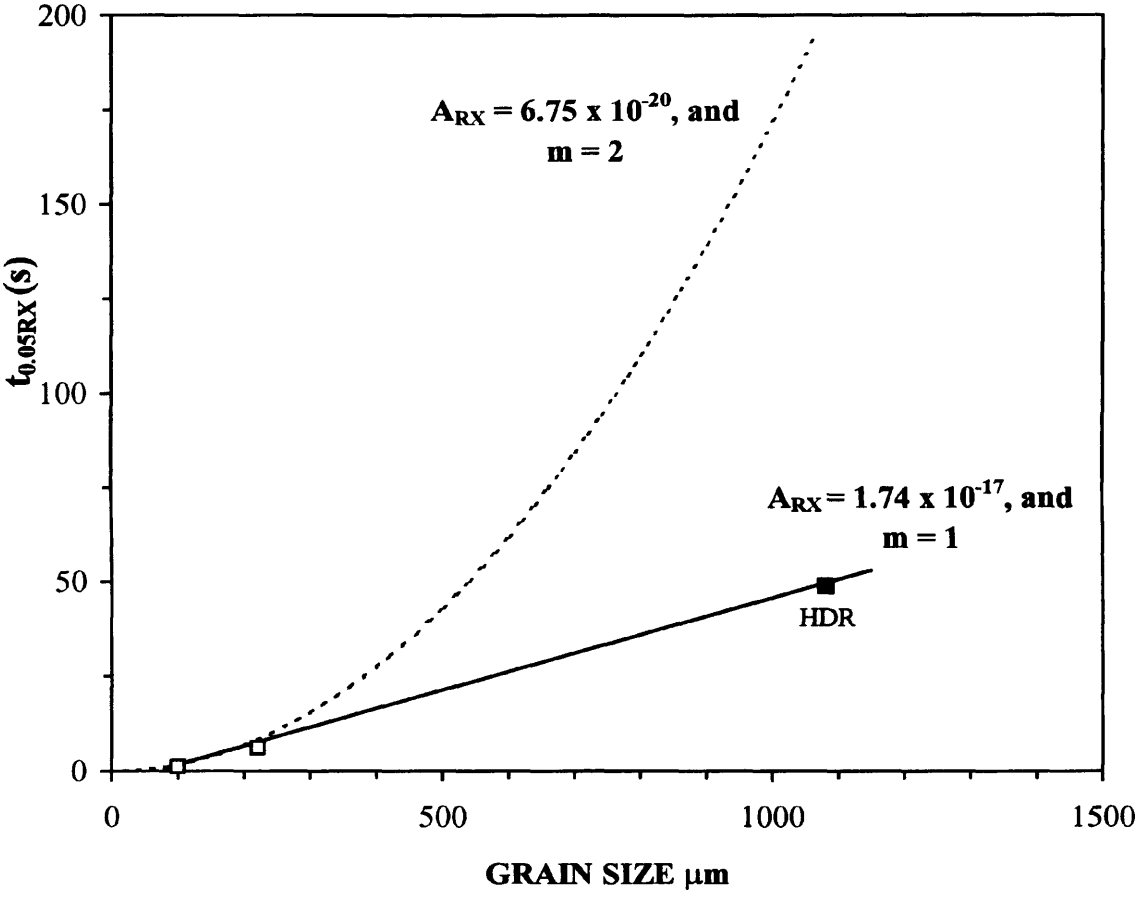

Fig. 5.2 Effect of austenite grain size on $t_{0.05RX}$.

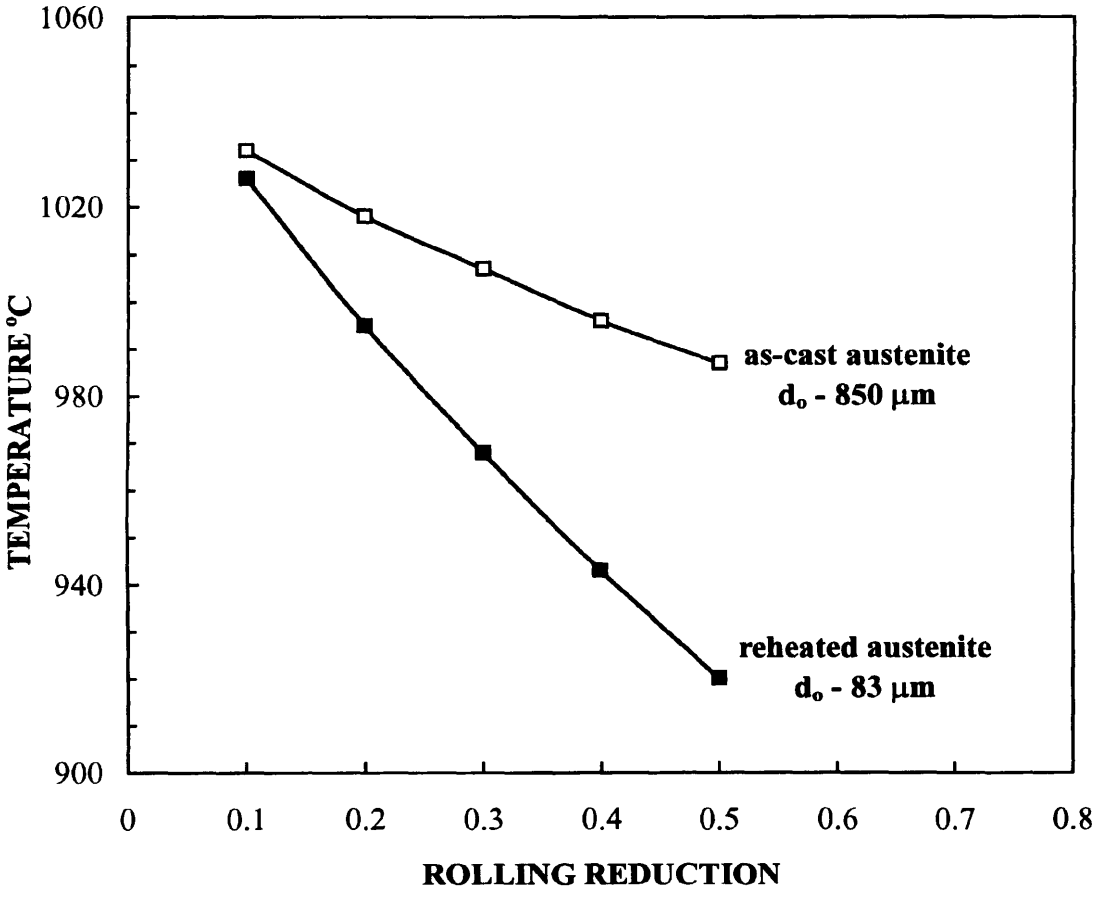

Fig. 5.3 **Experimental RST's of reheated and as-cast austenite of 0.01% C, 0.04% Nb, after Priestner *et al* [101].**

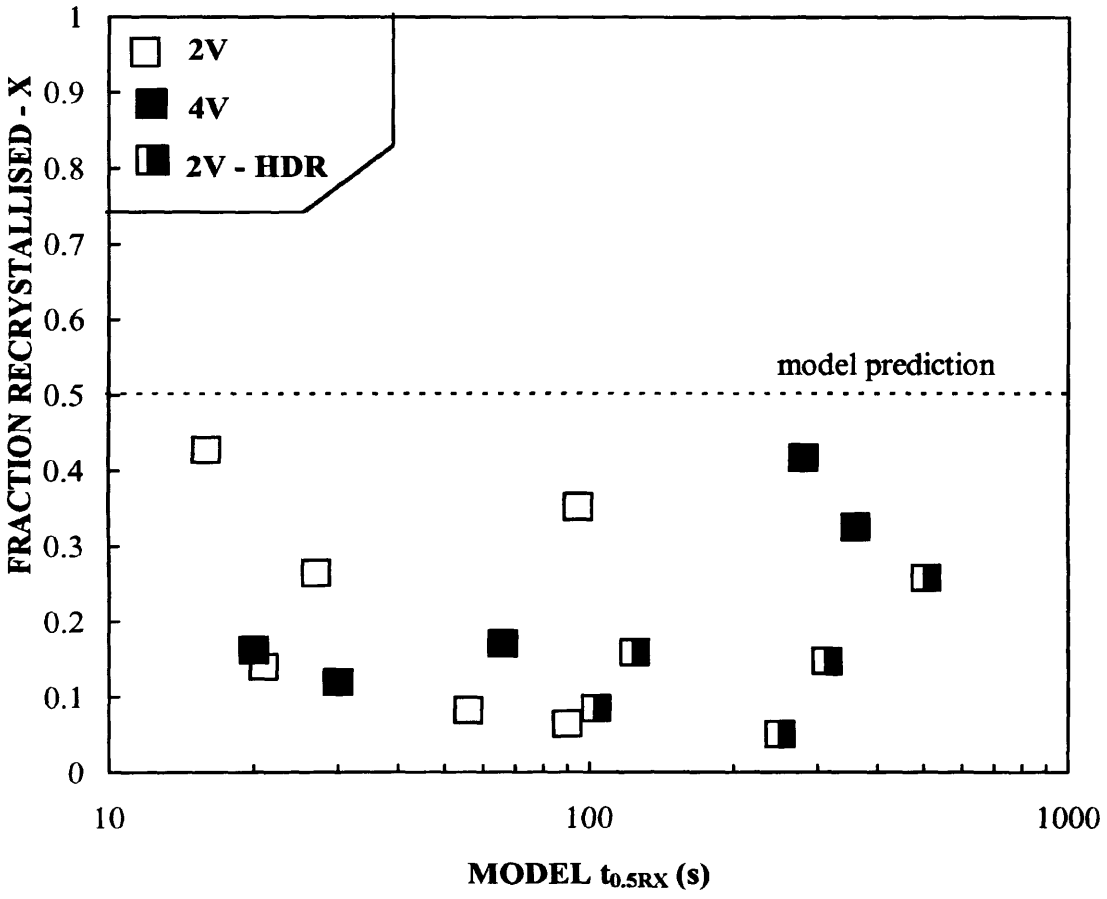

Fig. 5.4 **Relationship between the model time to 50% recrystallisation and the experimental fraction recrystallised for all partially recrystallised slabs.**

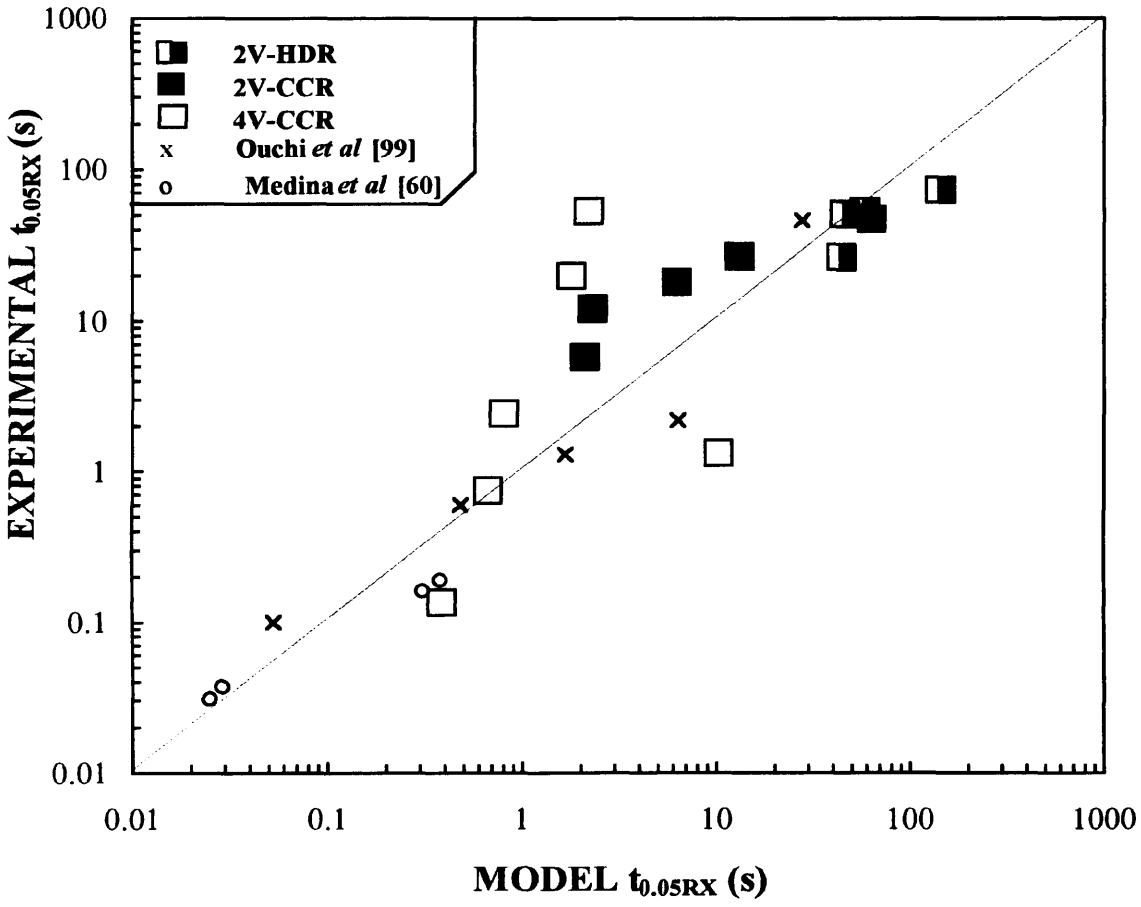

Fig. 5.5 **Relation between the model and experimental $t_{0.05RX}$.**

The $t_{0.05RX}$ values of the steels in this investigation (2V, 2V-HDR and 4V) plotted in the figure are values converted from experimental results using the Avrami equation. The results of Ouchi and Medina are the actual experimental times to $t_{0.05RX}$.

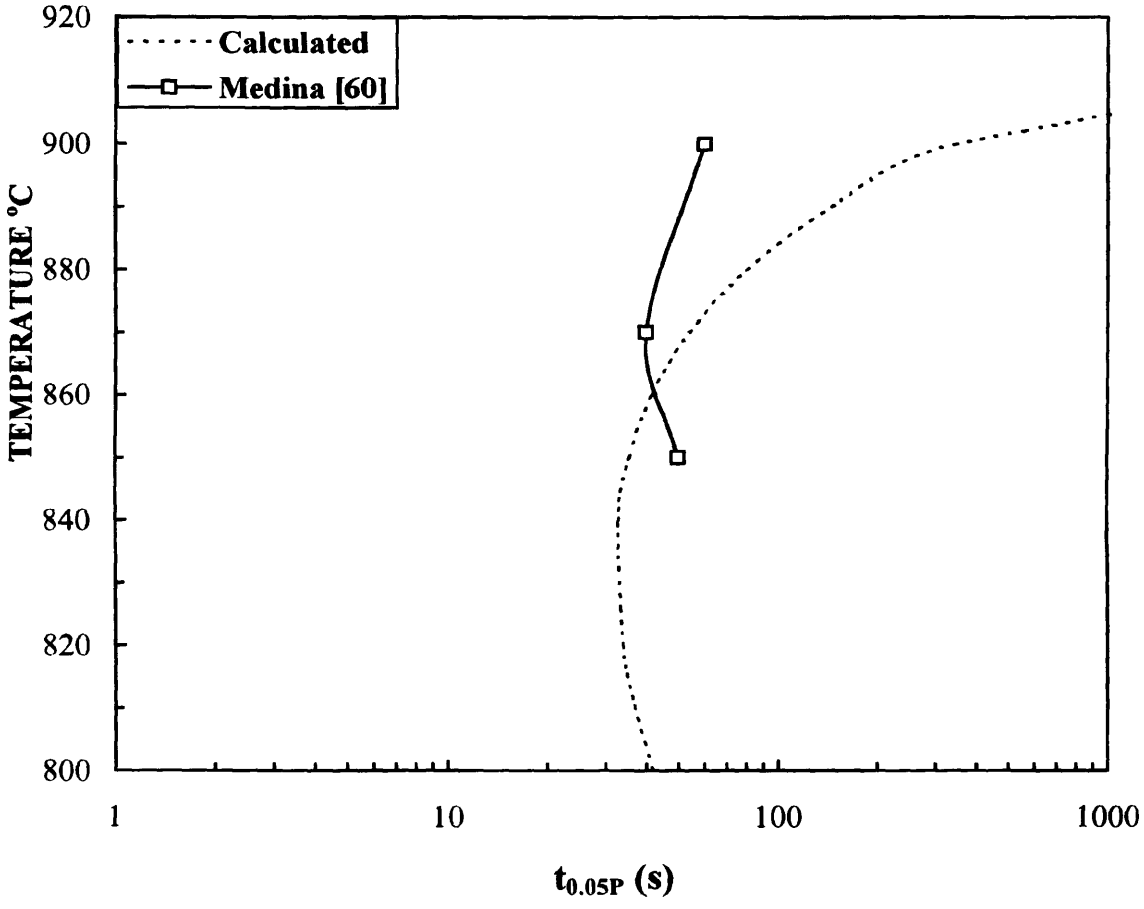

Fig. 5.6 **Comparison of the modified model and Medinas' experimental strain induced precipitation start times at the relevant temperatures of 0.06 wt% V steel.**

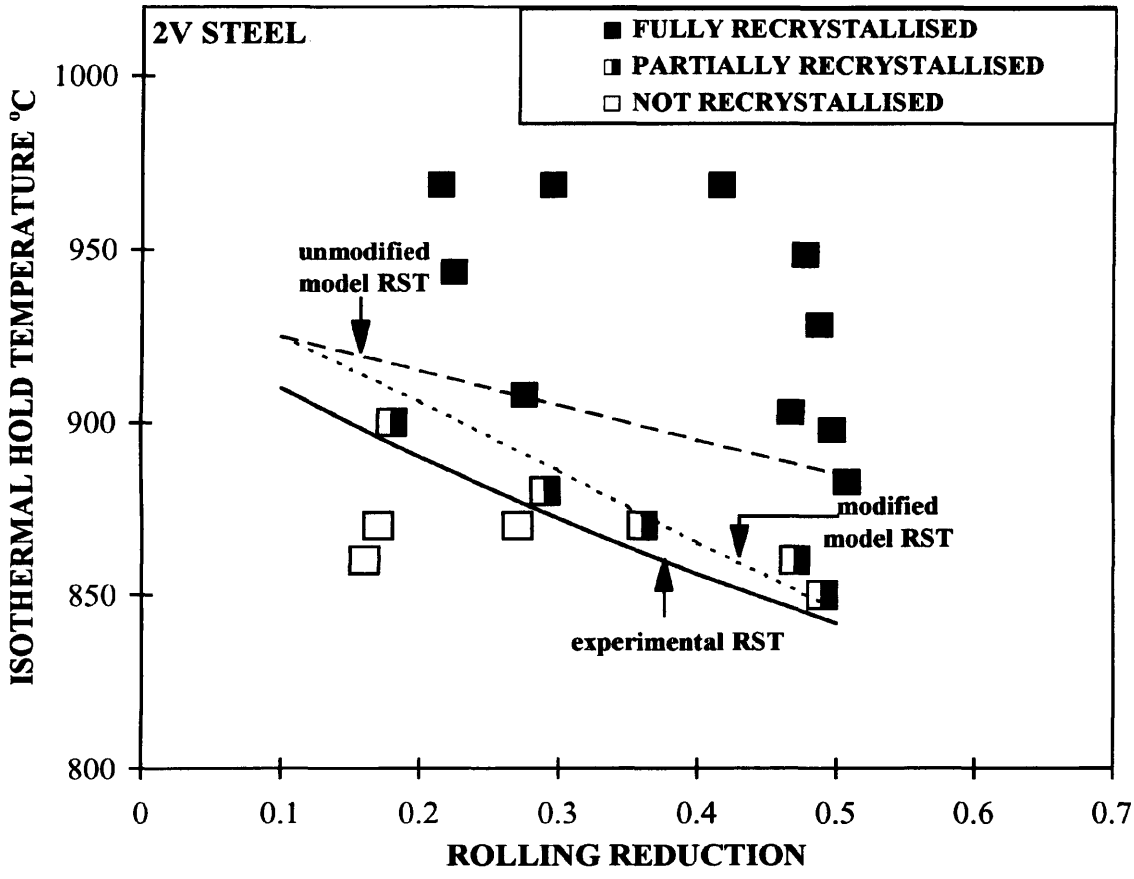

Fig. 5.7 **Comparison of the unmodified and modified model RST with the experimental RST of the reheated austenite of 2V.**

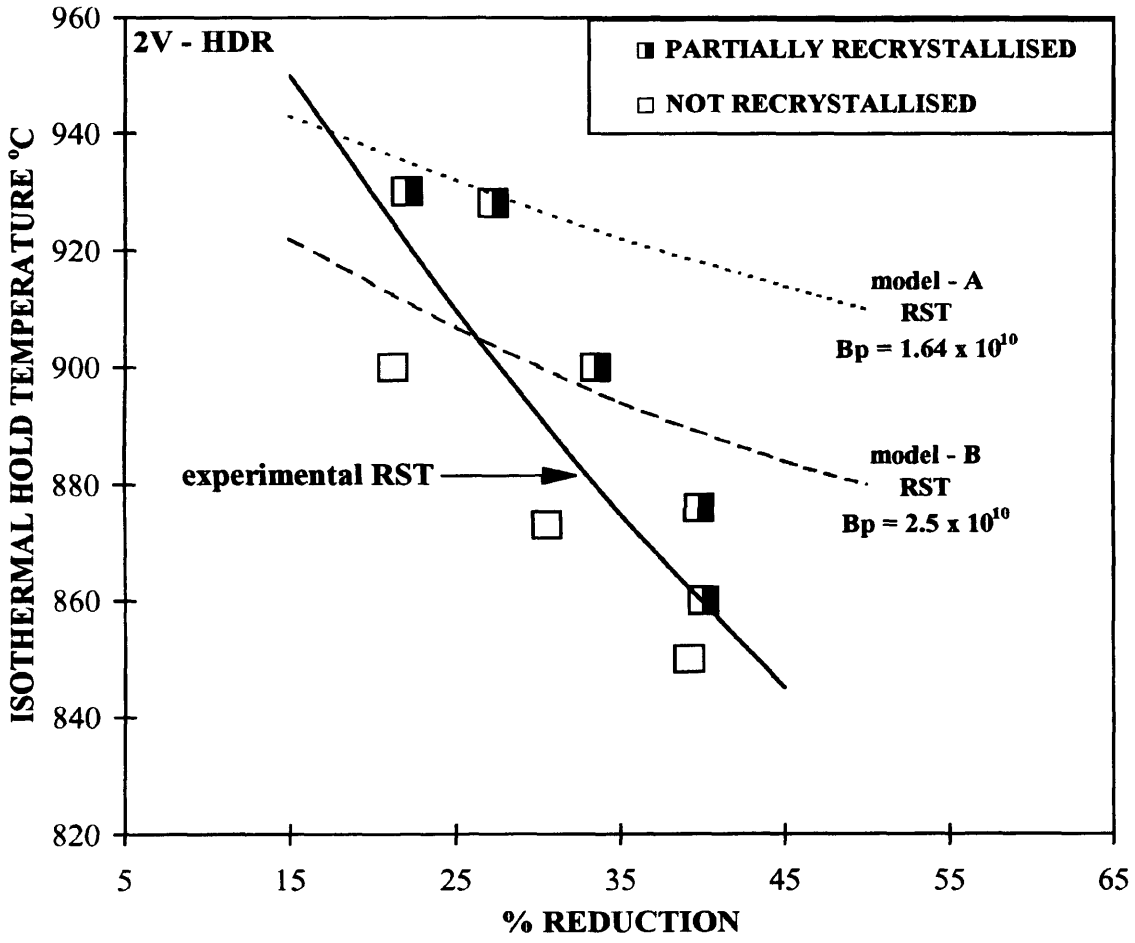

Fig. 5.8 Effect of the variation of constant B_P on the RST of steel 2V-HDR.

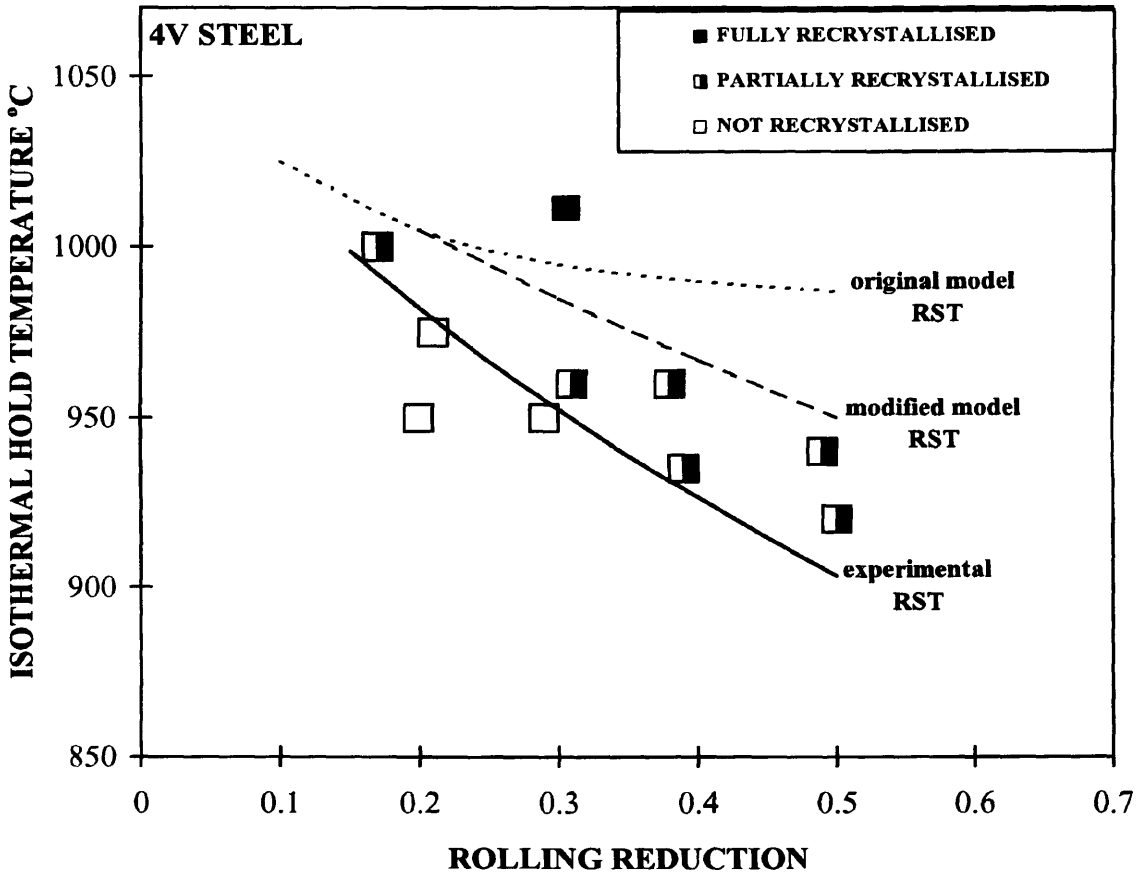

Fig. 5.9 **Comparison of the unmodified and modified model RST with the experimental RST of the reheated austenite of 4V.**

CHAPTER 6

CONCLUSIONS AND SUGGESTIONS FOR FURTHER WORK

6.0 Summary and conclusions

For vanadium steels, the experimental RST is higher, as predicted by the model, for the higher solute content and decreased in the order 4V, 2V-HDR and 2V. The RST decreases with increasing deformation.

Dutta and Sellars model has been modified

(i) to introduce a factor F, reflecting the lower solute drag effect on the time to 5% recrystallisation, $t_{0.05RX}$,

(ii) to assume a linear dependence of $t_{0.05RX}$ on the grain size, and

(iii) to assume appropriate constants A_{RX}, A_{PPT} and B_P.

The modified model is then in reasonable agreement with the experimentally determined RST's of the three steels.

In the CCR and HDR steels of similar compositions, the differences between the RST's is much smaller than would be expected from the model despite a large difference in grain size. In part, this is corrected by assuming a linear instead of a quadratic, dependence of $t_{0.05RX}$ on d_o, and assuming slower strain induced precipitation kinetics in the coarse grained as-cast austenite. The differences between the RST's of the two processes may be influenced by the segregation ratio of vanadium and the deviation from thermodynamic predictions of as-cast austenite.

6.1 Suggestions for further work

In deducing the value of $t_{0.05RX}$ from the experimental value of fraction recrystallised at selected temperatures and deformations using the Avrami equation, assumptions have been made in selecting the value of the exponent k. This is because the nature of the experimental data in this investigation did not permit the evaluation of the true value of the exponent k. It would be of benefit if k is determined experimentally for the two compositions which will yield some indication of the time interval from $t_{0.05RX}$ - $t_{0.95RX}$. Having established this, the results may provide a more clearer indication of the interaction between recrystallisation and the nature of strain induced precipitation kinetics, permitting a more appropriate choice of the constants in the Dutta and Sellars equations and hence better compatibility between prediction and experimental RST's.

Investigation of precipitation phenomenon particularly of the HDR material merits further study. The behaviour of such an as-cast austenite may not be adequately predicted from thermodynamic considerations based on reheated austenite. Modelling supported by STEM and TEM investigations may better explain the differences and the deviations from equilibrium considerations. This is important as much research and industrial practices are tending towards HDR.

Knowledge of the above two will permit a more appropriate choice of the values of the constants for input into the model where necessary, resulting in enhanced agreement between the predicted and experimental RSTs'.

REFERENCES

[1] **T.M. NOREN.** Special report on Columbium as a microalloying element in steels and its effect on welding technology. Ship Structure Committee, Washington D.C.1962.

[2] **J.H. WOODHEAD and S.R. KEOWN.** Proc 2nd Int Conf, HSLA STEELS-Processing, Properties and Applications. 28 Oct - 2nd Nov 1990, Beijing, China. Eds G.Tither and Z.Shouhua. Publ: TMS, p15-27.

[3] **T. TANAKA**. International Metals Reviews, 1981, No 4, p185-212.

[4] **A.J. DeARDO, C.I. GARCIA and E.J. PALMIERE.** 'THERMOMECHANICAL PROCESSING OF STEELS'. ASM Int, Materials Park, OHIO, 1991. ASM Handbook, Vol 4, Heat Treating, p237-255.

[5] **F.B. PICKERING.** Microalloying 75. Eds, M. Korchynsky et al. Union Carbide Corp, N.York, 1977, p9

[6] **R. K. AMIN, M. KORCHYNSKY and F.B. PICKERING.** Metals Technology, 8, 1981, p. 250.

[7] **B. DUTTA and C.M. SELLARS.** Materials Science and Technology. Vol 3, March 1987, p197-206.

[8] **G.H. WALTER.** Proceedings, "Microalloying 75." 1-3 Oct, 1975. Washington, D.C. U.S.A, p623-633.

[9] **E. M. H. LIPS and H. VAN ZUILIP.** Metal Progress, 66, 1954, p103.

[10] **M. COHEN and S.S. HANSEN**. Proc Conf, " HSLA STEELS - Metallurgy and Applications." Eds J.M. Gray, T. Ko, Z. Shouhua, W. Baorong and X. Xishan. 4-8 Nov 1985, Beijing, CHINA, p61-71.

[11] **F.B. PICKERING.** Proc Conf " HSLA Steels - Technology and Applications". Philadelphia, USA. 1984. ASM, Metals Park, OH, USA, p1-31.

[12] **R.A GRANGE.** Fundamentals Of Deformation Processing. Syracuse University Press, p299-320.

[13] **R.A. GRANGE.** ASM Trans. Quarterly. Vol 59, 1966, p26-48.

[14] **I. TAMURA, C. OUICHI, T. TANAKA and H. SEKINE.** THERMOMECHNICAL PROCESSING OF HIGH STRENGTH LOW ALLOY STEELS. Butterworths. 1988.

[15] **A. KERN, J. DEGENKOLBE, B. MUSGEN and U. SCHRIEVER.** ISIJ International, Vol 32, No 3, 1992, p387-394.

[16] **R. W. K. HONEYCOMBE.** STEELS. Microstructure and properties.Metallurgy and Materials Science Series. Publisher, Edward Arnold.

[17] **A.M. SAGE.** Int Conf on Physical Metallurgy of Thermomechanical Processing of Steels and Other Metals. THERMEC-88. Tokyo, Japan, 6-10 June 1988, The Iron and Steel Institute Of Japan, Chiyoda-ku, Tokyo 100 Japan, 1988, p11-19.

[18] **A.M. SAGE.** Ref [17], p51-60.

[19] **R.A. WALSH and A.J. DeARDO.** 4th International Steel Rolling Conference. The Science and Technology of Flat Rolling. Vol 1. Deauville - France. June 1-3 1987, p A.1.1-A.2.1.

[20] **I. KOZASU.** 'HSLA Steels, Technology andApplications.' ASM, 1984, p593.

[21] **A.AKIRA, M. KIOSHI and K. KAKUTO.** *Tetsu-to-Hagane*, 48, 1962, p1436.

[22] **I. WEISS , G.L. FITZSIMONS, K.MIELITYINEN-TIITTO and A.J.DeARDO.** Proc Int Conf, " Thermomechnical processing of microalloyed Austenite." Editors A.J. Deardo, G.A. Ratz and P.J. Wray. Publication TMS-AIME,Pittsburg, Pennsylvania, 17-19 Aug, 1981,p33-56.

[23] **R.K. AMIN and F.B. PICKERING.** Ref [22], p1-30.

[24] **P.T. MAZZARE, S.W. THOMPSON and G. KRAUSS.** Proc Int Conference on Processing, Microstructure and Properties of Microalloyed and Other Modern High Strength Low Alloy Steels. Editor A.J. DeArdo. June 3-6 Pittsburgh, PA, 1991, p497.

[25] **Y. SAITO, M. TANAKA, T. SEKINE and H. NISHIZAKI.** High Strength Low Alloy Steels. Proc Int Conf. Wollogong University, Wollogong, Austrialia. Aug 20-24, 1984. Edited by D.P. Dunne and T. Chandra, p28-32.

[26] **C. S. SMITH.** Transactions, AIME, Vol 175, 1948.

[27] **T. GLADMAN and F.B. PICKERING.** JISI, June 1967, p653-664.

[28] **T. GLADMAN.** Ref [2], p3-14.

[29] **K. NARITA.** Trans ISIJ, Vol 15, 1975, p145-152.

[30] **K.J. IRVINE, F.B. PICKERING and T. GLADMAN.** JISI, Vol 205, 1967, p161.

[31] **R.W. FOUNTAIN and J. CHIPMAN.** Trans TMS-AIME, Vol 212, 1958, p737

[32] **A.J. DeARDO.** Ref [17], p20-29.

[33] **J.G. SPEER, J.R. MICHAEL and S.S. HANSEN.** Metallurgical Transactions A. V18A, Feb 1987, p211-222.

[34] **G. BRAUER and W. D. SCHNELL.** Journal of Less Common Metals, vol 7,1964, p 23.

[35] **T. GLADMAN , D. DULIEU and I.D. McIVOR.** Ref [8], p32-56.

[36] **J. H. WOODHEAD.** Vanadium in High- Strength Steel, Vanitec Publ, No V140, London, 1979, p3-10.

[37] **W. ROBERTS.** Reprint of papers on Vanadium Steels from the ASM HSLA Steels Technology and Applications Conference, Philadelphia, 1983. Publ ASM, p1-32.

[38] **W. ROBERTS, A. SANDBERG and T. SIWEKI.** Presented at VANITEC conference, Krakow, Poland, 1980, p D1-D12.

[39] **J.G. SPEER, S. MEHTA and S.S. HANSEN.** Scripta Metallugica Vol 18, 1984, p1241.

[40] **P.R. RIOS.** Material Science and Eng, A142, 1991, p87-94.

[41] **H. ADRIAN.** Material Science and Technology, Vol 8, May 1992, p406-420.

[42] **R. KASPAR, J.S. DISTL and O. PAWELSKI.** Ref [17], p713-720.

[43] **J. JONAS, C.M. SELLARS and W.J. McTEGART.** Met Rev, 14, 1, 1969.

[44] **R.A.P. DJAIC and J.J. JONAS.** *Metall Trans*, 1973, 4, p621.

[45] **C.M. SELLARS.** Extended abstract. Mat Sci Tech, Vol 8, 1992, p134.

[46] **C.M. SELLARS.** " Hot working and Forming Processes ". Eds C.M. Sellars and G.J. Davies. Met Soc, London, 1988, p3-15.

[47] **C.M. SELLARS and J.A. WHITEMAN.** " Controlled Processing of HSLA Steels ", Product Technology Conf, York, England, 1976.

[48] **J.H. BEYNON and C.M. SELLARS.** ISIJ International, Vol 32, No 3, 1992, p359.

[49] **H. HU, R.B. BATH and R.A. VANDERMEER.** Recrystallisation '90. Proc Int Conf on Recrystallisation of metallic materials, Wollongong, Austrialia, TMS, 1991, p3.

[50] **S.F MEDINA and J.E. MANCILLA.** ISIJ International, Vol 33, No12, 1993, p1257- 1264.

[51] **C.M. SELLARS.** Ref [50], p448-457.

[52] **R.A.P. DJAIC and J.J. JONAS.** J.I.S.I., 210, 1972, p256.

[53] **R. SANDSTROM and R. LAGNEBORG.** Acta Metall, 23, 1975, p387.

[54] **S.F. MEDINA and P. FABREGUE.** Journal of Materials Science, 26, 1991, p 5427.

[55] **P.D. HODGSON and R.K. GIBBS.** ISIJ International, Vol 32, No 12, 1992, p1329.

[56] **S.F. MEDINA and J.E. MANCILLA.** Scripta Metallurgica *et* Materialia, V31, No 3, 1994, p315-320.

[57] **D.R. BARRACLOUGH and C. M. SELLARS.** Met Sci, 13,1979, p257.

[58] **I. KOZASU, C. OUCHI, T. SAMPEI and T. OKITA.** Ref [8], p100.

[59] **I. KOZASU, T. SHIMIZU and H. KUBOTO.** Trans I.S.I.J, 11, 1097, p367-375.

[60] **S.F MEDINA, J.E. MANCILLA and C.A. HERNANDEZ.** ISIJ International, Vol 34, No 8, 1994, p689-696.

[61] **T. TANAKA, N. TABATA, T. HATOMURA and C. SHIGA.** Ref 66, p107-119.

[62] **R.K. AMIN and F.B. PICKERING.** Ref [22], p1-30.

[63] **K.J. IRVINE, F.B. PICKERING and T. GLADMAN.** JISI, Vol 208, 1970, p717.

[64] **J. N. CORDEA and R.E HOOK.** Metall Trans, 1, 1970, p111.

[65] **M. KORCHYNSKY and H. STUART.** Symposium 'HSLA steels', Dusseldorf Metallurg Co, 1970, p17.

[66] **H.L. ANDRADE, M.G. AKBEN and J.J. JONAS.** Metallurgical Transactions A, Vol 14A, Oct 1983, p1967-1977.

[67] **M.G. AKBEN, I. WEISS and J.J. JONAS.** *Acta Met*, Vol 31, 1983, p161.

[68] **M.G. AKBEN and J.J. JONAS.** Proc Conf " HSLA Steels - Technology and Applications". Philadelphia, USA. 1984. ASM, Metals Park, OH, USA, p149-161.

[69] **M.J. LUTON, R. DORVEL and R.A.P. PETKOVIC.** *Metall Trans*,11A.1980.

[70] **M.J. WHITE and W.S. OWEN.** Metallurgical Transactions A, Vol 11A, April 1980, p597-604.

[71] **J.J. JONAS and M.G. AKBEN.** Metals Forum, Vol 4, 1981, p92.

[72] **H.J. McQUEEN.** Metal Progress, Vol 95,1969, p131.

[73] **W. ROBERTS.** Swedish Inst Metals Report No IM-1211,1977.

[74] **N.E. HANNERZ and F. de KAZINCZY.** J. Iron Steel Inst, Vol 208,1970.

[75] **A. le BON, J. ROFES-VERNIS and C. ROSSARD.** Metal Science, Vol 9, 1975, p36.

[76] **H. WATANABE, Y.E. SMITH and R.D. PEHLKE** in 'Hot Deformation of Austenite', J.B. Ballance ed, AIME, NY 1977, pp140.

[77] **M.F. ASHBY and R. EBLING.** Trans TMS-AIME, V 236, 1966, pp1396.

[78] **C.M. SELLARS and A.F. SMITH.** J. Mat Sci, V 2, 1966, pp521.

[79] **J. JIZAIMARU, H. KOBAYASHI and T. KOSAKA.** *Tetsu-to-Hagane*, V 60, 1974, No 4, p177

[80] **R. SIMONEAU, G. BEGIN and A.H. MARQUIS.** Metal Science, V 12, 1978, p8.

[81] **M. COHEN and S.S. HANSEN.** 'MiCon 78', 34,1979. Philadelphia. Pa. ASTM.

[82] **J.M. CHILTON and M.J. ROBERTS.** *Metall Trans*, 11A,1980, p1711-1721.

[83] **O. KWON and A.J. DeARDO.** *Acta Metall Mater,* Vol 39, No 4, 1991, p529-538.

[84] **B. DUTTA, E. VALDES and C.M. SELLARS.** *Acta Metall Mater.* Vol 40, No 4, 1992, p653-662.

[85] **L.J. CUDDY.** Ref [22], p129-140.

[86] **T WADA, H. TSUKAMOTO and M. SUGA.** *Tetsu-to-Hagane*, Vol 74, 1988, p242.

[87] **K. KUNISHIGE and N. NAGAO.** Trans ISIJ, Vol 25, 1985, p315.

[88] **R. K. GIBBS, R. PETERSON and B.A. PARKER.** Proc Int Conf "Processing, Microstructure and Properties of Microalloyed Steels." June 1991, Pgh, Pa., USA, publ ISS-AIME, Warrendale, Pa, 1992, p201-207.

[89] Special Issue on Technology of Direct Linkage between continuous Casting and Hot Rolling Processes. Tetsu-to-Hagane, Vol 74, 1988, No 7, complete issue.

[90] **T. KOYANO, O. TERADA, S. UCHIDA and M. ISHIKAWA**. "Operation of High Speed Slab Caster for Hot Direct Rolling2", Steelmaking Proceedings. ISS-AIME, Warrendale, PA, USA, Vol 69, p456.

[91] **R. PRIESTNER and C. ZHOU.** MICOSTRUCTURES " sponsored by TMS and ASM Int, Materials week, Pgh, PA.. Ed, J.J.Jonas et al. Publ - TMS. Oct 18-20. 1993, pp 121-138.

[92] **J. E. HILLIARD.** Metal Progress. May 1964, p99-102.

[93] **B.S. 4490. 1989.** Micrographic determination of the grain size of steel.

[94] **ASTM Standards Book**. Section 3, Vol 03.01, 1994, p227-252.

[95] Ref 14, p136.

[96] **ASTM Standards Book**. Section 3, Vol 03.03, 1994, Procedure E562-83.

[97] **R. PRIESTNER, C.C. EARLEY and J.H. RENDALL.** JISI, December 1963, p1252.

[98] **L.A. ERASMUS.** JISI, Feb 1964.

[99] **S. YAMAMOTO, C. OUCHI and T. OSUKA.** Ref [22], Publication TMS-AIME, p613.

[100] **S. F. MEDINA , J. E. MANCILLA and C.A. HERNANDEZ.** Journal of Material Science, 28, 1993, p5317-5324.

[101] **C. ZHOU, A.A. KHAN and R. PRIESTNER.** 1st Int Conf 'Modelling of Metal Rolling Processes'. 21-23 Sept, 1993, Imperial College, London. The Inst of Materials, p212-223.

[102] **K.C. RUSSEL.** Adv Colloid Interface Sci, 13, 1980, p205-318.

[103] **C.D. MORTON.** PhD Thesis, The University of Sheffield, 1975.

[104] **X. WENCHUNG and F. FUYUS.** *Acta Metallurgica Sinica*, 3, 1990, pB211.

[105] **C. ZHOU and R. PRIESTNER.** ISIJ Int, Vol 36, No 11, 1996, p1397-1405.

[106] **I.M LIFSHITZ.** J of Physics, Chem Solids, Vol19, 1961, p335.

[107] **C. WAGNER. Z ElectroChem,** Vol 65, 1961, p581.

PUBLISHED PAPER

ReX' 96

Third International Conference on Recrystallisation and Related Phenomena

Monterey, California, October 21-24, 1996.

THE DEFORMATION AND RECRYSTALLISATION BEHAVIOR OF AS-CAST V MICROALLOYED AUSTENITE DURING HOT DIRECT ROLLING

P. Patel, C. Zhou and R. Priestner

University of Manchester/UMIST Materials Science Centre, Grosvenor Street, Manchester M1 7HS, England

ABSTRACT

Small castings of a low carbon, vanadium microalloyed steel were solidified slowly enough to simulate thin slab casting. Hot direct rolling (HDR) was simulated by single-pass rolling of the as-cast austenite as it cooled. Conventional controlled rolling (CCR) was simulated by reheating slabs of similar composition to 1200° C. The recrystallisation stop-temperature (RST) model, proposed by Dutta and Sellars for niobium steels, was modified to suit the current material and the experimental methodology. The experimental RST of both the as-cast and reheated austenites agreed well with that predicted by the modified model. The initiation of recrystallisation was more rapid in the vanadium steel than in Nb steels, and not so strongly dependent upon grain size as proposed by the Dutta and Sellars model, exhibiting a linear relationship. Also, vanadium segregated less than Nb during solidification.

INTRODUCTION

Hot direct rolling (HDR) is an economic way of producing steels due to the energy saved by eliminating the reheating procedure in conventional processing. In HDR processing, the grain structure of the as-cast austenite before hot rolling is quite different from reheated austenite, being almost ten times larger than that observed in conventional processing[1-3]. Introduction of microalloying elements to as-cast austenite raises the degree of supersaturation of solutes, and results in segregation of solutes[2]. The slow recrystallisation of the very coarse as-cast austenite in Nb, Nb-Ti and Nb-Ti-B systems[2,3,4], exacerbated by the high supersaturation of

microalloying elements, tends to produce mixed ferrite grain size during HDR, with the resultant deterioration of toughness in the final products[3]. Interdendritic segregation of niobium results in large precipitates during solidification[5],depleting the matrix of the element for subsequent strain induced precipitation and precipitation hardening. Among HSLA steels, vanadium microalloyed steels may not be the ideal candidate for conventional controlled rolling due to their low recrystallisation stop- temperature[6]. However, they may be suitable for HDR processing, as the low RST may improve the homogenisation of austenite grain structure by recrystallisation controlled rolling, resulting in uniform ferrite grain structure. Compared with Nb steel, vanadium steel exhibits higher hot ductility[7], and a lower segregation ratio in as-cast austenite[8]. Owing to the greater solubility of V(C,N) than Nb(C,N), V(C,N) does not precipitate so extensively in austenite, hence, vanadium is more effective as a precipitation-strengthening addition[9]. For such a potential HDR steel, it is therefore of interest, to model the recrystallisation stop temperature of as-cast austenite, and examine the kinetics of vanadium carbonitride precipitation.

There is a large amount of data including a model for evaluating the RST proposed by Dutta and Sellars[10], for Nb steels, but relatively few studies have been reported for steels microalloyed with vanadium only. The objective of the present research, therefore, was to investigate the recrystallisation stop temperature of directly rolled, as-cast austenite of a vanadium microalloyed steel and to compare this with reheated austenite of similar composition. Based on the available data for recrystallisation and precipitation in vanadium steel[11, 12], the Dutta and Sellars model was modified to compare quantitatively with the experimental results.

EXPERIMENTAL

Steel castings of 1 kg weight were made by vacuum/ argon induction melting. A flow diagram of the HDR process that was developed during the research is shown in Fig.1. Two kinds of mould systems were designed to obtain two different casting structures. In one situation, the ceramic mould was preheated to 1050° C and was itself insulated with a ceramic fibre blanket, in order to simulate the cooling rate of thin slab casting. The macrostructure of the ingots in this mould system consisted of an outer layer between 1.5 - 2mm deep of columnar grains, the

remainder consisting of equiaxed grains having a mean linear intercept grain size of 1150 μm. In the other mould system, a cast iron chill block was placed at the bottom of ceramic mould to obtain a longer length (about 12mm) of columnar layer from the chill side, the remainder consisting of a 1.5-3mm deep of an outer layer of columnar grains and equiaxed grains in the centre of ingot. In the present experiments, observations were confined to the equiaxed grain region.

The ingots were in the shape of plates measuring approximately 100×75×15mm, and beveled along the bottom edge for entry into the rolling mill. A thermocouple in a quartz tube was located in the lower third of the ingot. This part of the ingot cooled at approx. 1.9 Ks^{-1} from 1400-1200°C.

To simulate HDR, ingots were allowed to cool in the mould to a few degrees above the aim rolling temperature. The rolls were preheated by blowing hot air from electric fans to minimise roll chill. The slab was stripped from the mould, inserted into the roll gap, and rolled directly into another furnace which was preset at the aim isothermal holding temperature. The entire thermal history was plotted on a chart recorder connected to the thermocouple. It was not possible to accurately predict the temperature of the slab on exit from the rolls, however, from previous experiments a temperature drop of approximately 30°C occurred during a roll pass. This was allowed for in the experiments, and the recorded isothermal hold temperatures during a roll pass is the temperature of the slab while in the furnace, estimated from the chart recorder printout. For CCR, slabs of similar composition to the HDR experiments were machined to different thicknesses selected so that on subsequent rolling to various reductions they all finished at the same thickness, namely 5mm. The slabs were reheated to 1200° C for 30 min to completely dissolve VCN. The austenite grain size was 92 μm. The rolling schedule was the same as that used in HDR experiments.

After rolling and isothermal holding, the slabs were quenched immediately in iced brine. Longitudinal sections from the quenched out slabs were polished and etched in saturated aqueous picric acid to reveal austenite grains. Precipitated particles were extracted onto carbon replicas from polished metallographic sections after etching in 2% nital. Precipitates on

the carbon replica were analyzed using Phillips EM400T and EM430T transmission electron microscopes with an EDAX 9100 energy dispersive analyzer.

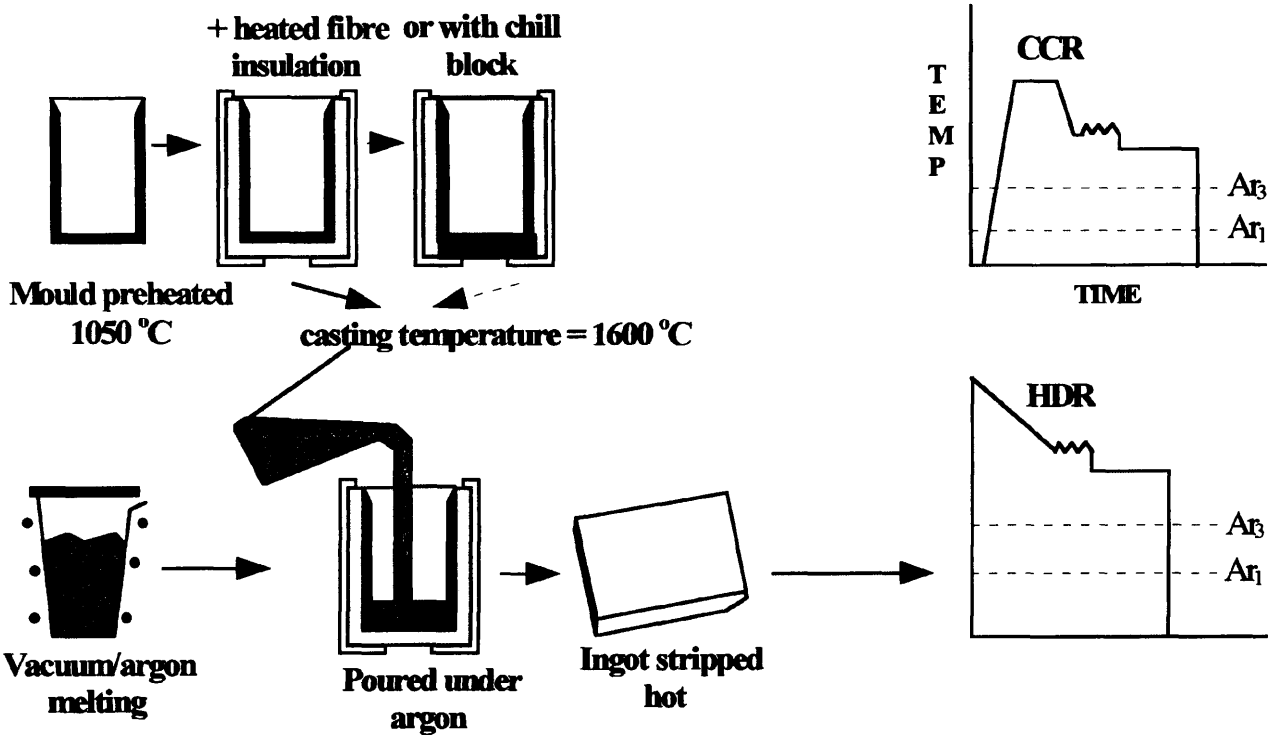

Fig 1. Schematic of CCR and HDR experimental procedures.

The occurrence of recrystallisation was detected by measuring austenite grain sizes (mean linear intercept) and their aspect ratios, and by inspection of microstructures for the presence of new grains. The fraction recrystallised, where appropriate, was determined by point counting.

The composition of each ingot was determined on a plane at the quarter-thickness of the plate. Considerable care was taken to standardise all the melting procedures to minimise the variation from the aim composition. Compositions of the steels are listed in Table 1.

Table 1. Compositions of steels (wt%)

Steel	C	Si	Mn	P	S	V	Al	N
CCR	0.14	0.31	1.4	0.006	0.005	0.2	0.026	0.0053
HDR	0.12-0.14	0.3-0.35	1.32-1.41	0.005-0.008	0.0035-0.006	0.2-0.22	0.01-0.03	0.005

MODIFICATION OF THE STANDARD MODEL

Dutta and Sellars[10] proposed that if strain induced precipitation went to 5% completion before recrystallisation went to 5% completion, then recrystallisation would be inhibited. A critical assessment of recrystallisation and precipitation kinetics led them to propose the following equations for Nb microalloyed steels:

For 5% recrysallisation

$$t_{0.05RX} = A \cdot d_o^{m} \cdot \varepsilon^{-4} \cdot \exp\left(\frac{300000}{RT}\right) \cdot \exp\left[\left(\frac{275000}{T} - 185\right)[Nb]\right] \quad (1)$$

For 5% precipitation

$$t_{0.05P} = C \cdot [Nb]^{-1} \cdot Z^{-0.5} \cdot \varepsilon^{-1} \cdot \exp\left(\frac{270000}{RT}\right) \cdot \exp\left(\frac{B}{T^3 \cdot \ln(k_s)^2}\right) \quad (2)$$

where d_0 is the initial grain size, ε is the true strain, [Nb] is Nb concentration in solution in wt%, Z is the Zener-Holloman parameter, temperature T in Kelvin, and R is the gas constant. k_s is the supersaturation ratio at T. Dutta and Sellars found the following values of the constants:

$A = 6.75\times10^{-20}$; $B = 2.5\times10^{10}$, $C = 3\times10^{-6}$ and $m = 2$.

Start of Recrystallisation

Ouchi et al[11] investigated the role of V and Nb solute atoms in the retardation of static recovery and the onset of recrystallisation in deformed extra-low carbon (0.002 wt%) austenite. It was assumed that retardation of recrystallisation was due to solute drag. They found that recrystallisation of the V austenite was much faster than the corresponding Nb austenite with the same concentration of solute. To assess this effect in terms of Dutta and Sellars' model, the niobium concentration in Equation (1) was substituted by F · [conc] where [conc] is the concentration of either Nb or V, and F is a factor that can be varied to fit Equation (1) to Ouchi's data. Such comparison as was possible is shown in Fig 2. For the Nb steel Equation (1) fits Ouchi's data reasonably well in unmodified form, i.e. with F = 1. For the V steel it was necessary to reduce F to 0.1 in order to obtain the same degree of agreement between Equation (1) and Ouchi's data.

The grain size in the present experiments ranged from 92μm to 1150μm, a much greater range than considered by Dutta and Sellars (25-250μm). A typical $t_{0.05RX}$ HDR result, rolled to 27.3% reduction at 958° C and then held at 928° C, is plotted in Fig.3 and compared with the prediction of Dutta and Sellars (Equation1) fitted to data at smaller grain sizes. Clearly the quadratic dependence of $t_{0.05RX}$ on d_o is inappropriate to the large grain size range applying in the present research. As in previous research on Nb-steel[4], a linear dependence of $t_{0.05RX}$ on d_o was found to be more appropriate, together with a change in the pre-exponential constant, A, to 1.74×10^{-17}. From the above considerations, Equation (1) can be rewritten for vanadium steel as:

$$t_{0.05RX} = 1.74 \times 10^{-17} \cdot d_o \cdot \varepsilon^{-4} \cdot \exp\left(\frac{300000}{RT}\right) \cdot \exp\left[\left(\frac{275000}{T} - 185\right) \cdot 0.1 \cdot [V]\right] \qquad (3)$$

Some data on the recrystallisation of V austenite exists in the literature[10,11]. The fraction recrystallised can be calculated using the Avrami equation[12].

$$X = 1 - \exp(-0.693(t/t_{0.5})^n) \qquad (4)$$

where X is fraction recrystallised at time t, $t_{0.5}$ is time for 50% recrystallisation and n the Avrami time exponent. The present research also yielded value of fraction recrystallised after selected times and deformations at selected temperatures. Values of $t_{0.05RX}$ were deduced from these data using Equation (4) and values of n of 1 for CCR and 0.8 for HDR materials. These "experimental" values are compared with values calculated using the modified Dutta and Sellars model, Equation (3), in Fig. 4. It is seen that the modified model for the start of recrystallisation is a reasonable predictor of the data that was available.

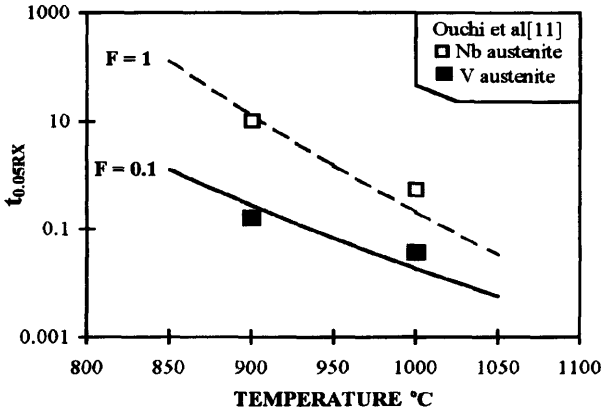

Fig 2. Effect of solute drag factor F on $t_{0.05RX}$.

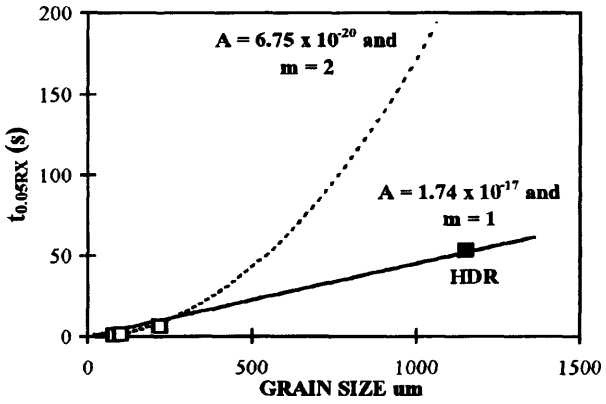

Fig 3. Effect of austenite grain size on $t_{0.05RX}$.

Start of Strain Induced Precipitation

Equation (2) was based on an inversion of the standard equation for steady state nucleation rate, J, of the form:

$$J \approx \left(\frac{N}{a_\alpha^2}\right) \cdot D_{eff} \cdot X_\alpha \cdot \exp\left(\frac{-\Delta G^*}{k_\beta T}\right) \qquad (5)$$

where N is the density of nucleation sites per unit volume, ΔG^* is the critical free energy for nucleation, X_α is solute concentration and D_{eff} is the diffusion coefficient of the solute. The values [13] of $D_o=3.65\times10^{-4}$ m^2s^{-1} and $Q_d=293$ kJ mol^{-1} for diffusion of vanadium in austenite are used to calculate D_{eff} in Equation(5). The larger D_o for vanadium than for Nb in austenite

effectively decreases the value of the constant C in Equation (2) by a factor D_{oNb}/D_{oV}, where D_{oNb} is 1.4×10^{-4} m^2s^{-1}[10]. The new value of constant A equals 1.15×10^{-6}. That is, the more rapid diffusion of vanadium results in a shorter time to the onset of strain induced precipitation. The constant B in Equation (2) is defined as $16\pi\gamma^2V_m^2N_of_o/3R^3$, where V_m is the molar volume of precipitate, γ is interfacial energy and f_o is a modifying factor for heterogeneous nucleation. If it is assumed that f_o is the same in both Nb and V steel, then the smaller V_m for V(CN) will reduce the constant B by a factor V_{mV}^2/V_{mNb}^2 $((a_{V(CN)}^3)^2/(a_{Nb(CN)}^3)^2)$. Here, 'a' is the lattice parameter whose values[14] are V(CN) = 0.415nm and Nb(CN) = 0.443nm. By substitution, the new value of the constant $B = 1.64\times 10^{10}$.

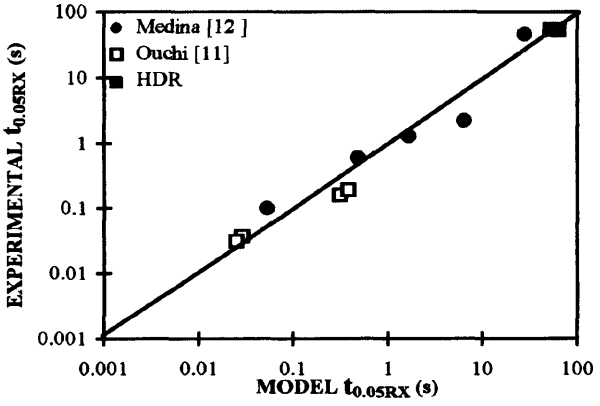

Fig. 4 Relationship between model and experimental $t_{0.05RX}$.

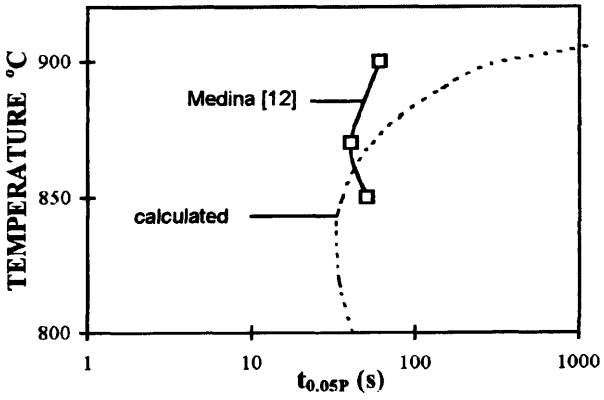

Fig. 5 Relation between the model and experimental $t_{0.05P}$..

In the VCN system, the precipitate nucleus is assumed to be predominantly VN due to the high solubility of VC in austenite. AlN precipitation is very sluggish and AlN is not generally precipitated in deformed austenite at as low as 800° C, provided the product [Al][N] in steel does not exceed 3×10^{-4}[7]. The value of [Al][N] in the steels used in the present research is much less than the suggested value, so that the amount of N removed from solution as AlN could be ignored. The supersaturation ratio k_s is defined as the ratio of the actual amount of VN in solution to the equilibrium amount. The solubility product used by Speer et al[15] was adopted here, i.e. $\log K_{VN} = -7840/T+3.02$. For the reasons discussed above, Equation (2) can then be modified for vanadium steel as:

$$t_{0.05P} = 1.15 \times 10^{-6} \cdot [V]^{-1} \cdot Z^{-0.5} \cdot \varepsilon^{-1} \cdot \exp\left(\frac{293000}{RT}\right) \cdot \exp\left(\frac{B}{T^3 \cdot \ln(k_s)^2}\right) \quad (6)$$

where B is 1.64 x 10^{10}. Fig.5 shows reasonable agreement between values calculated by Equation (6) and Medina's[12] data.

EXPERIMENTAL RESULTS COMPARED WITH MODIFIED MODEL

Recrystallisation Stop Temperature in Reheated Austenite

Fig.6 shows the results of recrystallisation experiments on reheated austenite. The data points represented by solid squares are for specimens in which the austenite grain aspect ratio was very close to that calculated from the applied rolling reduction and the fraction recrystallised was less than 5%. The solid line separating the two sets of data represents the experimentally determined RST, and the dashed line is the RST predicted by the modified model using Equations (5) and (6).

Recrystallisation Stop Temperature in As-cast Austenite

Fig.7 shows the results for as-cast austenite rolled directly after casting. The ingots were isothermally held for between 100-480 seconds after deformation, sufficient time to establish whether recrystallisation had started or not. The dashed line in Fig. 7 labeled "Model - A" represents the RST predicted by Equations (5) and (6) using the new value of the constant B. The model over estimates the RST for HDR. In their original paper, Dutta and Sellars anticipated that SIP may be slower in austenite of extra-ordinarily large grain size, and that the constant B may be larger for large grain sizes. The dashed line in Fig. 7 labeled "Model - B" is the prediction of the modified model if the constant B is increased from 1.64 x 10^{10} to 2.5 x 10^{10}. Clearly, the RST is very sensitive to the kinetics of SIP, which appears to be slower in the very coarse austenite grains of the present HDR experiments.

Fig.8 shows two kinds of VCN precipitation in as-cast austenite after deformation at below the RST. The linear group of larger, cuboidal particles, Fig.8 (a), about 50nm in size were

probably precipitated on austenite grain boundaries during holding after rolling. The intragranular precipitation of VCN particles, Fig.8(b), in the size range 2-5nm appears to strain induced after rolling, and was responsible for the inhibition of recrystallisation. It may be that the slower SIP in the large-grained austenite is a secondary effect on the incidence of precipitation on grain boundaries.

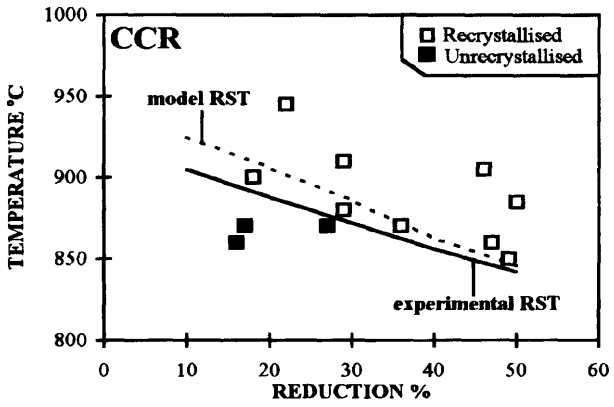

Fig.6 Model and experimental RST for CCR.

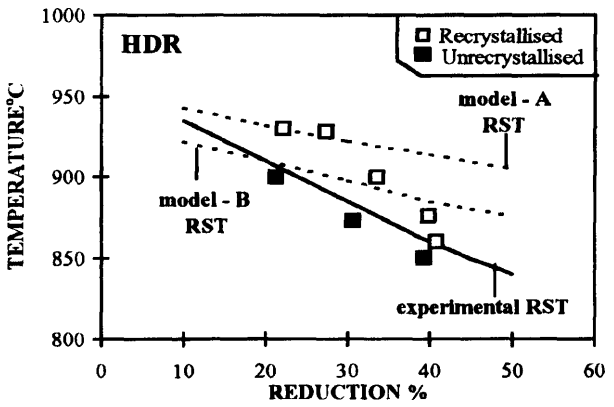

Fig. 7 Model and experimental RST for HDR.

SUMMARY AND CONCLUSIONS

Fig.9 summarises the RST's for the CCR and HDR experiments on the V steel described here, and compares these results with previous ones for a Nb-steel. For vanadium steel, Dutta and Sellars model has been modified

(i) to introduce a factor F, reflecting the lower solute drag effect on $t_{0.05RX}$,
(ii) to assume a linear dependence of $t_{0.05RX}$ on grain size, and
(iii) to assume appropriate constants A and B.

The model then explains with reasonable accuracy the difference between the RST's of the two types of steel. In both types of steel the RST is higher for HDR than for CCR. In view of the large differences in initial austenite grain size in the HDR and CCR processing, the differences between the RST's for the two processes is much smaller than would be expected on the basis of the original model. In part, this is corrected by assuming a linear, instead of quadratic, dependence of $t_{0.05RX}$ on d_o.

(a)

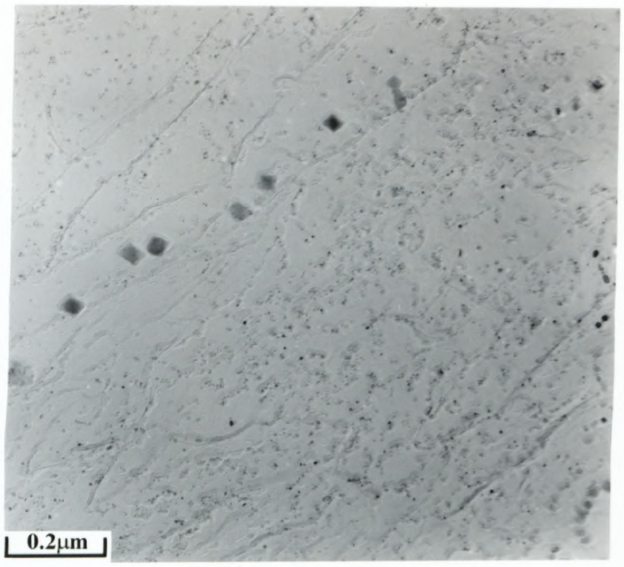

(b)

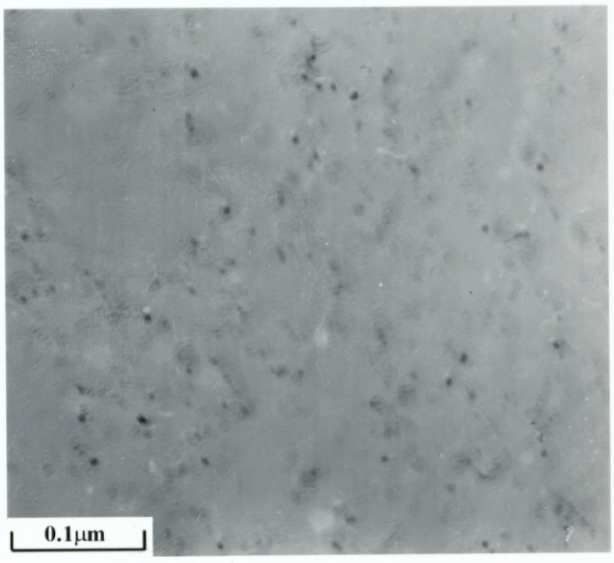

Fig.8 Precipitates in as-cast austenite, 39.2% reduction at 880℃ and isothermally held for 180 seconds at 850℃.

(a) Linear grouped coarse precipitates.

(b) Fine matrix precipitates.

However, in the V steel it was also necessary to assume that SIP was slower in the very coarse austenite grains of the HDR material. The difference between the RST's for the two processes may be influenced by the segregation ratio of vanadium or niobium, and the smaller difference in vanadium steel and the absence of large dendritic vanadium precipitates in as-cast austenite would suggest weaker segregation of vanadium during solidification.

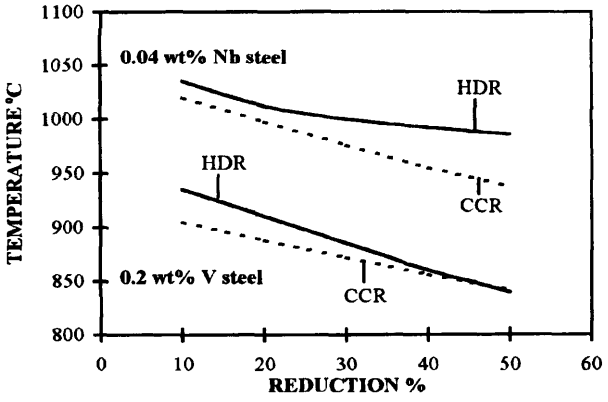

Fig.9 Comparison of RSTs during HDR and CCR of 0.04 wt % Nb and 0.2 wt % V steels.

REFERENCES

1. A. Yoshie, T. Fujita, Y. Onoe and K. Okamoto, 33rd MWSP CONF. PROC., ISS-AIME, Vol. XXIX, 1992, p. 87.
2. R. Priestner and C. Zhou, Ironmaking and Steelmaking, 22, p. 326.
3. M. Murata, K. Nishioka, and H. Tamehiro, Tetsu-to-Hagane, 74, 1988, p. 258.
4. C. Zhou, A. A. Khan and R. Priestner, 1st Inter. Conf. on Modelling Metal Rolling Processes, Sept. 1993, Publ. The Institute of Materials, p. 212.
5. C. Zhou and R. Priestner, ISIJ International, 36, 1996, p. 1397.
6. M. Cohen and S.S. Hansen, HSLA Steels, Metallurgy and Applications, ASM International, Ohio, 1986, p. 61.
7. B. Mintz and R. Abushosha, Ironmaking and Steelmaking, 20, 1993, p. 445.
8. Z. Chen, M.H. Loretto and R.C. Cochrane, Mater. Sci. Techno., 3, 1987, p.836.

9. R. K. Amin, M. Korchynsky and F.B. Pickering, Metals Technology, 8, 1981, p. 250.
10. B. Dutta and C. M. Sellars, Materials Science and Technology, 3, 1987, p. 197.
11. S. Yamamoto, C. Ouchi, and T. Osuka, Thermomechanical Processing of Microalloyed Austenite, ed. by A.J. DeArdo et al, AIME, Warrendale, Penn, 1982,p. 613.
12. S. F. Medina, J. E. Mancilla and C.A. Hernandez, ISIJ International, 34, 1994, p. 689.
13. C.D. Morton, PhD Thesis, The University of Sheffield, 1975.
14. X. Wenchung and S. Fuyus, Acta. Metallurgica Sinica, 3, 1990, p.B211.
15. J.G. Speer, S. Mehta, and S.S. Hansen, Scripta Metallurgica, 18, 1984, p.1241.